Numerical Studies of Open Swirl-Stabilized Turbulent Premixed Flames

Zhao Qiwei

M.Phil.

The Hong Kong Polytechnic University

2001

Acknowledgements

I am indebted to Dr. Chan, C.K. for his supervision, constructive criticism and encouragement, which have never ceased throughout the years. He was also helpful in his critical editing of this paper and in the original suggestion of the research topic. For suggestions during this study and for reviewing the dissertation, I am grateful to Professor Zhao, H.F., my co-supervisor.

The financial aid from The Hong Kong Polytechnic University is also greatly appreciated. The author acknowledges this support as more than monetary.

Finally, the author extends his gratitude to those all in the Department of Applied Mathematics, The Hong Kong Polytechnic University, with whom he shared many wonderful experiences and friendly ideas.

Abstract of thesis entitled "Numerical Studies of Open Swirl-stabilized Turbulent Premixed Flames" submitted by Zhao Qiwei for the degree of Master of Philosophy at the Hong Kong Polytechnic University in September 2001.

Abstract

In the current study, numerical methods are used to investigate an open swirl-stabilized turbulent premixed flame. It is assumed that swirl distributes uniformly along the circumference, and that the turbulent reacting flow is two-dimensional, symmetric, steady and incompressible.

Flame stabilization by swirl flow is a common feature of many combustors. However, most of the swirl combustors are enclosed, there have been relatively few studies of open swirl-stabilized flames. Presently, freely propagating open swirl-stabilized turbulent premixed flames are studied systematically. The purpose of this work is to obtain a better understanding of the flame properties by simulating the flow field, combustion and heat transfer. Spalding's Stretch-Cut-Slide model is modified to determine the mixing controlled fuel burning rate, $S_{fu,T}$, which is defined by

$$S_{fu,T} = -\rho \min\left[M_{fu}, \frac{M_{O_2}}{s}\right]\left(0.5\left|\frac{\partial u}{\partial y} + \frac{\partial v}{\partial x}\right| + \frac{S_L}{l_o}\right)$$

The results reveal that intense combustion occurs in a narrow region. A stationary planar flame is maintained above the burner exit, where the turbulent flame speed is equal to local flow velocity. Although the flame is stabilized by swirl, the flame zone is in fact free of swirl. Compared with previous experiments, predictions reveal that a central re-circulation zone is located downstream of the flame. However, flame stabilization does not rely on re-circulation, but on flow divergence. Combustion helps to drive the re-circulation: the re-circulation zone becomes wider and longer under combustion than in cold swirling jets. The maximum reversal velocity also increases when combustion occurs. Strong impingement occurs between swirling jet and reverse flow, which makes the flame planar. Effects of swirl intensity, fuel to air equivalence ratio and burner configuration on flame properties are also presented in this thesis. It is found that chemical reaction itself has stronger influence on re-circulation zone length than swirl intensity and equivalence ratio. A more planar flame can be obtained by modifying the burner configuration.

Table of Contents

Nomenclature iii

1 Introduction 1

1.1 Premixed and Non-Premixed Combustion 1

1.2 Flame Stabilization and Application of Swirl Flows 2

1.3 Experimental Studies of A New Kind of Swirl Burner 5

1.4 General Description of Turbulence Models 8

1.5 Numerical Studies of Combustion 9

1.6 Objectives of the Present Study 11

2 Mathematical Models 12

2.1 Conservation Equations and Averaging Process 12

2.2 Standard Two-equation k-ε Turbulence Model 17

2.3 Simplification of Species Conservation Equation 18

2.4 Simplification of Energy Conservation Equation 21

2.5 Combustion Model 21

2.5.1 Derivation Process of *SCS* Model 23

2.5.2 Simplification of *SCS* Model 26

2.5.3 Closure of *SCS* Model 28

2.6 Auxiliary Information 30

3 Derivation of Finite Difference Equation 33

3.1 Control Volume for Two-Dimensional Situation 33

3.2 The Staggered Grid Arrangement 34

3.3 Finite Difference Equation 35

3.4 Pressure Correction Equation 37

4 Application of Fluid Dynamic and Combustion Models 39

4.1 Computational Domain 39

4.2 Computational Grid 42

4.3 Boundary Condition 45

4.3.1 Inlet Boundary Condition 45

4.3.2 Entrainment Boundary Condition 46

4.4 Computational Details 50

5 Aerodynamics and Combustion in Open Swirl Flow 52
5.1 General Aerodynamic Characterisics 53
5.1.1 Axial Velocity 54
5.1.2 Radial Velocity 58
5.1.3 Tangential Velocity 59
5.1.4 Turbulent Kinetic Energy and its Dissipation Rate 61
5.2 Flame Properties 62
5.2.1 Temperature and Fuel Burning Rate 62
5.2.2 Species Concentrations 66
5.2.3 Reactedness 67
5.3 Effects of Re-circulation on Combustion 69
5.4 Comparison with other Combustion Models 71

6 Effects of Aerodynamics and Burner Configuration 74
6.1 Influence of Swirl Intensity 74
6.1.1 Influence of Swirl on Centerline Velocity 74
6.1.2 Influence of Swirl on Turbulent Kinetic Energy 75
6.1.3 Influence of Swirl on Flame Temperature 76
6.1.4 Influence of Swirl on Species Mass Fraction 78
6.2 Influence of Methane to Air Equivalence ratio 79
6.2.1 Influence of Equivalence Ratio on Axial Velocity 79
6.2.2 Influence of Equivalence Ratio on Turbulent Kinetic Energy 80
6.2.3 Influence of Equivalence Ratio on Flame Temperature 81
6.2.4 Influence of Equivalence Ratio on Species Mass Fraction 82
6.3 Influence of Burner Configuration 84
6.3.1 Influence of Burner Configuration on Axial Velocity 86
6.3.2 Influence of Burner Configuration on Flame Properties 87

7 Conclusions 90

References 92

Nomenclature

x	Axial coordinate in the cylindrical coordinates system
r, y	Radial coordinate in the cylindrical coordinates system
u	Axial velocity
v	Radial velocity
w	Tangential velocity
ρ	Density of gas mixture
μ	Molecular viscosity of the gas mixture
μ_T	Turbulent dynamic viscosity of the flow
M_i	Mass fraction of species i
Γ_i	Transport coefficient of species i
D_i	Diffusion coefficient of species i
S_i	Source term of M_i due to chemical reaction
H	Total enthalpy per unit mass of mixture
Γ_H	Transport coefficient of enthalpy
C_p	Specific heat capacity at constant pressure
C_{pi}	Specific heat capacity at constant pressure of species i
λ	Thermal conductivity of the fluid
P_r	*Prandtl* number
S_c	*Schmidt* number
φ	Generalized variable
Γ_φ	Transport coefficient of φ
S_φ	Source term of in the transport equation of φ
σ_y	Turbulent *Schmidt* number
σ_H	Turbulent *Prandtl* number
λ_T	Turbulent thermal conductivity
k	Turbulent kinetic energy
ε	Dissipation rate of turbulent kinetic energy
σ_k, σ_ε, C_μ, C_1, C_2	Empirical constants used in k-ε turbulence model
s	Stochiometric coefficient of based on mass
Ψ	Mixing fraction
A	Pre-exponential factor in *Arrhenius Law*
E	Activation energy of the chemical reaction
R	Universal gas constant

C_R	Empirical constant used in *EBU* model
g_{fu}	Mean square concentration fluctuation of fuel
S_L	Local laminar flame speed
l	Thickness of the block layer
$M_{fu,u}$	Fuel mass fraction of totally unburned gas
$M_{fu,b}$	Fuel mass fraction of fully burned gas
C_l	Empirical constant
T_1	Temperature of unburned fuel-air mixture
$\overline{T'^2}$	Mean square of temperature fluctuation
C_{T1}, C_{T2}	Empirical constants for temperature fluctuation model
W	Molecular weight of the gas mixture
Φ_P, Φ_E, Φ_W, Φ_N, Φ_S	Discretized values of generalized variable φ at different grid points
A_P, A_E, A_W, A_N, A_S	Corresponding coefficients for Φ_P, Φ_E, Φ_W, Φ_N, Φ_S
P_e	*Peclet* number
P′	Pressure correction
P	Pressure in the flow field
S	Swirl number
Φ	Fuel to air equivalence ratio
c	Reactedness (Progress Variable)

1. Introduction

Presently, numerical method is used to study an open swirl-stabilized turbulent premixed flame. The following sections provide some relevant information on this topic.

1.1 Premixed and Non-Premixed Combustion

Combustion phenomenon is a complicated chemical activity, usually in the presence of oxygen. They are characterized by a spectrum of time scales associated with chemical reactions, heat release and the concomitant change in density of the fluid mixture. During the combustion process, heat and mass transfer, fluid flow and chemical reactions play vital roles. Generally, technical processes in combustion are subdivided into two classes: premixed or non-premixed combustion. Combustion in gasoline driven automobile engines is a typical instance of premixed combustion. On the other hand, combustion in diesel engines is an instance for which non-premixed combustion occurs. In either case, chemical reaction can occur only when fuel and oxidizer are mixed at the molecular level.

In premixed flames, fuel and oxidizer are mixed down to the molecular level by molecular diffusion or turbulence during a sufficiently long time before combustion is initiated. The overall rate of burning in a turbulent flow depends to a large extent on the extent of interfacial area between premixed fuel and the combustion products. The larger this area, as in highly turbulent flows, the more rapid is the consumption rate of fuel and hence the overall rate of energy release. Premixed flames appear with a blue to bluish-green color. The blue color of this mode of combustion is due to chemiluminescence of some of the existing species (C_2 or CH radicals). Premixed flames are used whenever intense combustion within a small volume is required. This is the case in gasoline driven automobile engines.

In non-premixed flames, fuel and oxidizer are initially unmixed. In laminar flows, they are mixed entirely by the molecular diffusion process. In turbulent reacting flows, turbulence adds two effects: mixing at large scales through formation of coherent structures, and at small scales through turbulent fluctuations. However, molecular mixing at the smallest scales is still the rate-limiting step. In most cases combustion is much faster than diffusion and diffusion is the rate-limiting step that controls the entire process. This is the reason why those flames, where the reactants are non-premixed, are called diffusion flames. Diffusion flames radiate in a bright yellow color. This is due

to the presence of radiating particles in the diffusion flame. These particles may dominate over the chemiluminescence that is also present in non-premixed combustion. However, some highly stretched flames also appear blue since the local residence time is too short for soot particles to form. Large combustion devices such as furnaces usually operate under non-premixed conditions with diffusion flames, since the premixing of large volumes of fuel and air represents a serious safety problem.

It is clear, that in addition to premixed and non-premixed combustion, partially premixed combustion plays, at least locally, an important role in technical applications. An important example is modern gas turbine combustion chambers, where fuel rich region is used for flame stabilization. However, in order to minimize NO_x formation, most combustion occurs under premixed fuel lean conditions.

1.2 Flame Stabilization and Application of Swirl Flows

There are many research topics in combustion problems of technological interest, such as flame structure, flame stabilization, flame ignition/extinction, chemical kinetics, turbulence-kinetics interaction and so on. Of all these topics, flame stabilization is a very important subject. This problem arises when flow velocity in the combustion field exceeds the local flame speed. For example, the values of laminar flame speeds for hydrocarbon fuels in air are rarely greater than 45cm/s. Hydrogen is unique in its laminar flame speed, which approaches 240 cm/s. If one could attribute a turbulent flame speed to hydrocarbon mixtures, it would be at most a few hundred centimeters per second. However, in many practical devices, such as furnace burners and turbojets in which high volumetric heat release rates are necessary, the flow velocities of the fuel-air mixture are of the order of 30 m/s or higher. Furthermore, for such velocities, the boundary layers are too thin in comparison to the quenching distance for stabilization to occur by the same means as that obtained in Bunsen burners. Thus, some means for flame stabilization is needed. In practice, stabilization is accomplished by causing some of the combustion products to re-circulate, thereby continuously igniting the fuel mixture. Based on this principle, there are many methods to stabilize the flame in high-velocity streams, as depicted in Fig. 1.1.

(1) Bluff-body stabilization—by inserting solid obstacles in the stream, as in ramjet technology.

(2) Step stabilization—by using a step in the wall enclosure, as in the so-called "dump" burners.

(3) Aerodynamic stabilization—by directing part of the flow or one of the flow constituents, usually air, opposed or normal to the main stream, as in gas turbine combustion chambers.

A complete review of flame stabilization of turbulent premixed gases was given by *Edelman* and *Harsha* [14].

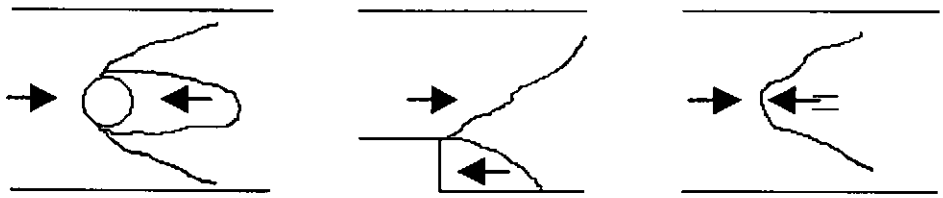

(A) Bluff Body Method, (B) Step Method, (C) Opposed Jet

Fig.1.1 Stabilization Methods for High-Velocity Reacting Flows

Among aerodynamic methods, swirl has been widely used for a number of years for the stabilization of high-intensity combustion processes [3,30,61]. Swirl flows are very important in combustion application. *Syred* and *Beer* [61] summarized the main effects of swirl as follows:

(1) To reduce flame lengths by producing higher rates of entrainment of the ambient fluid and fast mixing close to the exit nozzle and on the boundaries of re-circulation zones.
(2) To improve flame stability as a result of the formation of re-circulation zone in strongly swirling zones.
(3) As the blockage is aerodynamic, flame impingement on the burner may be minimized, thus ensuring minimum maintenance and extended life for the unit.

These re-circulation zones, which re-circulate heat and radical species to the root of the flame, thus reducing velocity requirements for flame stabilization, are only formed when swirl is sufficiently strong [8]. Though most significant effects of swirl are produced by re-circulation, non-recirculation swirl flows have also been investigated [21,34,47, 49] and used in flame stabilization [2,5,9,60].

Flame stabilization by swirl is a common feature of many turbines and furnaces. In most cases, flames are stabilized by reversal flow caused by strong swirl. Many fundamental aspects of the complex interaction between swirl and non-premixed flames [17,63], premixed flames [18,20] and spray combustion [15] have been investigated experimentally in laboratories using turbine and furnace simulators. Since most swirl burners are enclosed, there have been

relatively few studies of unconfined swirl stabilized flames. The following discussion will primarily concentrate on previous studies of unconfined jet flames stabilized by swirl flow.

Chigier and *Chervinsky* [9] studied the aerodynamic behavior of free butane-air flames with swirl. This is the earliest study about open swirl stabilized flame. Velocity and temperature measurements had been made in a series of turbulent swirl flames. Premixed butane-air jet issued from a round orifice with exit velocity of 60 m/s and the degree of swirl was varied by varying the ratio of the flow rates of air supplied tangentially and axially to the burner. The flames were stabilized some 4 diameters from the burner exit in the shape of an annular ring and were confined for a distance of 24 diameters. The measurements made in this region for three different degrees of swirl show that the decay of axial and swirl velocities is slower in a flame than that in cold swirl jets. The turbulent flame speed was found to be 80 times greater than the laminar flame speed. Theoretical expressions describing the decay along the axis of maximum values of axial velocity, swirl velocity and temperature have been obtained by integration of the turbulence equations of motion, energy and state. These expressions together with the semi-empirical expressions obtained for the radial spread of velocity and temperature provide a means of determining these quantities at each point in the flame as a function of swirl.

Starner and *Bilger* [60] investigated a non-premixed turbulent jet flame interacting with moderate swirl. They argued that much could be learned from the unconfined system because it is more accessible to probing by laser diagnostics. Their results show that the flame expands into the free stream, which does not act as a confinement, and is shortened one third and widened around one quarter by the swirl. This contrasts with results in the literature for confined swirling flames, which lengthen with increasing swirl. It is found that the effect of swirl on flame length can depend on the degree of confinement. When the flow is unconfined, the angular momentum will diffuse quickly into the free stream. The resulting adverse axial pressure gradient retards and widens the jet initially, whilst the normalized downstream turbulence components and stresses are close to those in non-swirling flames. By contrast, narrow confinement appears to lengthen the flame due to suppression of shear stress by the pressure-gradient terms, as the angular momentum cannot diffuse freely, thus maintaining a high radial pressure gradient.

Tangirala et al [63] studied the effect of heat release and swirl on the re-circulation within swirl-stabilized flames. The amount of heat release was

varied through changing the overall fuel to air equivalence ratio. The swirl was varied in order to assess the advantages or disadvantages of very high swirl operation. The velocity fields in nine non-premixed flames and three cold flows were mapped out using laser velocimetry. It was found that increasing the heat release resulted in a number of benefits, including an increase in the re-circulation, the turbulence levels, and the flame stability. Heat release helped to drive the re-circulation, since in some cases the cold flow did not have re-circulation but the corresponding flames did. Turbulent kinetic energy levels increased by a factor of three as heat release increased. The effect of increasing swirl was to improve the mixing and flame stability when swirl intensity is lower than a critical value; further increase in swirl actually reduced the turbulence levels and flame stability. Excessive swirl also had the disadvantages of forcing the flame to move upstream to a position closer to the burner walls, resulting excessive wall heating. It is interesting to note that, in the nine flames there is no significant change in the re-circulation zone length as either equivalence ratio or swirl is varied. This shows that chemical reaction has a strong effect on the re-circulation zone length.

Fujii et al [18] studied the unconfined, swirling turbulent flow with and without combustion. LDV (Laser Doppler Velocimetry) measurement system was employed to quantify the velocity characteristics of jets emerging from the annular swirl burner. It was found that a large re-circulation zone existed downstream of the flow axis under both reacting and non-reacting conditions. Flow field was drastically altered by combustion. The swirl component was significantly distorted around the flame stabilization zone with sharp axial velocity gradients, whereas a solid-body rotation was maintained in the isothermal flow. This deviation was probably due to unstable effects caused by the viscous forces, which outweighed the centrifugal forces. It was also found that the axial length of the re-circulation zone was diminished, and the point of maximum re-circulation strength necessary for the flame stabilization shifted further downstream due to heat release. Turbulence levels were higher in the reacting flow than in the isothermal jet.

These studies indicate that open swirl stabilized flames have no common regularities. Their behavior is strongly influenced by the burner configuration, swirl intensity, mixing extent of fuel and oxidizer, and etc.

1.3 Experimental Studies of A New Kind of Swirl Burner

Chan et al [5] developed a novel means for using weak swirl to stabilize freely propagating open premixed turbulent flames. The schematic of the swirl

burner is shown in Fig.1.2. This burner consists of a central flow of premixed fuel/air surrounded by co-flow air. Swirl is generated via injecting air tangentially through two air inlets. For conditions of weak swirl, they discovered that it provides a novel means of stabilizing freely propagating yet steady premixed flames, which maintain a distance above the burner exit. This interesting and useful phenomenon of flame stabilization by swirl has yet to be reported in the literature before. Moreover, the absence of physical surfaces in the vicinity of the flame provides free access to laser diagnostics. This gives such kind of burner the potential of being one of the most ideally suited configurations for investigating fundamental properties of premixed turbulent flames, such as turbulent flame speeds, flame generated turbulence, burning rates and extinction or local quenching by turbulence.

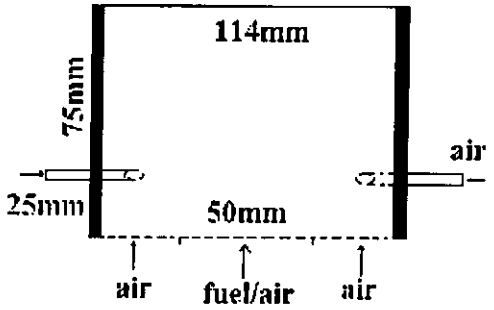

Fig.1.2 Schematics of the co-flow swirl burner

The flow fields for six reacting and non-reacting conditions with and without incident turbulence are investigated using two-component laser Doppler anemometry. The most distinct characteristic of the flame is that flame stabilization does not rely on flow re-circulation, since no re-circulation zone is detected in the vicinity of the flame. The velocity profiles show that the flames are stabilized by swirl-induced flow divergence, and the flame is maintained where the local mass flux equals the burning rate. Despite the fact that the flame is stabilized by swirl, the flame zones are in fact free of the influence of swirl. Because the flames are axisymmetric, turbulent flame speed can be estimated based on the centerline velocity vector, which is locally normal to the flame brush. The flow lines show that the flame flow fields are close approximations to the normal one-dimensional planar premixed turbulent flames of many theoretical models. It is also interesting to note that the turbulence level peaks in the flame zone, indicating the production of turbulence by the flame.

Several refinements have been made to reduce some of the flame asymmetries and damp flow perturbations after *Chan et al*'s swirl burner was put forward.

Bedat and *Cheng* [2] used a similar system in studying premixed flames with intense isotropic turbulence. The coflow system is replaced by central premixed fuel/air flow. The swirl generator is placed far upstream of the burner exit in order to allow the swirl to develop. It consists of four tangential air-inlets, individually adjustable, compressed air jets inclined at 20°. Such arrangement would be most useful to ensure an axi-symmetric flow fields. This setup can produce stable premixed turbulent flames under a wide range of mixture conditions and turbulence intensities, where the flames can be classified as wrinkled laminar flames, corrugated flames, and flames with distributed reaction zones. Compared to *Chan et al*'s [5] experiments, *Bedat* and *Cheng* [2] found that, in the intense turbulence, the flames are found to produce very little changes in the mean and rms velocities. Though *Bedat* and *Cheng* [2] detect no re-circulation zone in the vicinity of the flame, they did find a re-circulation zone under the isothermal conditions. It is not clear whether this re-circulation zone is overcome or moved downstream by chemical reaction. *Plessing et al* [42] measured the turbulent burning velocity in planar turbulent premixed flames using *Bedat* and *Cheng*'s [2] swirl burner. The measurements of the two-dimensional flow field show a re-circulation zone downstream of the flame stabilization area. However, *Plessing et al* [42] did not concentrate on the role and variation of the re-circulation zone. Recently, this kind of swirl burner has been scaled to the thermal input levels of a small industrial burner [7]. The purpose is to demonstrate its viability for commercial and industrial furnaces and boilers. Industrial scale-up experiments show that this swirl burner can achieve very high combustion efficiency with low NO_x emission. Between 210 and 280 kW thermal input and fuel to air equivalence ratio of about 0.85, NO_x emission is lower than 15ppm, while CO emission is lower than 10ppm. These results indicate that this burner is a simple, low-cost and promising environmental energy technology that can be further developed to meet future air-quality rules.

The above studies indicate that much research has been carried out on this new swirl burner. *Peters* [41] argued that such swirl burner can be used as standard device in studying turbulent burning velocities, since it can generate a freely stabilized flame which has a one-dimensional steady structure in the mean. However, there remain some uncertainties about this burner. For example, *Chan et al* [5] detected no re-circulation zone in their studies, while *Bedat* and *Cheng* [2] and *Plessing et al* [42] measured reversal flow in their experiments. Since the testing section is restricted within 100 mm from the burner exit in *Chan et al*'s [5] study, it is not clear whether there exists a re-

circulation zone downstream of the flame area. Another dispute is about turbulence generation in the flame zone. *Chan et al* [5] measured a peak value of turbulence in the flame zone, while *Bedat* and *Cheng* [2] found that flame produces very little turbulence. Furthermore, the previous studies did not explain why a planar flame can be maintained by the weak swirl flow. These facts indicate that much work need be done to make up for the previous studies.

In our current study, primary attention is focused on this open premixed turbulent flames stabilized by weak swirl flow. Numerical methods will be used to study this flame in a larger open space. The purposes of our study are twofold. One is to improve our understanding about the combustion process of this special flame. The other is to provide detailed information about the distribution of flow velocities, gas temperature and species concentrations. Since the flow is turbulent, and there occurs chemical reaction in the flow, the following two sections will provide some information about numerical simulation of turbulence and combustion.

1.4 General Description of Turbulence Models

As is well known, turbulence is one of the most difficult, unsolved theoretical problems in fluid mechanics [66]. Turbulent flow is highly complex, unsteady and three-dimensional The fundamental approach to turbulence studies is the direct numerical simulation (*DNS*) by solving the transient three-dimensional *Navier-Stokes* (*N-S*) equation without using any turbulence models. Another approach is the large-eddy simulation (*LES*), which is to solve the *N-S* equation in the grid size of large eddies, but still needs to model the small-scale turbulence (sub-grid modeling). Both of these two methods need extremely large computer capacity and computational time. Thus, they are impractical for engineering predictions. In the opinion of many fluid-dynamists, the only practical method today is the method of turbulence modeling based on solving the *Reynolds* time-averaged equations and transport equations of correlation terms.

The basic idea of turbulence modeling is to simulate the unknown higher-order correlation terms by using lower-order correlations or mean flow properties, in order to close the time-averaged equations or the transport equations of correlation terms. A turbulence model is an approximation of the effects of turbulence on the governing flow conditions. The earliest and simplest turbulence model is the mixing-length model or algebraic model (zero-equation model) proposed by *Prandtl* in 1925. The model is based on the

concept of analogy between laminar viscosity and turbulent viscosity, mean motion and turbulenet fluctuation. The merits of this model are simple and intuitive, without adding differential equations. However, it neglects the turbulence convection and diffusion and has less generality.

Historically, a one-equation or energy-equation model was developed. It is to use a modeled turbulent kinetic energy equation and a presumed algebraic expression of the turbulence scale l to predict turbulence viscosity, defining $\mu_T = C_\mu \rho K^{0.5} l$. This model is more reasonable than the mixing-length model, since it takes account of turbulent convection and diffusion. But for complex flows, it is difficult to give a generalized expression of the turbulent scale l. Therefore, the k-equation model can be considered as an intermediate step that leads to the development of two-equation models.

In fact, not only the turbulent kinetic energy, but also the other turbulent properties are transported in the flow field. *Launder* and *Spalding* [27] summarized the second turbulence parameters as $z = k^m l^n$, proposed by different authors [10,48,54]. Among them the well-known k-ε model [28] is most widely used and tested. This model assumes that the turbulent flow characteristics can be found from the knowledge of the turbulent kinetic energy k and its dissipation rate ε. During the last 20 years, numerous modifications of the k-ε turbulence model have been proposed, with certain extent of success, to account for effects of buoyancy, streamline curvature and swirling flows.

In recent years, the *Reynolds* stress transport equation model (*DSM*) has been applied to predict strongly swirling and buoyant flows in burners and furnaces. In many cases it gives better results than that given by the k-ε model, showing the merits in its ability to account for the swirling effect, buoyancy effect, curvature effect, near-wall effect, etc. However, its drawbacks prevent the *Reynolds* stress model from being widely used nowadays, as explained by *Zhou* [66].

As a compromise between the number of unknowns and computational time, the standard k-ε model is chosen for the current study.

1.5 Numerical Studies of Combustion

Due to the complicated nature of chemically reacting turbulent flow, the attempts to numerically solve for the combustion variables were attempted only after a number of advances had been made in modeling of turbulence.

Chemical reactions pose a complicated problem. Even a simple type of combustion process occurs via a large number of elementary reactions. If we want to describe the turbulent flame behavior rigorously, the calculation from first principles will require the detailed kinetics calculation simultaneously with the calculation of time-dependent three-dimensional flow, concentration and temperature fields. The required computational load would be enormous and would be almost impossible to implement even by the most sophisticated super-computers [45]. Thus, it is necessary to develop some plausible physical models to make the numerical calculation actually possible.

One possibility is to separate the kinetics calculation from the flow calculation [33, 51,62]. However, this will not be always possible, and only in certain limited cases can these calculations be made separately. Since combustion involves many intermediate steps, most of the fast processes can be neglected and only one or two slow processes are considered to govern the combustion rate. Based on this idea, various methods and models have been suggested, and they have been reviewed by *Khalil* [25].

Since our current study deals with turbulent premixed combustion, we shall briefly examine current approaches to modeling turbulent premixed combustion in general. Turbulent combustion models in use today may be classified in order of increasing complexity as [64,65]:

(1) Single-step reaction models

(2) Mixing- controlled models

(3) Models based on probability density functions (*PDF*)

Single-step reaction model aims to curve fit the energy release rate over a narrow range of operating conditions without considering the structure of the flame. Moment method has been extended to reaction rate expressions of the *Arrhenius* type by expanding the exponential temperature relation in an infinite series. However in such approaches higher moments have to be modeled. No well-founded methods of modeling such moments to achieve closure have been suggested. In fact the series is often truncated without justification in order to achieve closure.

Mixing-controlled models postulate a structure for the turbulent flame. It is assumed that conversion of reactants to products is limited by the rate at which the hot products mix with cold reactants, which in turn is a function of the turbulent eddy turnover time. Thus in these models, unlike in single-step reaction model, the rate of conversion of reactants to products is not kinetically

controlled. The *EBU* (Eddy-Break-Up) model [53,58] and *SCS* (Stretch-Cut and Slide) model [55] developed by *Spalding* are such mixing-controlled models.

The probability density function approach has following three variants:

(1)The probability density function for locating the flame front at a point in space at a given time is specified a priori.

(2)The probability density function is calculated from a finite number of moments.

(3)An evolution equation for the probability density function is solved.

Detailed information about these *PDF* combustion models can be obtained in *Refs.* [4,29,43,44].

With modern computational tools and facilities, numerical simulations with large code to predict the performance of combustion devices such as furnaces and gas turbines are feasible and start to compete with practical experiments. Whether they will partly or fully replace experimental study will largely depend on the efficiency of the numerical methods and on the reliability of the turbulence and combustion models.

1.6 Objectives of the Present Study

In our current study, numerical methods is used to study this swirl flame in a larger, open space. The purpose of this research is to obtain a better understanding of the open premixed turbulent flames stabilized by swirl flow through simulating the flow, combustion and heat transfer in the open space. Since turbulent flow and turbulent combustion have been studied quite extensively, fairly satisfactory methods are available for their prediction. Specific objectives of our study are as follows:

(1) Velocity field with or without combustion

(2) Temperature and gas species distribution

(3) Premixed flame position and turbulent flame speed

(4) Swirl influence on flame properties

(5) Effect of fuel to air equivalence ratio on flame properties

(6) Effect of burner configuration on open premixed flames

2. Mathematical Models

There are many physical and chemical processes taking place in the combustion equipment, namely, transport of mass, momentum, species and energy [25]. Except for radiation energy transfer, all the physical quantities are transported together with the mass, i.e., they are properties of mass. The radiation energy is transported by means of electro-magnetic waves or photons [50]. The transport phenomena of the related physical quantities are governed by the conservation principles, which can be expressed in terms of differential equations [25,59]. The physics of the problem can be determined only by solving the system of the transport equations. However, the entire set of the "exact" equations is not readily manageable even for the simplest laminar flow cases. This requires simplification of the general transport equations. Furthermore, when the flow is turbulence, the time-dependent fluctuating solution is neither possible nor necessary [24]. Therefore, time averaging of the fluctuating transport processes is required. This leads to turbulence modeling of all the transport processes [24].

2.1 Conservation Equations and Averaging Process

The schematic of the co-flow swirl burner has been shown in Fig.1.2. The configuration chosen is same as that employed by *Chan et al* [5]. The burner is supplied by a 50mm diameter inner core of fuel/air mixture surrounded by an annular co-flow air jet of 114mm diameter. Swirl is induced via injecting air tangentially through two air inlets of 6.1mm diameter.

To formulate this problem, the cylindrical coordinate system will be used. The flow is considered to be two-dimensional (i.e., $\partial/\partial\theta=0$, where θ is the tangential coordinate in the cylindrical coordinate system), steady (i.e., $\partial/\partial t=0$), and incompressible (the density fluctuation $\rho'=0$). The initial velocity, temperature and species mass fractions are assumed to be uniform at the burner inlet. Unlike some models in which diffusion in the axial direction is neglected [58], we consider the fully elliptic problem. The governing transport equations of mass, momentum, species and energy may be written in their primitive form as (Note that, since $\partial/\partial\theta=0$, the θ coordinate will not appear in the equation):

1. Mass Conservation Equation

$$\frac{\partial(\rho u)}{\partial x}+\frac{1}{r}\frac{\partial(r\rho v)}{\partial r}=0 \qquad (2.1)$$

Where,

ρ: Density of gas mixture

u: Velocity component in the axial direction, x

v: Velocity component in the radial direction, r

2. Momentum Conservation Equation (*N-S* Equation)

(1) Axial-momentum

$$\frac{\partial(\rho uu)}{\partial x}+\frac{\partial(r\rho uv)}{r\partial r}=\frac{\partial}{\partial x}(\mu\frac{\partial u}{\partial x})+\frac{\partial}{r\partial r}(r\mu\frac{\partial u}{\partial r})$$

$$-\frac{\partial p}{\partial x}+\frac{\partial}{\partial x}(\mu\frac{\partial u}{\partial x})+\frac{\partial}{r\partial r}(r\mu\frac{\partial v}{\partial x}) \qquad (2.2)$$

Where,

μ: Molecular viscosity of the fluid mixture

(2) Radial-momentum

$$\frac{\partial}{\partial x}(\rho uv)+\frac{\partial}{r\partial r}(r\rho vv)=\frac{\partial}{\partial x}(\mu\frac{\partial v}{\partial x})+\frac{\partial}{r\partial r}(r\mu\frac{\partial v}{\partial r})-\frac{\partial p}{\partial r}+\frac{\partial}{\partial x}(\mu\frac{\partial u}{\partial r})$$

$$+\frac{\partial}{r\partial r}(r\mu\frac{\partial v}{\partial r})-\frac{2\mu v}{r^2}+\frac{\rho w^2}{r} \qquad (2.3)$$

(3) Tangential-momentum

$$\frac{\partial}{\partial x}(\rho uw)+\frac{\partial}{r\partial r}(r\rho vw)=\frac{\partial}{\partial x}(\mu\frac{\partial w}{\partial x})+\frac{\partial}{r\partial r}(r\mu\frac{\partial w}{\partial r})$$

$$-\frac{\partial}{r\partial r}(\mu w)-\frac{\rho vw}{r}+\frac{\mu}{r}(\frac{\partial w}{\partial r}-\frac{w}{r}) \qquad (2.4)$$

3. Species Conservation Equation

$$\frac{\partial}{\partial x}(\rho uM_i)+\frac{\partial}{r\partial r}(r\rho vM_i)=\frac{\partial}{\partial x}(\Gamma_i\frac{\partial M_i}{\partial x})+\frac{\partial}{r\partial r}(r\Gamma_i\frac{\partial M_i}{\partial r})+S_i \qquad (2.5)$$

Where,

M_i: Mass fraction of species i

Γ_i: Transport coefficient of species i, $\Gamma_i=\rho D_i$ (kg/m·s)

D_i: Diffusion coefficient of species i, m^2/s

Si: Source term of M_i per unit volume due to chemical reaction

4. Energy Conservation Equation

$$\frac{\partial}{\partial x}(\rho uH)+\frac{\partial}{r\partial r}(r\rho vH)=\frac{\partial}{\partial x}(\Gamma_H\frac{\partial H}{\partial x})+\frac{\partial}{r\partial r}(r\Gamma_H\frac{\partial H}{\partial r})$$

$$+\Gamma_H(1-\frac{P_r}{S_c})\sum_i H_i(\frac{\partial^2 M_i}{\partial x^2}+\frac{\partial^2 M_i}{r^2\partial r^2})+S_H \qquad (2.6)$$

Where,

H_i: Enthalpy of species i per unit mass (including formation enthalpy),

$$H_i = H_i^\circ + \int_{T^\circ}^{T} C_{pi}(T)dT \qquad (2.7)$$

H_i° : Formation enthalpy of species i at T° K

C_{pi}: Specific heat capacity at constant pressure of species i, J/kg·K

H: Total enthalpy per unit mass of mixtures (neglecting the kinetic energy)

$$H = \sum_i M_i H_i \qquad (2.8)$$

Γ_H: Transport coefficient of enthalpy, $\Gamma_h \equiv \lambda/C_p$ (kg/m·s)

λ: Thermal conductivity of the fluid, J/m·s·K

C_p: Specific heat capacity at constant pressure of the fluid, J/kg·K

P_r: *Prandtl* number, $P_r \equiv C_p\mu/\lambda$

S_c: *Schmidt* number, $S_c \equiv \mu/\Gamma_i$

S_H: Source of enthalpy per unit volume

For any quantity that obeys the conservation law, we can write its transport equation in the following generalized form as [38],

$$\frac{\partial}{\partial x}(\rho u\varphi)+\frac{\partial}{r\partial r}(r\rho v\varphi)=\frac{\partial}{\partial x}(\Gamma_\varphi\frac{\partial \varphi}{\partial x})+\frac{\partial}{r\partial r}(r\Gamma_\varphi\frac{\partial \varphi}{\partial r})+S_\varphi \qquad (2.9)$$

Note that S_φ here does not exactly coincide with the source terms defined earlier, rather S_φ denotes the rest of terms after the conservation equation has been written in the above form, and Γ_φ is the transport coefficient of φ.

The above equations are applicable to any local position. However, when the flow is highly turbulent, the local velocity and physical quantities fluctuate in a non-steady and random fashion. The non-steady motion of fluid particles is too complicated to be solved by direct application of the above transport equations. Moreover, a complete numerical solution of the turbulent flow is impractical with today's computers, because the turbulence eddies are only millimeters in size in a flow domain of several meters. At the same time, the non-steady solution, even if possible, is not useful for practical engineering purpose. The engineering interest is mainly in the averaged behavior of the

flow. Thus, an averaging process of the above equations to obtain transport equations of the mean quantities is necessary. This leads to turbulence and combustion models.

Before proceeding, it is necessary to discuss the methods of averaging. Two methods of averaging, i.e., *Reynolds* mean (or time-mean) and *Favre* (or density-weighted) mean are available [24]. The density is not uniform due to temperature and composition variation as a result of chemical reaction and heat transfer. For time-mean quantity, $\bar{\varphi}$, one has,

$$\varphi = \bar{\varphi} + \varphi' \tag{2.10}$$

$$\bar{\varphi'} = 0 \tag{2.11}$$

While for density-weighted mean, $\bar{\varphi}^{\circ}$, one has,

$$\varphi = \bar{\varphi}^{\circ} + \varphi'^{\circ} \tag{2.12}$$

$$\overline{\rho\varphi} = \bar{\rho}\bar{\varphi}^{\circ} \tag{2.13}$$

$$\overline{\rho\varphi'^{\circ}} = 0 \tag{2.14}$$

Time-averaging methods have a clearer physical meaning than the density-weighted method, although many of the measured quantities do actually represent the *Favre* mean [24] values. In our current study, the *Reynolds* averaging method will be employed, which starts with time-averaged governing equations and employs empirical input for turbulent transport terms to close the system of transport equations. This involves a set of equations that determine the turbulent transport terms in the time-averaged system of equations.

When using time-mean method, the transport equation in general form, i.e., equation (2.9) can be written as:

$$\frac{\partial}{\partial x}(\rho\bar{u}\bar{\varphi}) + \frac{\partial}{r\partial r}(r\rho\bar{v}\bar{\varphi}) = \frac{\partial}{\partial x}(\overline{\Gamma_{\varphi}\frac{\partial\varphi}{\partial x}} - \rho\overline{u'\varphi'}) + \frac{\partial}{r\partial r}(r\overline{\Gamma_{\varphi}\frac{\partial\varphi}{\partial r}} - r\rho\overline{v'\varphi'}) + \overline{S_{\varphi}} \tag{2.15}$$

Note that the molecular diffusion terms, $\overline{\Gamma_{\varphi}\frac{\partial\varphi}{\partial x}}$ and $\overline{\Gamma_{\varphi}\frac{\partial\varphi}{\partial r}}$, are usually much smaller than the turbulent diffusion terms, $-\rho\overline{u'\varphi'}$ and $\rho\overline{v'\varphi'}$. Therefore, one can approximate these terms by writing,

$$\overline{\Gamma_{\varphi}\frac{\partial\varphi}{\partial x}} = \Gamma_{\varphi}\frac{\partial\bar{\varphi}}{\partial x} \tag{2.16}$$

$$\overline{\Gamma_\varphi \frac{\partial \varphi}{\partial r}} = \Gamma_\varphi \frac{\partial \bar{\varphi}}{\partial r} \tag{2.17}$$

This set of equations is not a closed system due to the unknown second order turbulence correlation terms, i.e., $-\rho\overline{u'\varphi'}$ and $-\rho\overline{v'\varphi'}$. These quantities expressed the transport of momentum, mass and energy caused by turbulent fluctuation, or known as the turbulent stresses or the Reynolds stresses ($-\rho\overline{u'u'}$, $-\rho\overline{u'v'}$, $-\rho\overline{v'v'}$, $\rho\overline{u'w'}$ and $\rho\overline{v'w'}$), turbulent mass flux ($-\rho\overline{u'M_i'}$ and $-\rho\overline{v'M_i'}$) and turbulent heat flux ($-\rho\overline{u'H'}$ and $-\rho\overline{v'H'}$) respectively. These turbulent diffusion terms should be modeled by some approximate closure. In the case of isotropic turbulent flows, the concept of an isotropic scalar turbulent viscosity (or eddy viscosity) can be introduced, and these correlation terms in the above equations can be expressed in the so-called *Boussinesq* form as [25]

$$-\rho\overline{u'u'} = \mu_T\left(\frac{\partial \bar{u}}{\partial x} + \frac{\partial \bar{u}}{\partial x}\right) \tag{2.18}$$

$$-\rho\overline{u'v'} = \mu_T\left(\frac{\partial \bar{u}}{\partial r} + \frac{\partial \bar{v}}{\partial x}\right) \tag{2.19}$$

$$-\rho\overline{v'v'} = \mu_T\left(\frac{\partial \bar{v}}{\partial r} + \frac{\partial \bar{v}}{\partial r}\right) \tag{2.20}$$

$$-\rho\overline{u'w'} = \mu_T \frac{\partial \bar{w}}{\partial x} \tag{2.21}$$

$$-\rho\overline{v'w'} = \mu_T \frac{\partial \bar{w}}{\partial r} - \frac{\mu_T \bar{w}}{r} \tag{2.22}$$

$$\rho\overline{w'^2} = -\frac{2\mu_T \bar{v}}{r} \tag{2.23}$$

$$-\rho\overline{u'M_i'} = D_T\rho \frac{\partial \overline{M_i}}{\partial x} = \frac{\mu_T}{\sigma_y}\frac{\partial \overline{M_i}}{\partial x} \tag{2.24}$$

$$-\rho\overline{v'M_i'} = D_T\rho \frac{\partial \overline{M_i}}{\partial r} = \frac{\mu_T}{\sigma_y}\frac{\partial \overline{M_i}}{\partial r} \tag{2.25}$$

$$-\rho\overline{u'H'} = \frac{\lambda_T}{C_p}\frac{\partial \bar{H}}{\partial x} = \frac{\mu_T}{\sigma_H}\frac{\partial \bar{H}}{\partial x} \tag{2.26}$$

$$-\rho\overline{v'H'} = \frac{\lambda_T}{C_p}\frac{\partial \bar{H}}{\partial r} = \frac{\mu_T}{\sigma_H}\frac{\partial \bar{H}}{\partial r} \tag{2.27}$$

Where,

μ_T: Turbulent dynamic viscosity

D_T: Turbulent mass diffusion coefficient

λ_T: Turbulent thermal conductivity

σ_y or σ_H: Turbulent *Prandtl* or *Schmidt* number

Now, the above set of *Reynolds* time-averaged equations, i.e., equation (2.15) can be rewritten in the following generalized form as

$$\frac{\partial}{\partial x}(\rho\bar{u}\bar{\varphi}) + \frac{\partial}{r\partial r}(r\rho\bar{v}\bar{\varphi}) = \frac{\partial}{\partial x}(\overline{\Gamma_{\varphi,eff}}\frac{\partial\bar{\varphi}}{\partial x}) + \frac{\partial}{r\partial r}(r\overline{\Gamma_{\varphi,eff}}\frac{\partial\bar{\varphi}}{\partial r}) + \overline{S_\varphi} \qquad (2.28)$$

Where, $\overline{\Gamma_{\varphi,eff}} = \Gamma_\varphi + \mu_T/\sigma_\varphi$ is the generalized transport coefficient of quantity φ, σ_φ stands for turbulent *Prandtal* or *Schmidt* number. Note that the turbulent *Prandtl* and *Schmidt* numbers can be assumed to be constant [25,59], while the turbulent dynamic viscosity is calculated from other equations of turbulence. The task of turbulence modeling is either to direct simulate the second order correlation terms $-\rho\overline{u'\varphi'}$ and $-\rho\overline{v'\varphi'}$, or to simulate the turbulent dynamic viscosity μ_T.

2.2 Standard Two-equation k-ε Turbulent Model

The k-ε model was originally proposed by *Launder* and *Spalding* [28] and has been tested by many researchers and found to yield reasonable result. In the current study, the transport equations of k and ε were given directly. Detailed derivation process of these two equations can be found in *Ref.* [66].

1. Transport equation for turbulent kinetic energy, k

$$\frac{\partial}{\partial x}(\rho\bar{u}k) + \frac{\partial}{r\partial r}(r\rho\bar{v}k) = \frac{\partial}{\partial x}((\frac{\mu_T}{\sigma_k} + \mu)\frac{\partial k}{\partial x})$$

$$+ \frac{\partial}{r\partial r}(r(\frac{\mu_T}{\sigma_k} + \mu)\frac{\partial k}{\partial r}) + G - \rho\varepsilon \qquad (2.29)$$

Where,

σ_k: Turbulent *Prandtl* number for k, assumed to be constant

G: Stress production term

$$G = \mu_T(2((\frac{\partial\bar{u}}{\partial x})^2 + (\frac{\partial\bar{v}}{\partial r})^2 + (\frac{\bar{v}}{r})^2) + (\frac{\partial\bar{u}}{\partial r} + \frac{\partial\bar{v}}{\partial x})^2)$$

$$+ \mu_T((\frac{\partial\bar{w}}{\partial x})^2 + (\frac{\partial\bar{w}}{\partial r} - \frac{\bar{w}}{r})^2) \qquad (2.30)$$

2.Transport equation for turbulent kinetic energy dissipation rate, ε

$$\frac{\partial}{\partial x}(\rho \bar{u}\varepsilon)+\frac{\partial}{r\partial r}(r\rho \bar{v}\varepsilon)=\frac{\partial}{\partial x}((\frac{\mu_T}{\sigma_\varepsilon}+\mu)\frac{\partial \varepsilon}{\partial x})+\frac{\partial}{r\partial r}(r(\frac{\mu_T}{\sigma_\varepsilon}+\mu)\frac{\partial \varepsilon}{\partial r})$$

$$+\frac{\varepsilon}{k}(c_1 G-c_2\rho\varepsilon) \qquad (2.31)$$

Where,

σ_ε: Turbulent *Prandtl* number for ε, assumed to be constant

$C_1$and C_2: Empirical constants

In the standard two-equation k-ε model, the turbulent dynamic viscosity is related to k and ε as [66]

$$\mu_T = C_\mu \rho k^2/\varepsilon \qquad (2.32)$$

The presently accepted empirical constants for the k-ε model are listed in Table2-1 [66]:

Table 2-1 Empirical Constants Used in k-ε Model

C_1	C_2	σ_k	σ_ε	C_μ
1.44	1.92	0.90	1.30	0.09

2.3 Simplification of Species Conservation Equation

In a multi-component system, whether reacting or not, we can construct as many equations of the form of equation (2.5) as there are species. S_i is the mass rate of creation or consumption of species i by chemical reaction. For a chemical-inert species, S_i is zero, and equation (2.5) takes a particular simple form.

For example, combustion of methane with air as the oxidizer involves fuel (CH_4), oxygen (O_2), products (CO_2, H_2O) and inert gas (N_2). If we have to solve all these equations, the task may not be a small one in the reacting situation. In order to reduce the magnitude of this task in a reacting system, simplification can be introduced to render the number of species equations to be solved as small as practically possible. In our current study, *Spalding*'s Simple-Chemical-Reacting-System (*SCRS*) is assumed:

(1) The reaction is one-step and irreversible.

(2) Laminar mass diffusion coefficients, D_i, or exchange coefficients, Γ_i, are independent of the species i, i.e.,

$$D_i=D, \qquad \Gamma_i=D\cdot\rho=\Gamma_y$$

All are equal to one another at any point, but they need not be uniform.

These assumptions are commonly employed and have been verified to be reasonable [16,25,59].

In *SCRS*, the single-step reaction is between two reactants, called here for convenience *fuel* and *oxidant*, in which they combine in fixed proportions by mass to produce a unique product,

$$\begin{array}{ccc} \textit{fuel} + \textit{oxidant} & \rightarrow & \textit{product} \\ 1\text{kg} \quad s\text{ kg} & & (1+s)\text{ kg} \end{array} \qquad (2.33)$$

Where,

s: Stoichiometric coefficient based on mass

The quality, s, is a constant for a given reactant pair. It is assumed that there are no intermediate compounds produced. By virtue of the second assumption, species composition of the product is constant at all locations. Consequently, the mass fraction of the product determines the mass fraction of each product species uniquely. Thus, the unknowns are M_{fu}, M_{ox}, M_{pr} and M_{inert} (mass fraction of fuel, oxygen, product and inert gas, respectively). However, one of the unknowns can be eliminated using the condition that the sum of mass fraction is unity.

An important consequence of the reaction equation (2.33) is that the mass rates of consumption or creation by chemical reaction of fuel, oxidant and product, S_{fu}, S_{ox} and S_{pr} are related through:

$$S_{fu}=S_{ox}/s=-S_{pr}/(1+s) \qquad (2.34)$$

Equation (2.34) can be made use of to yield conservation equations that have zero source term. From Equation (2.5) we obtain two equations, one for M_{fu} (with i=fu) and the other for M_{ox} (with i=ox). Using the relationship (2.34) and the second assumption, we obtain an equation for function ψ_1, which is defined in the following expression:

$$\psi_1=M_{fu}-M_{ox}/s \qquad (2.35)$$

By dividing M_{ox}'s transport equation by s and subtracting the resulting equation from M_{fu}'s transport equation, the governing equation for ψ_1 can be written as:

$$\frac{\partial}{\partial x}(\rho u\psi_1)+\frac{\partial}{r\partial r}(r\rho v\psi_1)=\frac{\partial}{\partial x}(\Gamma_y\frac{\partial\psi_1}{\partial x})+\frac{\partial}{r\partial r}(r\Gamma_y\frac{\partial\psi_1}{\partial r}) \qquad (2.36)$$

Where, Γ_y is the common value of species transport coefficient. Similar source free equations can be obtained for other two functions ψ_2 and ψ_3, where ψ_2 and ψ_3 is defined as:

$$\psi_2 = M_{fu}+M_{pr}/(1+s) \qquad (2.37)$$

$$\psi_3 = M_{ox}/s+M_{pr}/(1+s) \qquad (2.38)$$

Although these three source free equations are available, in order to avoid duplication of information, only two of them are made use of. In our current study, ψ_1 and ψ_2 were chosen. The transport equation for ψ_2 is:

$$\frac{\partial}{\partial x}(\rho u\psi_2)+\frac{\partial}{r\partial r}(r\rho v\psi_2)=\frac{\partial}{\partial x}(\Gamma_y\frac{\partial\psi_2}{\partial x})+\frac{\partial}{r\partial r}(r\Gamma_y\frac{\partial\psi_2}{\partial r}) \qquad (2.39)$$

When the flow is turbulent, time-averaged forms of Equations (2.36) and (2.39) can be written as:

$$\frac{\partial}{\partial x}(\rho\bar{u}\bar{\psi})+\frac{\partial}{r\partial r}(r\rho\bar{v}\bar{\psi})=\frac{\partial}{\partial x}((\Gamma_y+\frac{\mu_T}{\sigma_y})\frac{\partial\bar{\psi}}{\partial x})+\frac{\partial}{r\partial r}(r(\Gamma_y+\frac{\mu_T}{\sigma_y})\frac{\partial\bar{\psi}}{\partial r}) \qquad (2.40)$$

It has been tested that solving a source-free equation is much easier to achieve convergence. However, for a premixed flame, solution of a source free equation alone, e.g. Equation (2.40), is insufficient to yield information on all the component mass fractions. We must solve in addition on conservation equations for one of the species. This could be any of the three: M_{fu}, M_{ox}, M_{pr}. In our study, the fuel mass fraction, M_{fu}, is taken as the unknown:

$$\frac{\partial}{\partial x}(\rho\bar{u}\overline{M_{fu}})+\frac{\partial}{r\partial r}(r\rho\bar{v}\overline{M_{fu}})=\frac{\partial}{\partial x}((\Gamma_y+\frac{\mu_T}{\sigma_y})\frac{\partial\overline{M_{fu}}}{\partial x})$$

$$+\frac{\partial}{r\partial r}(r(\Gamma_y+\frac{\mu_T}{\sigma_y})\frac{\partial\overline{M_{fu}}}{\partial r})+\overline{S_{fu}} \qquad (2.41)$$

Where, $\overline{S_{fu}}$ is the mass consumption rate of fuel by chemical reaction. It will be given in the section of combustion models.

Once ψ_1, ψ_2 and M_{fu} are available, the different mass fraction can be calculated from:

$$M_{ox}=s(M_{fu}-\psi_1) \qquad (2.42)$$

$$M_{pr}=(1+s)(\psi_2-M_{fu}) \qquad (2.43)$$

$$M_{inert}=1-M_{fu}-M_{ox}-M_{pr} \qquad (2.44)$$

2.4 Simplification of Energy Conservation Equation

Equation (2.6) has been obtained by neglecting the turbulence energy and kinetic energy of the mean motion to total enthalpy. According to the assumptions of *SCRS*, it can be further simplified.

It is known that, *Schmidt* number, S_c, is related to mass diffusion process, while *Prandtl* number, P_r, is related to heat diffusion. The quantity, P_r/S_c, in equation (2.6) is the inverse of *Lewis* number, $1/L_e$, which represents the ratio of heat exchange coefficient to species exchange coefficient. Usually, L_e can be safely taken as unity for most gases [16,25,59]. Based on *SCRS*, we can conclude that L_e is unity, too. Thus, P_r/S_c is taken as unity in our current study. Under this assumption, the third term on the right hand side of Equation (2.6) is zero. As a result, the time-averaged form of Equation (2.6) can be expressed as:

$$\frac{\partial}{\partial x}(\rho\bar{u}\bar{H})+\frac{\partial}{r\partial r}(r\rho\bar{v}\bar{H})=\frac{\partial}{\partial x}\left(\left(\Gamma_h+\frac{\mu_T}{\sigma_H}\right)\frac{\partial\bar{H}}{\partial x}\right)$$

$$+\frac{\partial}{r\partial r}\left(r\left(\Gamma_h+\frac{\mu_T}{\sigma_H}\right)\frac{\partial\bar{H}}{\partial r}\right)+\overline{S_H} \qquad (2.45)$$

The source term, $\overline{S_H}$, is the time-averaged form of S_H in Equation (2.6). Note that combustion does not affect S_H, since the total enthalpy is the sum of sensible heat and the enthalpy of formation. The direct thermal effect of chemical reaction is to increase the former one by decreasing the latter, but the sum of them remains unchanged [52]. Under ordinary combustion conditions, S_H results from the net absorption of radiation by the gas. In our current study, radiation heat transfer is not considered temporarily. Thus, S_H is taken to be zero, and equation (2.45) becomes a source-free one.

2.5 Combustion Model

So far, the only problem left unresolved is to treat the fuel-burning rate per unit volume ($\overline{S_{fu}}$ in Equation (2.41)), which plays a central role in the premixed combustion. When the combustion process is not physically controlled (as in the case of laminar premixed combustion), the chemical kinetics will exert influence on the chemical reaction. When turbulence is absent, the rate of fuel consumption per unit volume for one-step, irreversible reaction can be expressed in *Arrhenius* form as:

$$S_{fu,A} = -A\rho^2 M_{fu} M_{ox} EXP(-\frac{E}{RT}) \qquad (2.46)$$

Where,

A: Pre-exponential factor

E: Activation energy

R: The universal gas constant

The values of A and E depend on the reactant-pair under consideration.

Equation (2.46), however, can't be directly used for turbulent flames. For turbulent flows, we should also take separate account of the effect of turbulence on the reaction rates. It has been pointed out by *Spalding* [55] that, in many turbulent premixed flames the reaction rate often comes under the control of hydrodynamic effects, although it is still influenced by chemical kinetics. In *Ref.* [53], *Spalding* proposed that the gases in a confined turbulent premixed flame should be regarded as a mixture of alternating fragments of unburned gas with almost-fully-burned gas, the chemical reaction was supposed to occur on the interfaces between these two kinds of fragments. Hence, the chemical reaction rate was supposed to depend upon the rate at which fragments of unburned gas were broken into still smaller fragments by the action of turbulence, and this rate was assumed to be proportional to the rate of decay of turbulence energy. This model is called the Eddy-Break-Up model (*EBU*), in which chemical reaction rate combined with the k-ε model is expressed as:

$$\overline{S_{fu,T}} = -C_R \rho g_{fu}^{0.5} \varepsilon/k \qquad (2.47)$$

Where,

C_R: *EBU* constant, taken to be 0.35-0.4

g_{fu}: Local mean square concentration fluctuations of fuel

Although this model is based on intuitive arguments rather than on a rigorous derivation, it marks an important step in the development of models for turbulent premixed combustion [40].

The success of *EBU* model lied in that, it realized that turbulence mixing is the rate-determining process in turbulent premixed combustion. However, this model under-estimate the role of chemical kinetics in premixed combustion. In order to make up of this shortcoming, *Spalding* put forward the "Squashing and Stretching" concept in 1976 [55], which was integrated into the Stretch-Cut-

and-Slide model, known as *SCS* [56]. The main concepts of this model are depicted as follows.

The gases in a turbulent premixed flame are regarded as a mixture of alternating fragments of unburned gas with almost-fully-burned gas. Under the influence of turbulence, the lumps of unburned gas are broken down into smaller ones continuously. The block comprising layers of burned and unburned gas is firstly squashed until its thickness is halved and length doubled, as is shown in Fig. 2-2. Then it is cut, and its two parts put together to form again the original shape, but with four layers rather than two. These processes are continually repeated.

Through these processes, the turbulence length scales of mass concentration in a turbulent premixed flame are reduced, while the interface area between burned gas and unburned gas is increased, and so does the homogeneity of temperature of the gas entity. Hence, the reaction rate should be influenced by the broken down rate of the unburned gas lumps. In addition, chemical reaction is assumed to occur at the interface of burned gas and unburned gas. The flame propagates from the hot layer into the cold via heat conduction, molecular diffusion and chemical reaction. It is supposed that the flame front propagates at the corresponding laminar flame speed, S_L, relative to the unburned gas.

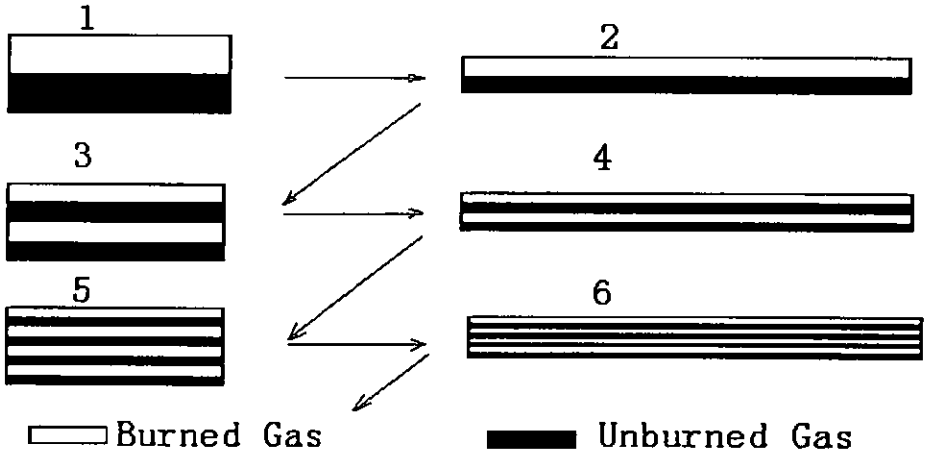

Fig. 2.1 Illustration of Stretch-Cut-and-Slide Model

In our current study, *SCS* model is employed to determine the fuel-burning rate per unit volume. The following section will provide some detailed information about the derivation process for the fuel-burning rate per unit volume.

2.5.1 Derivation Process of *SCS* Model

As is shown in Fig.2.1, the thickness of such a two-part layer, when first formed, is given the symbol, l_o. It is supposed that the gas layers formed in this way travel together through the flame, but the layer thickness, l, diminishes with time in accordance with the following equation [55,58]:

$$\frac{dl}{dt} = -lR_{st} \tag{2.48}$$

Where,

R_{st}: Local stretching rate, taken as a constant with time

In a two-dimensional flow, R_{st} may be approximately represented by:

$$R_{st} = \left|\frac{\partial u}{\partial y} + \frac{\partial v}{\partial x}\right| \tag{2.49}$$

According to assumptions of *SCS* model, the fuel consumption rate can be given by [58]:

$$\frac{dM_{fu}}{dt} = -\frac{1}{l}S_L(M_{fu,u} - M_{fu,b}) \tag{2.50}$$

Where,

M_{fu}: Averaged fuel mass fraction in the gas

$M_{fu,u}$: Fuel mass fraction of the unburned gas

$M_{fu,b}$: Fuel mass fraction of burned gas

S_L: Local laminar flame speed

l: Thickness of the gas layer

If the laminar flame front is thin compared with the gas layer in question, S_L can be regarded as independent of time until all the unburned fuel is consumed. The combination of equation (2.48), (2.49) and (2.50) leads to:

$$dM_{fu} = \frac{(M_{fu,u} - M_{fu,b})S_L}{\left|\frac{\partial u}{\partial y} + \frac{\partial v}{\partial x}\right|}\frac{1}{l^2}dl \tag{2.51}$$

Integration of the left-hand side of equation (2.51) yields:

$$\int_{M_{fu,u}}^{M_{fu,b}} dM_{fu} = M_{fu,b} - M_{fu,u} \tag{2.52}$$

While integration of the right hand side of equation (2.51) yields:

$$\frac{(M_{fu,u}-M_{fu,b})S_L}{\left|\frac{\partial u}{\partial y}+\frac{\partial v}{\partial x}\right|}\int_{l_o}^{l_1}\frac{1}{l^2}\,dl=-\frac{(M_{fu,u}-M_{fu,b})S_L}{l_o\left|\frac{\partial u}{\partial y}+\frac{\partial v}{\partial x}\right|}\left(\frac{l_o}{l_1}-1\right) \tag{2.53}$$

Where,

l_1: Prevailing value of l when the gas is fully burned

l_O: Prevailing value of l when the gas is fully unburned

According to the last three equations, we obtain the following expression for l_o/l_1 as:

$$\frac{l_o}{l_1}=1+\frac{l_o\left|\frac{\partial u}{\partial y}+\frac{\partial v}{\partial x}\right|}{S_L} \tag{2.54}$$

On the other hand, l is related to time, i.e., equation (2.48), which can be integrated to yield [55]:

$$\frac{l_o}{l_1}=\exp\left(t_1\left|\frac{\partial u}{\partial y}+\frac{\partial v}{\partial x}\right|\right) \tag{2.55}$$

Where,

t_1: Time needed for the gas to be fully burned.

According to equations (2.54) and (2.55), we get the expression for t_1 as:

$$t_1=\frac{\ln\left(1+\frac{l_o\left|\frac{\partial u}{\partial y}+\frac{\partial v}{\partial x}\right|}{S}\right)}{\left|\frac{\partial u}{\partial y}+\frac{\partial v}{\partial x}\right|} \tag{2.56}$$

Now, the fuel-burning rate per unit volume can be given by dividing total consumed mass of fuel, $\rho(M_{fu,u}-M_{fu,b})$, by the time t_1:

$$S_{fu,T}=-\frac{\rho(M_{fu,u}-M_{fu,b})\left|\frac{\partial \bar{u}}{\partial y}+\frac{\partial \bar{v}}{\partial x}\right|}{\ln\left(1+l_o\left|\frac{\partial \bar{u}}{\partial y}+\frac{\partial \bar{v}}{\partial x}\right|/S_L\right)} \tag{2.57}$$

Owing to turbulence fluctuation, a local point of the flame is not always occupied by the unburned gas or burned gas, but in an alternative manner between the two states. When it is at the state of fully burned gas, there will no reaction at all. Only when unburned gas prevails at this point can there occur chemical reaction at the fuel-burning rate of $S_{fu,T}$. Presently, we define α as the time fraction for the instantaneous fuel concentration at a point to exist at an upper state $M_{fu,u}$. For a premixed system, α can be given by:

$$\alpha = \frac{\overline{M_{fu}} - M_{fu,b}}{M_{fu,u} - M_{fu,b}} \tag{2.58}$$

Hence, the time-averaged fuel-burning rate, $\overline{S_{fu,T}}$ can be given as:

$$\overline{S_{fu,T}} = \alpha S_{fu,T} = -\frac{\rho(\overline{M_{fu}} - M_{fu,b})\left|\frac{\partial \bar{u}}{\partial y} + \frac{\partial \bar{v}}{\partial x}\right|}{\ln(1 + l_o\left|\frac{\partial \bar{u}}{\partial y} + \frac{\partial \bar{v}}{\partial x}\right|/S_L)} \tag{2.59}$$

2.5.2 Simplification of *SCS* Model

Equation (2.59) provides the time-averaged fuel-burning rates per unit volume. However, it is difficult to combine this complicated formula with turbulent models, and to understand its physical meanings. Hence, it is necessary to make some simplification of Equation (2.59). From Equation (2.54), one can get:

$$l_o = \frac{l_1}{1 - l_1\left|\frac{\partial u}{\partial y} + \frac{\partial v}{\partial x}\right|/S_L} \tag{2.60}$$

Substituting Equation (2.60) into Equation (2.59) would yield:

$$\overline{S_{fu,T}} = \frac{\rho(\overline{M_{fu}} - M_{fu,b})\left|\frac{\partial \bar{u}}{\partial y} + \frac{\partial \bar{v}}{\partial x}\right|}{\ln(1 - l_1\left|\frac{\partial \bar{u}}{\partial y} + \frac{\partial \bar{v}}{\partial x}\right|/S_L)} \tag{2.61}$$

In the case where $l_1\left|\frac{\partial u}{\partial y} + \frac{\partial v}{\partial x}\right|/S_L << 1$, *Taylor*-series expansion method can be used to eliminate logarithm operation on the right hand side of equation (2.61):

$$\ln(1 - l_1\left|\frac{\partial u}{\partial y} + \frac{\partial v}{\partial x}\right|/S_L) \approx -l_1\left|\frac{\partial u}{\partial y} + \frac{\partial v}{\partial x}\right|/S_L - 0.5\left(l_1\left|\frac{\partial u}{\partial y} + \frac{\partial v}{\partial x}\right|/S_L\right)^2$$

Thus, the turbulent controlled fuel-burning rate per unit volume, $\overline{S_{fu,T}}$, can be expressed as:

$$\overline{S_{fu,T}} = -\frac{\rho(\overline{M_{fu}} - M_{fu,b})}{\frac{l_1}{S_L}\left(1 + 0.5\frac{l_1}{S_L}\left|\frac{\partial u}{\partial y} + \frac{\partial v}{\partial x}\right|\right)} \tag{2.62}$$

Here, Taylor-series expansion method is used again on the right hand side of Equation (2.62):

$$\frac{1}{1+0.5\frac{l_1}{S_L}\left|\frac{\partial u}{\partial y}+\frac{\partial v}{\partial x}\right|} \approx 1-0.5\frac{l_1}{S_L}\left|\frac{\partial u}{\partial y}+\frac{\partial v}{\partial x}\right|$$

Hence, $\overline{S_{fu,T}}$ can be rewritten as:

$$\overline{S_{fu,T}} = -\rho\left(\overline{M_{fu}} - M_{fu,b}\right)\left(\frac{S_L}{l_1} - 0.5\left|\frac{\partial u}{\partial y}+\frac{\partial v}{\partial x}\right|\right) \qquad (2.63)$$

Combining Equation (2.54), the expression for $\overline{S_{fu,T}}$ can be defined by:

$$\overline{S_{fu,T}} = -\rho\left(\overline{M_{fu}} - M_{fu,b}\right)\left(0.5\left|\frac{\partial u}{\partial y}+\frac{\partial v}{\partial x}\right| + \frac{S_L}{l_o}\right) \qquad (2.64)$$

This equation is somewhat like that of the modified *EBU* model of *Spalding* [36]. Compared with equation (2.59), equation (2.64) is simple and easy to understand.

As is known, laminar flame speed, S_L, is one of the fuel/air mixture's physical and chemical properties, embodying the influence of molecular diffusion and chemical dynamics on combustion. The quantity, $\left|\frac{\partial u}{\partial y}+\frac{\partial v}{\partial x}\right|$, is the local stretching rate of the fluid, influenced by the hydrodynamic state of the flow, namely, by the turbulence in the flow. Hence, equation (2.64) explains how turbulence mixing process can dominate the reaction when $l_o\left|\frac{\partial u}{\partial y}+\frac{\partial v}{\partial x}\right|/S_L$ is fairly large, while molecular diffusion and chemical dynamics dominate at low values of $l_o\left|\frac{\partial u}{\partial y}+\frac{\partial v}{\partial x}\right|/S_L$. When $l_o\left|\frac{\partial u}{\partial y}+\frac{\partial v}{\partial x}\right|/S_L$ tends to zero, the laminar burning velocity S_L will have a significant influence on the reaction rate.

In a premixed flame system, $M_{fu,b}$ stands for the mass fraction of fuel that will prevail when, in the local mixture, the fuel is allowed to burn as much as possible. The magnitude of $M_{fu,b}$ depends on local fuel to air equivalence ration. Since the variable, $(M_{fu}-M_{ox}/s)$, remains unchanged during combustion, we have

$$(\overline{M_{fu}} - \overline{M_{ox}}/s) \le 0: \quad M_{fu,b}=0$$

$$(\overline{M_{fu}} - \overline{M_{ox}}/s) \ge 0: \quad M_{fu,b}=(\overline{M_{fu}} - \overline{M_{ox}}/s)$$

Both these relations can be expressed by the following equation:

$$M_{fu,b}=\max[(\overline{M_{fu}} - \overline{M_{ox}}/s), 0] \qquad (2.65)$$

Finally, $\overline{S_{fu,T}}$ can be rewritten in the following form as:

$$\overline{S_{fu,T}} = -\rho \min\left[\overline{M_{fu}}, \frac{\overline{M_{ox}}}{s}\right]\left(0.5\left|\frac{\partial u}{\partial y}+\frac{\partial v}{\partial x}\right|+\frac{S_L}{l_o}\right) \qquad (2.66)$$

Since significant chemical reaction is unlikely to occur in low temperature regions before ignition even where turbulence energy decay or stretching may proceed. In such regions, the reaction rate is assumed to be controlled by chemical kinetics, and to obey the familiar *Arrhenius* form of equation (2.46). At this time, $S_{fu,CK}$, M_{fu}, M_{ox} and T should taken their local time-averaged values respectively.

Thus, there are two expressions for the reaction rate, $\overline{S_{fu,A}}$ and $\overline{S_{fu,T}}$. It is supposed that the overall reaction is controlled by the one proceeding at a lower rate, hence,

$$\overline{S_{fu}} = -\min\left[\left|\overline{S_{fu,A}}\right|, \left|\overline{S_{fu,T}}\right|\right] \qquad (2.67)$$

2.5.3 Closure of *SCS* Model

There are still two unknowns in equation (2.66), i.e., the initial layer thickness of the unburned gas within a turbulence eddy, l_o, and local laminar flame speed, S_L.

In our current study, l_o is taken as proportional to the local turbulence length scale of mass concentration. For *Le*=1, this length scale becomes identical to the hydraulic turbulence length scale and thus can be related by the k-ε model to give [28]:

$$l_o = C_l k^{1.5}/\varepsilon \qquad (2.68)$$

Where, C_l is the empirical constant, C_l=0.09.

The local laminar flame speed, S_L, can't be taken as a constant in the calculation of $\overline{S_{fu,T}}$. For a given pair of reactants, it depends strongly on local thermodynamic parameters, especially on the temperature. As a result of the internal laminar burning process and the external heat exchange, temperature difference between unburned mixture and burned gas is very large. Hence, the temperature of the unburned mixture within a turbulence eddy, T_l, determines the local laminar flame speed. Presently, methane-air premixed flame is studied. According to *Refs.* [13,26], the laminar flame speed of methane can be given by the following expression:

$$S_L = 1.6\times10^{-6}T_l^{2.11}+0.08 \text{ m/s} \qquad (2.69)$$

Thus, in order to obtain S_L, we should solve for the local temperature of unburned mixture. Owing to temperature fluctuation, T_l is usually not equal to the local time-mean temperature, $\overline{T}$. However, T_l can be predicted by using the scalar-fluctuation model described below.

Under the isotropic turbulence assumption, the transport equation for the time-mean square value of the temperature fluctuation derived in the way similar to those for k and ε, can be given as [66]:

$$\frac{\partial}{\partial x}(\rho \bar{u}\overline{T'^2}) + \frac{\partial}{r\partial r}(r\rho \bar{v}\overline{T'^2}) = \frac{\partial}{\partial x}(\Gamma_{T,eff}\frac{\partial \overline{T'^2}}{\partial x}) + \frac{\partial}{r\partial r}(r\Gamma_{T,eff}\frac{\partial \overline{T'^2}}{\partial r})$$

$$+ C_{T1}\mu_T((\frac{\partial \overline{T}}{\partial x})^2 + (\frac{\partial \overline{T}}{\partial r})^2) - C_{T2}\rho\varepsilon\overline{T'^2}/k \qquad (2.70)$$

Where,

$\overline{T'^2}$: Time-mean square of the temperature fluctuation

$\Gamma_{T,eff}$: Effective transport coefficient of $\overline{T'^2}$

$$\Gamma_{T,eff} = \frac{\mu + \mu_T}{\sigma_T} \qquad (2.71)$$

C_{T1} and C_{T2}: Empirical constants, C_{T1}=1.44, C_{T2}=1.92

In our current study, it is assumed that there is no local fluctuation of either of the fresh mixture temperature and the fully burned mixture. In other words, the fluctuation of temperature inside the fresh mixture or inside the burned gas is negligible. The temperature fluctuation comes only from the fluctuation between the fresh mixture and the burned gas. It is simply assumed that the variation of the instantaneous temperature with time is "battle" shaped. The instantaneous temperature at a point is assumed to exist at a lower state T_l for a time fraction of α, and at an upper state T_2 for the rest of the time, 1-α. Hence, the two unknown temperatures T_l for the fresh mixture and T_2 for the burned gas can now be found from the knowledge of the mean temperature $\overline{T}$, mean square temperature fluctuation $\overline{T'^2}$ and time fraction α:

$$\overline{T} = \alpha T_l + (1-\alpha)T_2 \qquad (2.72)$$

$$\overline{T'^2} = \alpha(\overline{T} - T_l)^2 + (1-\alpha)(T_2 - \overline{T})^2 \qquad (2.73)$$

In this study, we do not consider any other possibilities of α, and simply assume that α is equal to 0.5. Hence,

$$T_1=\overline{T}-\sqrt{\overline{T'^2}} \tag{2.74}$$

$$T_2=\overline{T}+\sqrt{\overline{T'^2}} \tag{2.75}$$

On the other hand, T_1 should be greater than the initial temperature of the fuel and air mixture as they enter the domain of interest. Finally, the temperature of the fresh mixture can be expressed as:

$$T_1=\max[\overline{T}-\sqrt{\overline{T'^2}}\,,\ T_0] \tag{2.76}$$

Where, T_0 is the inlet temperature of the fuel air mixture.

2.6 Auxiliary Information

In order to close the above mathematical formulation, we should provide additional information on the boundary conditions, and the fluid thermodynamic properties, like μ, ρ and C_p. Because of the elliptic nature of the differential equations, boundary conditions must be supplied for each of the main dependent variables along a boundary completely enclosing the domain of interest. The definition of the boundary conditions will be discussed in Chapter 4. This section deals with the fluid thermodynamic properties only.

There are five species in the combustion space, i.e., fuel, oxygen, nitrogen, water vapor and carbon dioxide. In the open environment, pressure in the flow field can be taken to be constant. Thus, the density of the gas mixture is considered as a function of both mean temperature and species composition:

$$\rho=273.15\,\overline{W}/(22.4\,\overline{T}) \qquad kg/m^3 \tag{2.77}$$

Where,

$\overline{W}$: Averaged molecular weight of the fluid mixture

$\overline{W}$ can be calculated according to the following expression:

$$\frac{1}{\overline{W}}=\sum\frac{M_i}{W_i} \tag{2.78}$$

Where,

i: Refers to above five species

M_i: Mass fraction of the species i

W_i: Molecular weight of the species i

In the turbulent flow, the molecular viscosity of the gas mixture, μ, is very small compared with the turbulent viscosity, μ_T. Thus, μ can be taken as equal to that of air without introducing serious errors. In our current study, μ is obtained from the following expression [35]:

$$\mu = 1.709\times10^{-5}\times\frac{384}{T+111}\left(\frac{T}{273}\right)^{1.5} \text{ kg/m·s} \qquad (2.79)$$

The specific heat capacity at constant pressure is also a function of the gas mixture temperature and composition, defined by:

$$C_p=\Sigma M_i C_{pi} \qquad (2.80)$$

The specific heat capacity per unit mass of each species, C_{pi}, is given by:

$$C_{pi}=a_i+b_i T \ (C_{pi} \text{ in J/kg·K, T in K}) \qquad (2.81)$$

Table 2-2 lists constants a_i and b_i for each species (Data taken from *Ref.* [19]).

Table 2-2 Coefficients in the approximations for c_p

Quantity	a_i	b_i
C_p of CH_4	1775.0375	2.3821
C_p of O_2	898.8969	0.1582
C_p of N_2	990.6107	0.1615
C_p of CO_2	870.4045	0.294
C_p of H_2O	1884.4188	0.6858

A characteristic of our study is that there are many empirical constants in the turbulence model and combustion model. Values of the five constants given in Table 2.1 are widely accepted in the standard k-ε model [35,66] and we have employed these values in our study. In our numerical study, it is found that numerical results are not vey sensitive to different values of the turbulent *prandtl* and *Schmidt* number. Hence, values of these parameters, σ_y, σ_H, σ_T are chosen as 0.9 based on *Chuang et al.*[11] and *Zhou*[66].

There are also two empirical constants, C_{T1} and C_{T2}, in the transport equation for mean square temperature fluctuation. At the initial stage of our study, values of 2.0 and 1.0 respectively [67] were used. Numerical results reveal excessive large mean square temperature fluctuations with an

unreasonable distribution of T_1. There is little information about these two constants in the literature. Comparing eq.(2.70) with eq.(2.29), we can see that both of these equations are for the second-order correlation terms. Therefore, the values for C_1 and C_2 in eq.(2.29) are given to C_{T1} and C_{T2} respectively. Numerical results show that reasonable predictions are obtained for mean square temperature fluctuations and temperature of the unburned mixture.

3. Derivation of Finite Difference Equation

From the preceding sections, we see that the differential equations we are concerned with here are all non-linear and coupled together. In most practical situations, there is no possibility for obtaining analytical solutions to them, and numerical methods of one kind or other have to be used. Many methods have been put forward in the past decades. They vary enormously in complexity, ease of use, efficiency and width of applicability. Here, we shall employ a finite difference technique based on the well-tried *SIMPLE* (Semi-Implicit Method for Pressure Linked Equations) algorithm of *Patankar* and *Spalding* [36]. Details of *SIMPLE* algorithm can be found in *Ref.* [38]. The major aspects of this approach that are pertinent to the present work will be discussed in this chapter.

3.1 Control Volume for Two-Dimensional Situation

In order to solve those transport equations depicted in Chapter 2, the first step is to discretize those partial differential equations into finite difference form. In the present work, the control volume technique has been chosen to devise the finite difference equations. In this manner, the continuum calculation domain will be discretized into a number of macro volumes.

A typical control volume for the generalized variable φ in the cylindrical coordinates is shown in Fig. 3.1. For the grid point P, points E and W are its axial-direction neighbors, while N and S are the radial-direction neighbors. The dashed lines define the control volume and P is placed at its center in the current study. This control volume is the region traversed by a rectangle of sides Δx, Δr when it is rotated about an axis through an angle of unit radian.

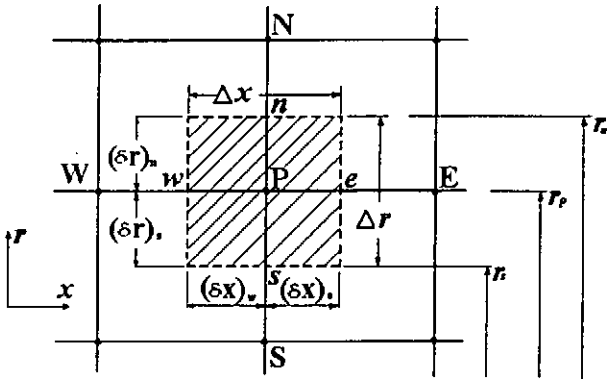

Fig. 3.1 Control Volume for variable φ except u and v

For the above control volume, the area of the face normal to the axial-direction will be $0.5(r_n+r_s)\Delta r$, where r_n and r_s are the outer and inner radii of the control volume. The areas of inner and outer face normal to the radial direction are $r_n\Delta x$ and $r_s\Delta x$ respectively. This control volume occupies a volume of $\Delta V=0.5(r_n+r_s)\,\Delta x\Delta r$.

3.2 The Staggered Grid Arrangement

In our current study, the staggered grid for the velocity components u and v is employed. That is to say, the control volumes for u and v are different from those for other dependent variables, as is shown in Fig. 3.2. Such grid arrangement was first used in the *MAC* (Marker And Cell) method [23]. It forms the basis of *SIMPLE* algorithm. By using staggered grid, the wavy phenomena in velocity and pressure field, which are known to be causes of computation instability, can be avoided.

In the staggered grid, the velocity components u and v are calculated for the points that lie on the faces of the control volumes. Thus, the axial-direction velocity, u, is calculated at the faces that are normal to the axial-direction. The locations for u are shown in Fig. 3.2 by short arrows, while the main grid points are shown by dots. It is noticed that, with respect to the main grid points, the u locations are staggered only in the axial-direction. Whether the u location is exactly midway between two adjacent main grid points depends upon how the main control volumes are defined. However, the u location must lie on the main control volume face, irrespective of whether the latter one happens to be midway between the main grid points. Similarly the v locations are staggered only in the radial-direction and lie on the main control volume faces that are normal to the radial-direction, as shown in Fig. 3.2.

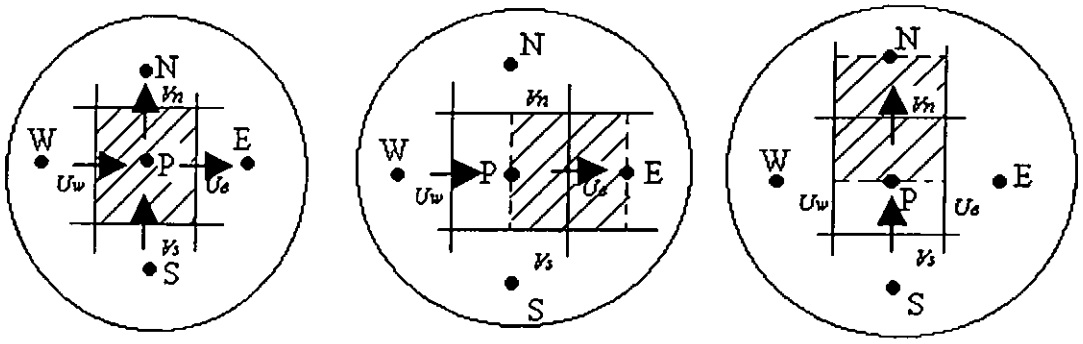

(a) main control volume (b) control volume for *Ue* (c) control volume for *Vn*

Fig. 3.2 Staggered Grid Arrangement

3.3 Finite Difference Equation

Integration over the control volume is employed to construct the finite difference equations in the present study. First, the generalized transport equation (2.28) for φ except velocity components u and v can be rewritten in the following form as:

$$\frac{\partial J_x}{\partial x} + \frac{1}{r}\frac{\partial (rJ_r)}{\partial r} = \overline{S_\varphi} \tag{3.1}$$

Where,

J_x: Total (convection plus diffusion) flux through corresponding control-volume face in the axial direction

J_r: Total (convection plus diffusion) flux through corresponding control-volume face in the radial direction

J_x and J_r are defined as:

$$J_x = \rho \bar{u}\bar{\varphi} - \overline{\Gamma_{\varphi,eff}}\frac{\partial \bar{\varphi}}{\partial x} \tag{3.2}$$

$$J_r = \rho \bar{v}\bar{\varphi} - \overline{\Gamma_{\varphi,eff}}\frac{\partial \bar{\varphi}}{\partial r} \tag{3.3}$$

The integration of equation (3.1) over the control volume shown in Fig. 3.1 would give

$$\iiint \left(\frac{\partial J_x}{\partial x} + \frac{1}{r}\frac{\partial (rJ_r)}{\partial r}\right) r\,dx\,dr = \iiint \overline{S_\varphi} r\,dx\,dr \tag{3.4}$$

During this integration, the Power Law differencing scheme [38] is used to evaluate J_x or J_r through the corresponding control volume face. The source terms, $\overline{S_\varphi}$, are linearized as suggested by *Patankar* [38]:

$$\bar{S}_\varphi = S_c + S_P \bar{\varphi}_P \tag{3.5}$$

Where,

S_c: The constant part of $\overline{S_\varphi}$

S_P: The coefficient of φ

It is obvious that S_P does not stand for $\overline{S_\varphi}$ evaluated at grid point P. As a rule of discretization, S_P must always be less than or equal to zero [38]. Details of the integration process of equation (3.4) can be found in *Ref.* [38] and will not be repeated here.

Finally, the discretized equation for equation (3.1) can be written as:

$$A_P\Phi_P=A_E\Phi_E+A_W\Phi_W+A_N\Phi_N+A_S\Phi_S+b \tag{3.6}$$

Where, Φ_P is the value of quantity φ at grid point P, Φ_W, Φ_E, Φ_S, Φ_N are values at neighboring grid points, A_P, A_E, A_W, A_N and A_S are their corresponding coefficients.

$$A_E=D_eA(|P_e|)+[[-F_e, 0]] \tag{3.7a}$$

$$A_W=D_wA(|P_w|)+[[F_w, 0]] \tag{3.7b}$$

$$A_N=D_nA(|P_n|)+[[-F_n, 0]] \tag{3.7c}$$

$$A_S=D_sA(|P_s|)+[[F_s, 0]] \tag{3.7d}$$

$$b=S_c\Delta V \tag{3.7e}$$

$$A_P=A_E+A_W+A_N+A_S-S_P\Delta V \tag{3.7f}$$

and

$$D_e=\Gamma_e r_P\Delta r/(\delta x)_e, \quad D_w=\Gamma_w r_P\Delta r/(\delta x)_w,$$

$$D_n=\Gamma_n r_n\Delta x/(\delta r)_n, \quad D_s=\Gamma_s r_s\Delta x/(\delta r)_s \tag{3.8}$$

$$F_e=(\rho u)_e r_P\Delta r, \quad F_w=(\rho u)_w r_P\Delta r,$$

$$F_n=(\rho u)_n r_n\Delta r, \quad F_s=(\rho u)_s r_s\Delta r \tag{3.9}$$

P_i (i=e, w, n, s) is the *Peclet* number for surface i, defined as

$$P_e=F_e/D_e,\ P_w=F_w/D_w,\ P_n=F_n/D_n,\ P_s=F_s/D_s \tag{3.10}$$

As the definitions indicate, F_i (i=e, w, n, s) is the convective flux at the control volume face of the quantity φ, D_i is the corresponding diffusive flux, while P_i is the ratio of the two fluxes. Hence, A_P, A_E, A_W, A_N and A_S take account of the convection and diffusion transport of the quantity φ comprehensively. $A(|P_i|)$ is a function of P_i. When using Power Law differencing scheme, $A(|P_i|)$ can be expressed as [38]:

$$A(|P|)=\max[0, (1-0.1|P|^5)] \tag{3.11}$$

It can be known according to above definitions, all these coefficients, A_P, A_E, A_W, A_N and A_S, are not less than zero. This is also a rule of discretization.

The finite difference equation (3.6) can be rewritten in the following more generalized form as:

$$A_P\Phi_P=\Sigma A_{nb}\Phi_{nb}+b \tag{3.12}$$

Where, subscript *nb* denotes a neighbor point and the summation is to be taken over all the neighbors.

In a similar method, we can derive the finite difference equations for velocity components u and v when integrating their corresponding transport equations over the staggered grid. Since the pressure field is unknown and need to be solved, the pressure gradient is not included in the source term quantities S_c and S_P. That is to say, the pressure gradients are separated from the term 'b'. Thus, the finite difference equations for u and v can be written as:

$$a_e u_e = \Sigma a_{nb} u_{nb} + b + (P_P - P_E) A_e \tag{3.13}$$

$$a_n v_n = \Sigma a_{nb} v_{nb} + b + (P_P - P_N) A_n \tag{3.14}$$

Where, $(P_P-P_E)A_e$ and $(P_P-P_N)A_n$ are the appropriate pressure forces. A_e and A_n are the corresponding face areas on which the pressure difference acts.

3.4 Pressure Correction Equation

In *SIMPLE* algorithm, the calculations start from an initially guessed pressure field. The resulting velocity field will not satisfy the continuity equation. Such an imperfect velocity field based on the guessed pressure field p^* will be denoted by u^* and v^*. Some methods should be taken to improve the guessed pressure p^*, such that the resulting starred velocity field will progressively get closer to satisfying the continuity equation.

One method to improve the guessed pressure p^* is to solve the pressure correction equation. Let us propose that the correct pressure p is obtained from

$$p = p^* + p' \tag{3.15}$$

Where, p' is called the pressure correction. It is sure that this change in pressure will lead to some change in the velocity field. The corresponding velocity corrections u' and v' can be introduced in a similar manner:

$$u = u^* + u', \qquad v = v^* + v' \tag{3.16}$$

The relationships between p' and u', v' can be obtained from equations (3.13-3.14):

$$u'_e = d_e(p'_P - p'_E),\ u'_w = d_w(p'_W - p'_P),$$

$$v'_n = d_n(p'_P - p'_N),\ v'_s = d_s(p'_S - p'_P) \tag{3.17}$$

Where,

$$d_e = A_e/a_e,\ d_w = A_w/a_w,\ d_n = A_n/a_n \quad ,\ d_s = A_s/a_s \tag{3.18}$$

Substituting for equation (3.17) into equation (3.16), one get

$$u_e=u^*_e+d_e(p'_P-p'_E) \tag{3.19}$$

$$u_w=u^*_w+d_w(p'_W-p'_P) \tag{3.20}$$

$$v_n=v^*_n+d_n(p'_P-p'_n) \tag{3.21}$$

$$v_s=v^*_s+d_s(p'_S-p'_P) \tag{3.22}$$

In order to get the discretized equation for the pressure correction, one can integrate the continuity equation over the main control volume and substitutes for equations (3.19-3.22) into it. This will yield a *Poisson*-type equation for the pressure correction:

$$A_P p'_P=A_E\, p'_E+A_W\, p'_W+A_N\, p'_N+A_S\, p'_S+b \tag{3.23}$$

where,

$$A_E=\rho_e d_e r_P \Delta r \tag{3.24a}$$

$$A_W=\rho_w d_w r_P \Delta r \tag{3.24b}$$

$$A_N=\rho_n d_n r_n \Delta x \tag{3.24c}$$

$$A_S=\rho_s d_s r_s \Delta x \tag{3.24d}$$

$$A_P=A_E+A_W+A_N+A_S \tag{3.24e}$$

$$b=[(\rho u^*)_w-(\rho u^*)_e]r_P\Delta r+[(r\rho v^*)_s-(r\rho v^*)_n]\Delta x \tag{3.24f}$$

Since the pressure correction equation is derived from the continuity equation, the latter one is not directly solved for during the computation.

By now, we have formulated all the finite difference equations for the dependent variable φ. These finite difference equations can be solved using the line-by-line method and *TDMA* (Tri-Diagonal Matrix Algorithm) [38].

4. Application of Fluid Dynamic and Combustion Models

The calculations presented here model the geometry, composition and flow rates used in the premixed flame experiments discussed in *Ref.* [5]. As is shown in the Fig.1.2, a fuel/air mixture flows vertically upward from a 50mm inner diameter nozzle. The velocity of the co-flow air matches that of the core mixture. In the experiment [5], swirl is generated via injecting air tangentially through two air inlets. Although such method may cause some asymmetry of the flow field, this phenomenon won't be serious when the tangential jets are introduced into the burner well upstream of the burner exit. In our current simulation, a symmetrical flow field is assumed. Swirl is introduced into the burner by the radial inflow with tangential momentum at an axial distance of 25mm downstream of the burner inlet plane, adjacent to the inner wall boundary (See Fig. 4.1). It is assumed that the tangential mass flow rate distributes uniformly along the burner circumference. Thus, the two tangential air pipes will not appear in the computational domain and the flow can be treated under the two-dimensional cylindrical coordinates system.

4.1 Computational Domain

Because of symmetry of the flow field, it is sufficient to consider only one-half of the field, as shown in Fig. 4.1. It is 1.0m long in the axial direction and 0.65m wide in the radial direction. The right boundary is the jet centerline of the axisymmetric flow. The lower boundary is the inlet plane of the coflow stream and the free-stream boundary I, or axial entrainment boundary for the swirl jet. The inlet and the axial entrainment boundaries are separated with a wall region with certain length and width. The axial entrainment boundary is taken far upstream from the burner exit to reinforce the assumption that the u-velocity gradient in the axial direction is identically zero at this free boundary. The left vertical boundary is the free-stream boundary II or radial entrainment boundary. The upper boundary is defined as the outlet of the computational domain.

There are two free-stream boundaries in our current study, i.e., the axial and radial entrainment boundary. This adds some difficulty in defining the magnitude of the computational domain. However, the current domain is not chosen randomly. It is based on the results of a series of numerical tests. At the initial stage of this study, the author of this paper did some calculations on the following computational domains: 0.8m×0.5m, 1.0m×0.5m and 1.3m×0.75m

(the former number denotes the axial length while the latter one denotes the radial width of the computational domain), as shown in Fig. 4.2.

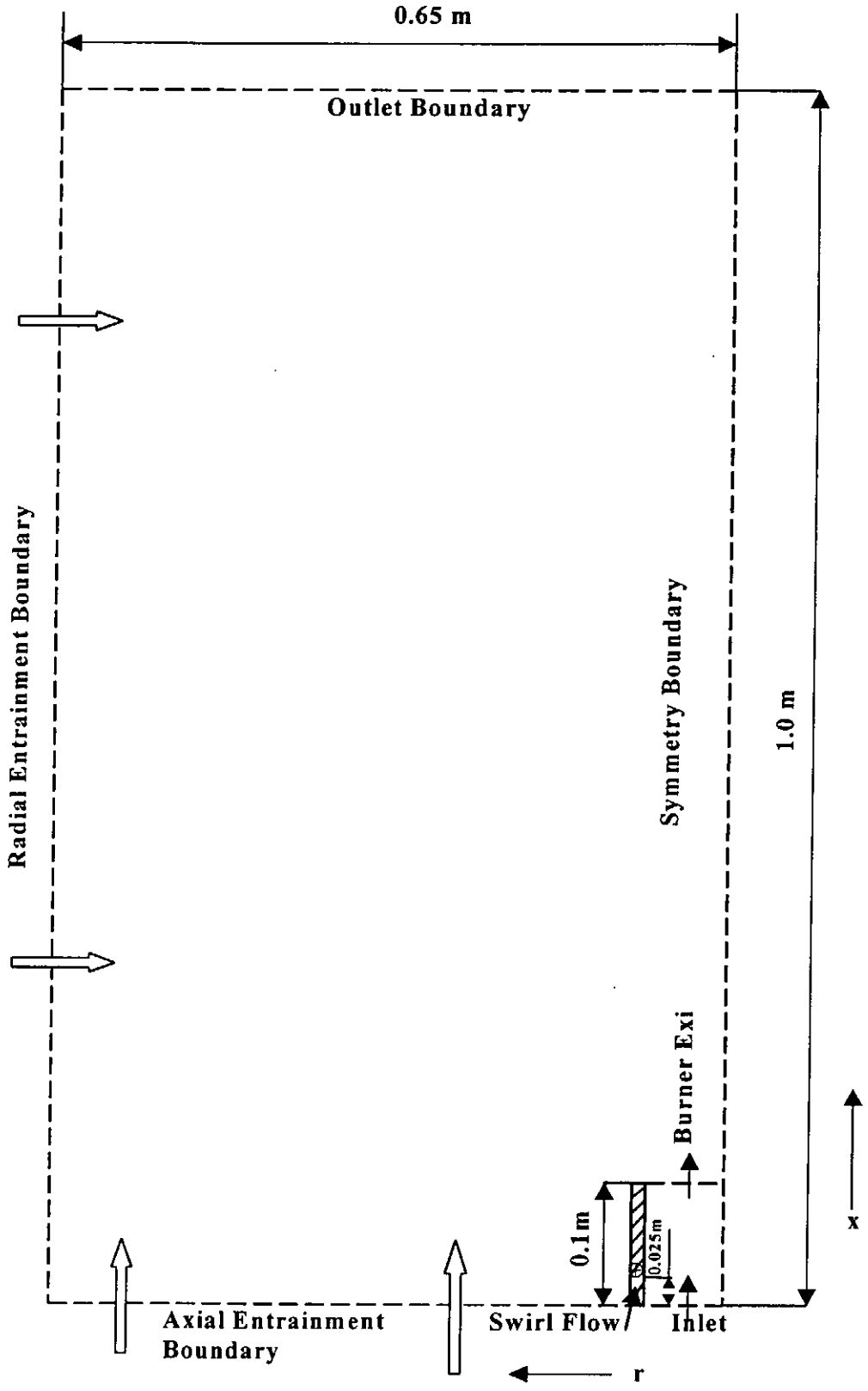

Fig.4.1 Computational Domain For Swirl Stabilized Premixed Flame

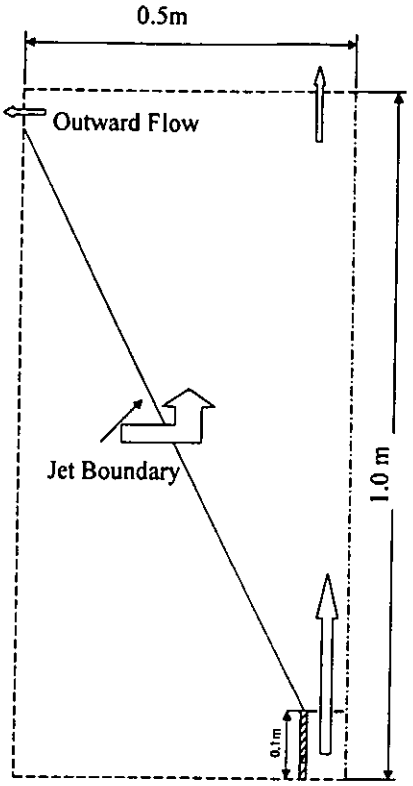

(a)Computational Domain of 1.0m×0.5m

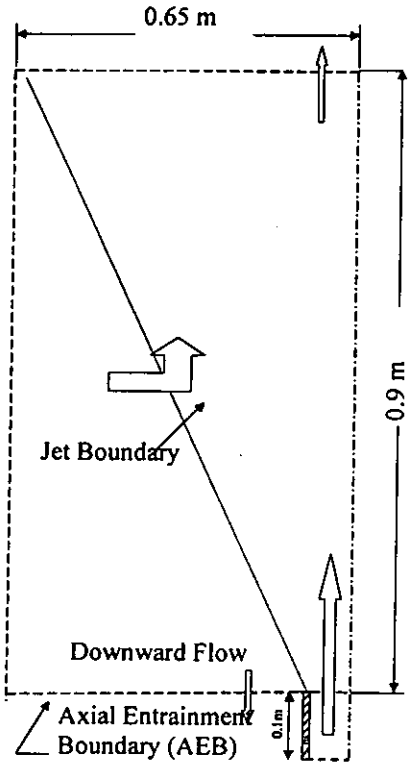

(c) Position Variation of AEB

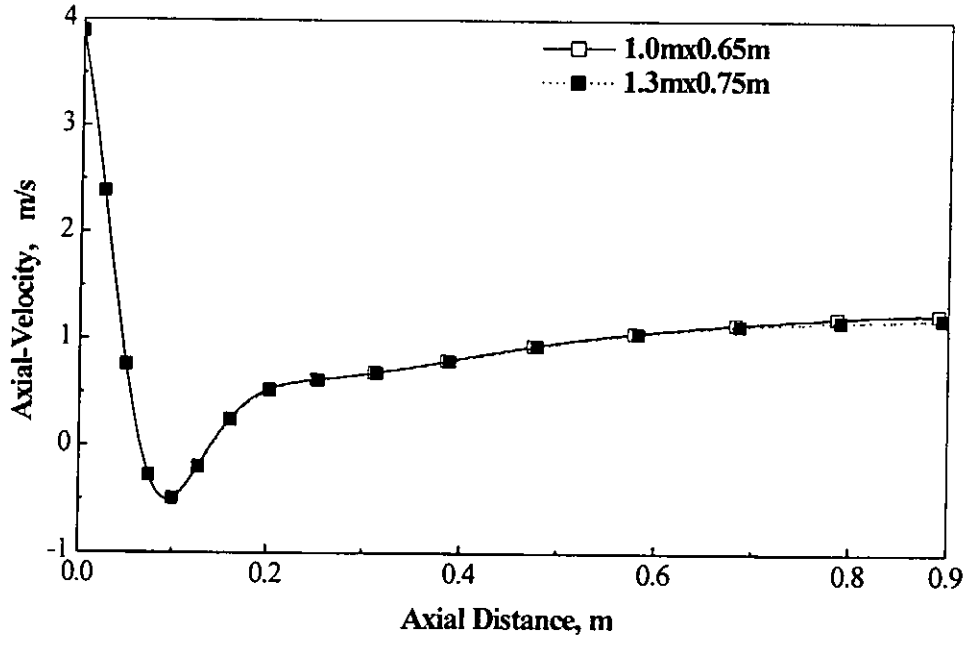

(b) Variation of Axial-Velocity with Computational Domain (Isothermal Condition)

Fig. 4.2 Influence of Computational Domain on Numerical Results

The main problem encountered when using the domain of 0.8m×0.5m is that the axial length is too short. Numerical results reveal that there exists a re-

circulation zone downstream of the swirl flow. Thus, the outlet boundary can't be defined as a fully developed boundary. A new problem appears when applying the domain of 1.0m×0.5m. As shown in Fig. 4.2 (a), there exists an outward flow on the radial entrainment boundary. This means that there are essentially two outlets for the computational domain. It is well known that this is a source of computational instability[38]. Employing the domain of 1.3m×0.75m or 1.0m×0.65m could eliminate the above two difficulties. Fig. 4.2 (c) reveals that there is little difference in the axial velocity when using these two domains. To ensure certain precision in calculation, larger amount of grid is needed for the bigger computational domain. This will lead to a heavier computational load. As a compromise between computation time and precision, we choose the domain of 1.0m×0.65m.

One may suppose that the computational load can also be reduced when locating the axial entrainment boundary on the burner exit plane. It is found that there exists a downward flow on this boundary, as shown in Fig. 4.2 (b), and the computation tends to divergence. Since the flow is swirl, flow divergence is very strong near the wall at the burner exit. This will account for possible reversal flow in the axial entrainment boundary. Such phenomenon can be avoided by extending the domain upstream of the burner exit. Numerical tests reveal that the negative u-velocity in the axial entrainment boundary or positive v-velocity in the radial entrainment boundary is a cause of computational instability. By employing a properly elongated domain, the most realistic and correct solution can be obtained.

4.2 Computational Grid

Chapter 3 has reported that control volume method is used to discretize the governing partial difference equations, and that staggered grid system is employed. Fig. 4.3 provides the grid system for all the dependent variables except velocity component u and v. This is a set of non-uniform grid, consisting of 192 nodes in the axial direction and 144 nodes in the radial direction. Usually, a non-uniform grid is used, in order that finer spacings in the region where large spatial gradients are expected can be achieved without increasing the total size of grid. Preliminary numerical tests reveal that these zones include the initial mixing region of the flow in the tube, the shear layers of the swirl jet, the boundary of the re-circulation zone and zones with intense chemical reaction.

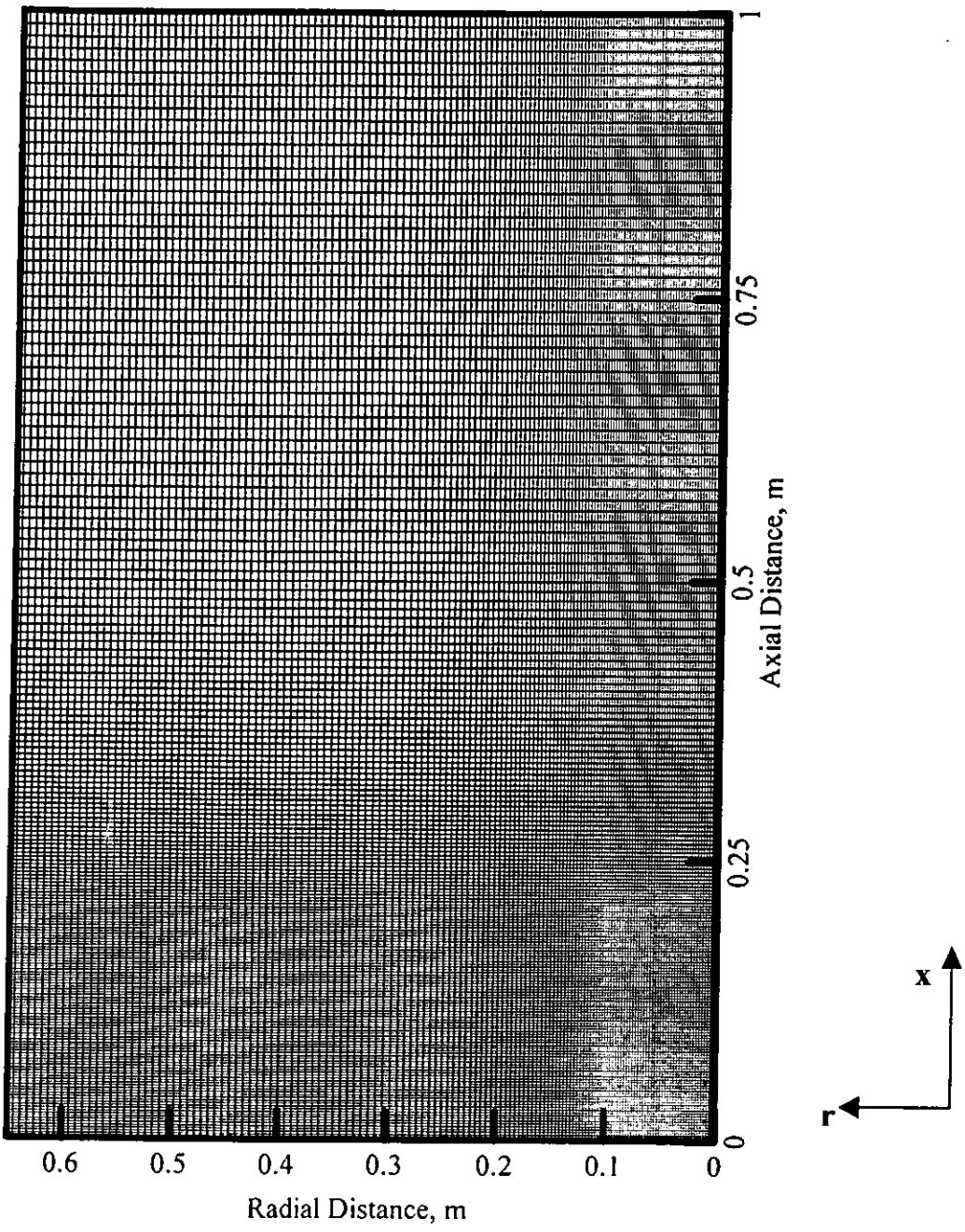

Fig.4.3 Computational Grid for Dependent Variable φ, except u and v

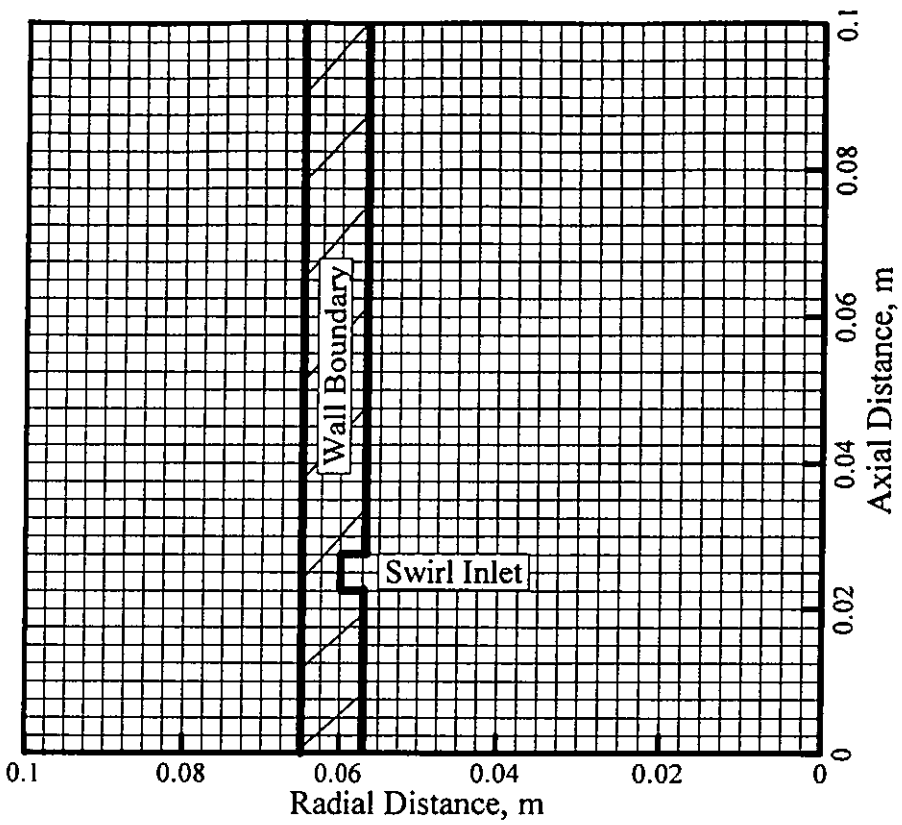

Fig.4.4 Expand View of High Resolution Grid near Inlet Boundary

The most important region is the intense chemical reaction zone, or known as the flame zone. Laboratory experiments [5] have shown that all the flames are stabilized within an axial distance of 0.1m from the burner exit. Thus, the densest grid is applied in this region, as shown in Fig. 4.4. Detailed information about the grid arrangement is as follows.

From 0 to 0.1m in the radial direction, the computational grid lines are uniformly spaced 2.5×10^{-3}m apart. Because the inner radius of the burner is 0.057m, the distance between the 23rd and the 24th grid lines in the radial direction is adjusted to be 2.0×10^{-3}m to make sure that the 24th grid line lies at 5.7×10^{-3}m radial location (resulting in a 3.0×10^{-3}m spacing between the 24th and 25th grid lines.). From 0.1m to 0.30235m, the grid spacing is progressively stretched by a factor of 1.02 resulting in a grid spacing of 6.47×10^{-3}m at the 0.30235m radial location. For grid lines at radial distances greater than 0.30235m, the grid lines are uniformly spaced again. The distance between two adjacent grids is 6.47×10^{-3}m. The grid in the axial direction is similarly constructed with a uniform axial spacing of 2.5×10^{-3}m from 0 to 0.2m, a stretching factor of 1.05 from 0.2 to 0.60304m (1.04×10^{-2}m grid spacing at 0.60304m), and a uniform grid for the remainder of the axial extent of the domain with grid spacing of 1.04×10^{-2}m.

Such grid arrangement is devised according to a series of preliminary numerical tests. It ensures that dense grid is located in the very important regions, and that the ratio of the axial length to the radial width of the grid node isn't too large or too small. Thus, the computation is easier to achieve convergence. In addition, numerical results based on this set of grid is, in fact, free of the influence of grid numbers. As is shown in Fig. 4.5, there is little difference in the axial velocity between the current grid and a denser grid.

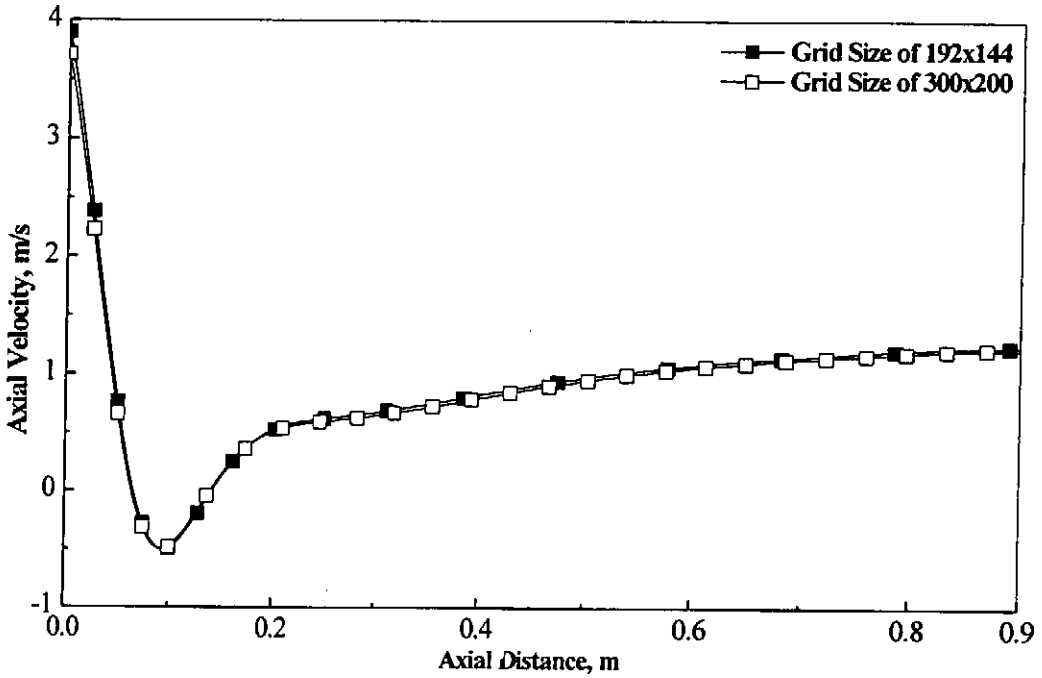

Fig. 4.5 Influence of Grid Size on the Axial Velocity

4.3 Boundary Conditions

Because of the elliptic nature of the governing differential equations, boundary conditions must be supplied for each of the main dependent variables along a boundary completely enclosing the domain of integration. An important and often difficult aspect of any numerical simulation is the choice of appropriate boundary conditions. The problem is even more difficulty when there exist free stream boundaries.

4.3.1 Inlet Boundary Conditions

At the inlet boundary, the conditions on the density, momentum, energy, turbulent parameters and composition of the inflowing gases are specified as a function of position. For radial distances less than 2.5×10^{-2} m from the jet centerline, the flow is composed of fuel/air mixture with a certain fuel to air equivalence ratio of Φ. The axial velocity u_0 and temperature T_0 are assumed to be uniform for the mixture at the inlet. The fuel/air mixture is surrounded by

coflow air stream for radial distances between 2.5×10^{-2} m and 5.7×10^{-2} m, with identical velocity and temperature to those of the core mixture, respectively.

The turbulent kinetic energy, k_0, at the inlet boundary is assumed to be a certain fraction of the inflowing kinematic energy. Its dissipation rate, ε_0, is defined by [11]:

$$\varepsilon_0 = C_\mu k_0^{1.5}/(0.03D) \tag{4.1}$$

Where, D is the inner diameter of the burner.

The enthalpy, H_0 and mixed fractions $\psi_{1,0}$ and $\psi_{2,0}$ at the inlet plane can be calculated via equations (2.8), (2.35) and (2.37).

Swirl is introduced into the burner by specifying the tangential velocity as w_0, between 2.25×10^{-2}m and 2.75×10^{-2}m in the axial direction at the radial location of 5.85×10^{-2}. w_0 is obtained according to the conservation of angular momentum:

$$2\pi R^{+2}v^{+}\Delta x^{+}w_0=2\pi r_t^2\ v_t^2 L_t \tag{4.2}$$

Where,

r_t: Inner radius of the tangential air inlet used in the experiments[5],

$r_t=3.05\times10^{-3}$m

v_t: Inflowing tangential velocity

L_t: The difference between the inner radius of the burner and the tangential air inlet, $L_t=5.395\times10^{-2}$m

R^+: Radius of the 25th grid node in the radial direction,

$R^+=5.85\times10^{-2}$ m

v^+: Radial velocity at the swirl inlet

Δx^+: The differnce of 2.75×10^{-2} m and 2.25×10^{-2} m.

In the current study, it is assumed that the tangential mass flux enters the burner through Δx^+ at the radial location of R^+. Thus, v^+ can be obtained from:

$$v^+=r_t^2 vt/(R^+\Delta x^+) \tag{4.3}$$

4.3.2 Entrainment Boundary Conditions

In the current study, the environmental air is assumed to enter the domain of interest through the axial and radial entrainment boundaries, as shown in Fig. 4.1. Our preliminary computation tests reveal that these two entrainment boundaries should be located far away enough from the burner exit. The

numerical results are very sensitive to the boundary conditions chosen for these two boundaries. Two types of boundary conditions have been tested in our preliminary studies:

Condition A: For the axial entrainment boundary, the axial gradients of all the governing parameters except the radial velocity are set to zero, while the radial velocity itself is set to zero. The radial entrainment boundary can be defined in a similar way. That is to say, the radial gradients of all the governing parameters except the axial velocity are set to zero, while the axial velocity itself is set to zero. Note that v is replaced by (rv) in the latter case.

Condition B: For the axial entrainment boundary, the radial velocity and the axial gradient of the axial velocity are still set to zero. Other governing parameters are specified according to the stagnant environment. Similarly, only the axial velocity and the radial gradient of (rv) are set to zero, while other parameters take their values from the stagnant environment for the radial entrainment boundary. For example, the turbulent kinetic energy and its dissipation rate at the entrainment boundaries are set to zero since the surrounding conditions are stagnant for the present problem.

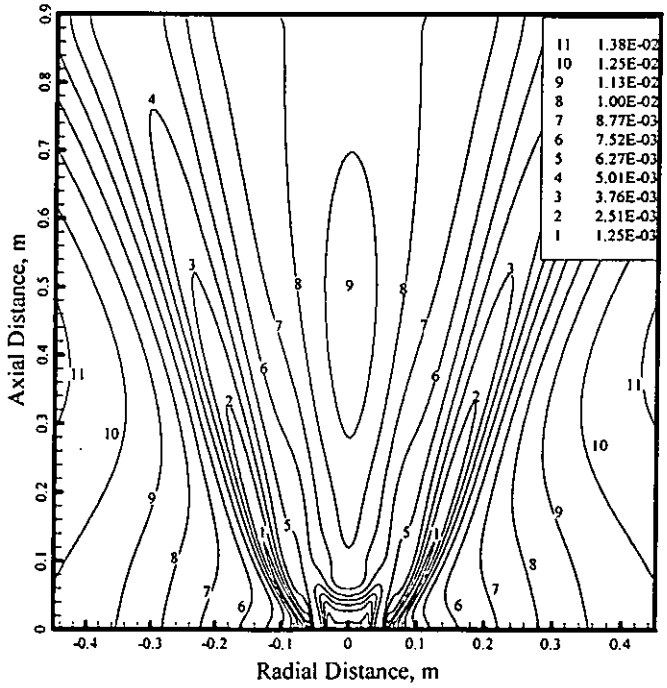

Fig. 4.6 (1) Distribution of Turbulent Viscosity Based on Condition A

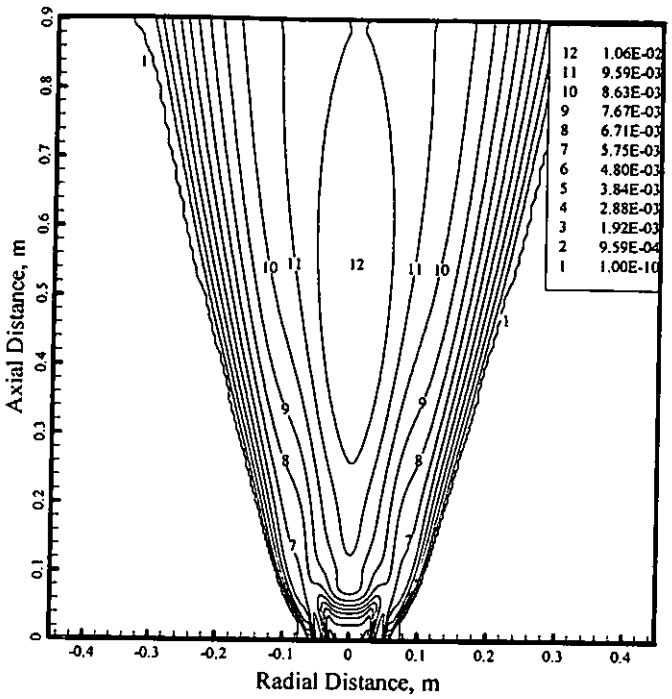

Fig. 4.6 (2) Distribution of Turbulent Viscosity Based on Condition B, kg/m·s

Fig. 4.6 Influence of Conditions A, B on the Predictions (Isothermal)

Condition A indicates that the swirl flow still has significant influence on the entrainment boundaries, though these two boundaries locate far away enough from the swirl jet. Compared with condition A, condition B is more realistic. It shows that the swirl jet has little influence on the remote entrainment boundaries. The computations under both of the two conditions can achieve convergence. Fig. 4.6 provides the distribution of turbulent viscosity from above two conditions. It can be seen from these figures that, condition A yields intense turbulence outside of the swirl flow, while condition B yields very little turbulence in the corresponding regions. Since the surrounding environment is stagnant, there should be no turbulence outside of the main swirl flow. Thus, the prediction based on condition B is more realistic and correct. In our current study, condition B is chosen for the entrainment boundaries.

At the outlet, the flow is assumed to be fully developed, i.e., the axial gradients of all the dependent variables are set to zero. By far, the easiest boundary to model is the symmetry plane. There is no flow across this boundary, so the radial velocity is zero. From the definition of the symmetry axis condition, the radial gradients of all other variables are zero. The standard log-law wall function, as outlined by *Launder* and *Spalding* [28], is used for the next to the wall grid points.

There are some special nodes in the computational domain. One of them is the node at the axial entrainment boundary adjacent to the wall boundary, as is shown in Fig.4.7.

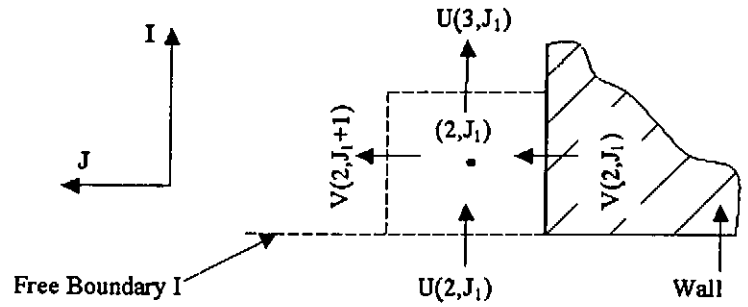

Fig. 4.7 The Node at the Axial Entrainment Boundary Adjacent to the Wall

At this node, the zero axial gradient assumption for u velocity is not valid any longer. It can be seen from Fig.4.7 that the normal velocity on the wall boundary, $V(2,J_1)$, should be equal to zero. Usually, $V(2,J_1+1)$ takes non-zero value. Thus, the relationship between $U(2,J_1)$ and $U(3,J_1)$ should be subject to the mass conservation principle for the main control volume, $(2,J_1)$. The implementation of the condition, $U(2,J_1)=U(3,J_1)$ in the program will cause computation instability and difficult to converge. Accordingly, the definition of u velocity at the node on the outlet boundary adjacent to the symmetry axis should be done in a similar way. However, the computational tests reveal that the zero axial gradient assumption for u velocity at this node brings no ill effect on the computation stability. This may be due to the relatively small v velocity near the symmetry axis. As a consequence, the zero axial gradient assumption is applied for this node.

As a summary of this section, the boundary conditions for the present problem are listed in the Table 4.1.

Table 4.1 Boundary Conditions for Jet Premixed Flame

Inlet Boundary	$u=u_0$; $v=0.0$; $k_0=0.005u_0^2$; $\varepsilon_0=C_\mu k_0^{1.5}/(0.03D)$; $T=T_0$;
	When $r\le 2.5\times10^{-2}$m:
	$M_{fuel}=(\Phi/i)/(4.31+\Phi/i)$; $M_{O2}=1.0/(4.31+\Phi/i)$; $M_{CO2}=0.0$;
	$M_{H2O}=0.0$; $M_{N2}=3.31/(4.31+\Phi/i)$; $H=\sum M_j H_j$; $\overline{T'^2}=0$
	When $r\le 5.7\times10^{-2}$m:
	$M_{fuel}=0$; $M_{O2}=0.232$; $M_{CO2}=0.0$;
	$M_{H2O}=0.0$; $M_{N2}=0.768$; $H=\sum M_j H_j$; $\overline{T'^2}=0$

Axial Entrainment	$\frac{\partial u}{\partial x} = v = w = k = \varepsilon = 0;\ T = T_0;\ \overline{T'^2} = 0;$ $M_{fuel} = M_{CO2} = M_{H2O} = 0.0;\ M_{O2} = 0.232;\ M_{N2} = 0.768;\ H = \sum M_j H_j$
Radial Entrainment	$\frac{\partial (rv)}{\partial r} = u = w = k = \varepsilon = 0;\ T = T_0;\ \overline{T'^2} = 0;$ $M_{fuel} = M_{CO2} = M_{H2O} = 0.0;\ M_{O2} = 0.232;\ M_{N2} = 0.768;\ H = \sum M_j H_j$
Symmetry	$\frac{\partial u}{\partial r} = v = w = \frac{\partial k}{\partial r} = \frac{\partial \varepsilon}{\partial r} = \frac{\partial M_j}{\partial r} = \frac{\partial H}{\partial r} = \frac{\partial \overline{T'^2}}{\partial r} = 0;\ \Gamma_{eff} = 0$
Outlet	$\frac{\partial u}{\partial x} = v = \frac{\partial w}{\partial x} = \frac{\partial k}{\partial x} = \frac{\partial \varepsilon}{\partial x} = \frac{\partial M_j}{\partial x} = \frac{\partial H}{\partial x} = \frac{\partial \overline{T^2}}{\partial x} = 0$

4.4 Computational Details

An existing computer program, *EL2D*, developed by *Patankar* [37,38] is modified and extended to fit our current investigation. The iteration starts from estimations of the values of all variables including boundary conditions. In the course of iteration, under relaxation factors are used to promote computation stability. These parameters are 0.5 for all the dependent variables except that a factor of 0.8 is used for pressure field. The other variables are not relaxed during the iteration. Generally, this set of parameters provides faster convergence and stability in the early stages of the computation for the flows considered in this thesis. The computation is terminated when the ratio of maximum mass imbanlance for each control volume is less than 0.01 percent of the incoming mass.

Fig. 4.8 shows the block diagram of the current program highlighting its structure. The user must supply part of the program (not data) for the code. The user-supplied program, named ***SUBROUTINE USER***, defines the problem to be solved. The roles of these subprograms can be found from the explanation, which is given below.

GRID and UGRID: Constructing grid system

START: Initialize the dependent variables

DENSE: Calculate the density distribution

BOUND: Find the boundary values of dependent variables

OUTPUT and PRINT: Output necessary data, iterative or final

GAMSOR: Provides the diffusion coefficients and source terms

SETUP1: Calculate the grid-related parameters and initialize the non-user supplied variables

SETUP2: Calculate the coefficients of the finite difference equations, call the subprogram GAMSOR and SOLVE

SOLVE: Using *TDMA* and alternating line-by-line method to solve the discretization equations

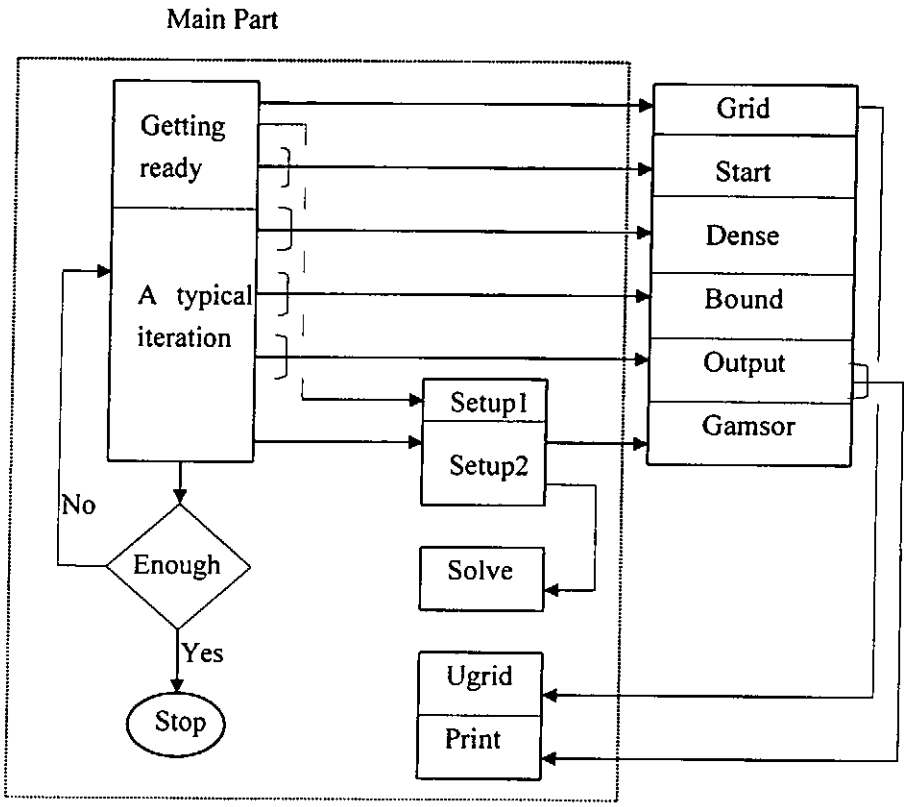

Fig. 4.8 Structure of the elliptic solver *EL2D*

5. Aerodynamics and Combustion in Open Swirl Flow

The current study aims to obtain a better understanding of the aerodynamic characteristics and flame properties of the open swirl-stabilized turbulent premixed flames. Presently, numerical simulation is made for the following operating conditions:

Burner inlet velocity: u_0=5.0 m/s

Methane to air equivalence ratio: Φ=1.0

Burner inlet temperature: T_0=298.15 K

Radial velocity at the swirl inlet: v^+=2.63 m/s

Tangential velocity at the swirl inlet: w_0=76.3 m/s

The geometric swirl number is 0.07 according to above parameters. Note that geometric swirl number, S_l, can be conveniently obtained from the burner geometry and mass flow rate by [12]

$$S_l = \frac{\pi r_t R}{A_t}\left(\frac{m_t}{m_t + m_a}\right)^2 \tag{5.1}$$

Where,

r_t: The radius of the tangential air inlet

R: The radius of the burner

A_t: The total area of the tangential air inlets

m_t: The tangential mass flow rates

m_a: The axial mass flow rates

It can be learnt from equation (5.1) that, S_l depends strongly on the ratio of r_t to R when the mass flow rates are fixed. Thus, whether the swirl is strong or weak is difficult to judge, directly according to S_l. Many studies have shown [6,32] that the theoretical swirl number, S, can be obtained more appropriately by the following definition:

$$S = \frac{\int_0^R 2\pi r^2 \rho u w dr}{R\int_0^R 2\pi r \rho\left(u^2 - \frac{w^2}{2}\right)dr} \tag{5.2}$$

This definition can be easily employed to tell the swirl intensity. When S is less than 0.6, the swirl is weak and there is no re-circulation zone in the flow domain. When S

is above 0.6, a re-circulation zone often appears and the flow is called strong swirl flow. However, the substitution of u(r) and w(r) into the integration of equation (5.2) leads to a negative swirl number at the burner exit. This shows that the definition of swirl number using equation (5.2) is not suitable for the current study.

Gouldin et al [1,20,22], *Ramos* [46] and *Cheng* [7] studied the swirling flows experimentally. In their studies, the swirl number is defined as the ratio of the axial flux of angular momentum to that of the axial flux of axial momentum normalized by the burner radius, R,

$$S = \frac{\int_0^R \rho u w 2\pi r^2 dr}{R \int_0^R \rho u^2 2\pi r^2 dr} \tag{5.3}$$

This definition of swirl number is applied in our current study. According to equation (5.3), the predicted swirl number at the burner exit is 1.156. This indicates that the swirl is very strong, not so weak as the geometric swirl number has showed.

5.1 General Aerodynamic Characteristics

Our current prediction models one of the flames, *SWF4*, as reported by *Chan et al* [5]. Firstly, predictions are compared with available data of *SWF4*. In *Chan et al*'s study, the testing section was limited to within 0.1m vertical distance from the burner exit. Presently, only the predicted centerline axial velocities are compared with those measured values.

Profiles of the centerline axial velocity are shown in Fig. 5.1. The burner exit is denoted as zero in the axial direction. Fig. 5.1 indicates that the predictions do not match well with experiments for the isothermal conditions. However, it is worth noting that during simulation, it is difficult for the swirl to reduce the centerline axial velocity at x=0.01m above the burner exit to a value below 2.0m/s without inducing re-circulation. A much better prediction is made for the reacting case, except that there appears to be discrepancy downstream of the flame zone. This may be due to the assumption of axisymmetry flow in our present study. *Tangirala et al.* [63] reported that the re-circulation strength (in terms of mass flow) would be reduced when the flame precessed and entrained air in a non-axisymmetric manner. In fact, the swirl jet is a non-axisymmetric flow. However, an axisymmetric pattern is assumed in this study. The sharper

decrease in the centerline axial velocity may also be due to over-predicted re-circulation strength.

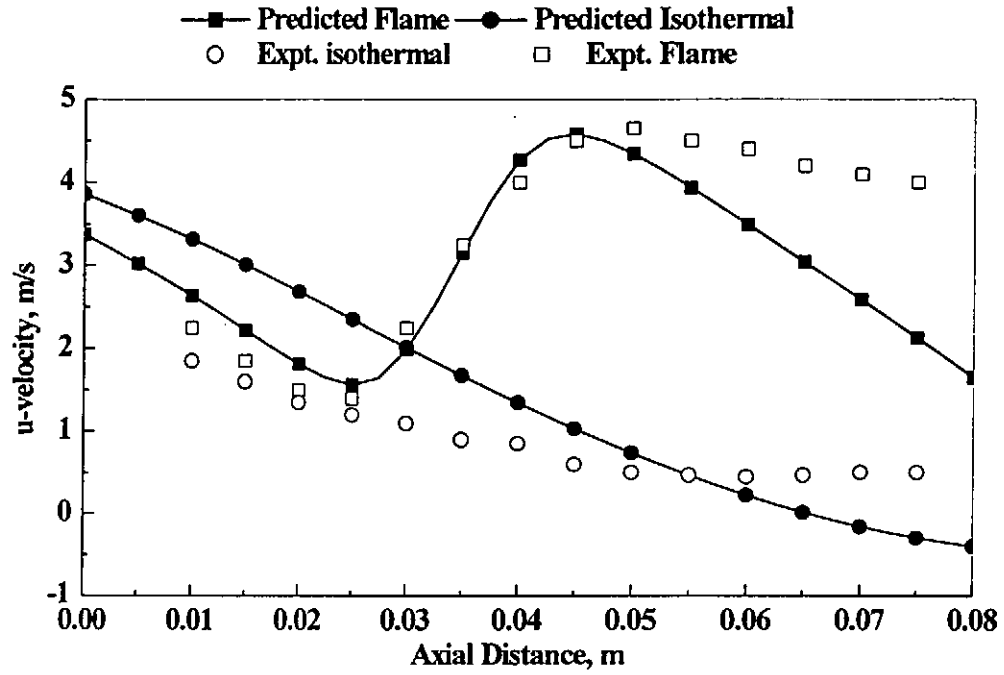

Fig. 5.1 Comparison between Predictions and Measurements

5.1.1 Axial Velocity

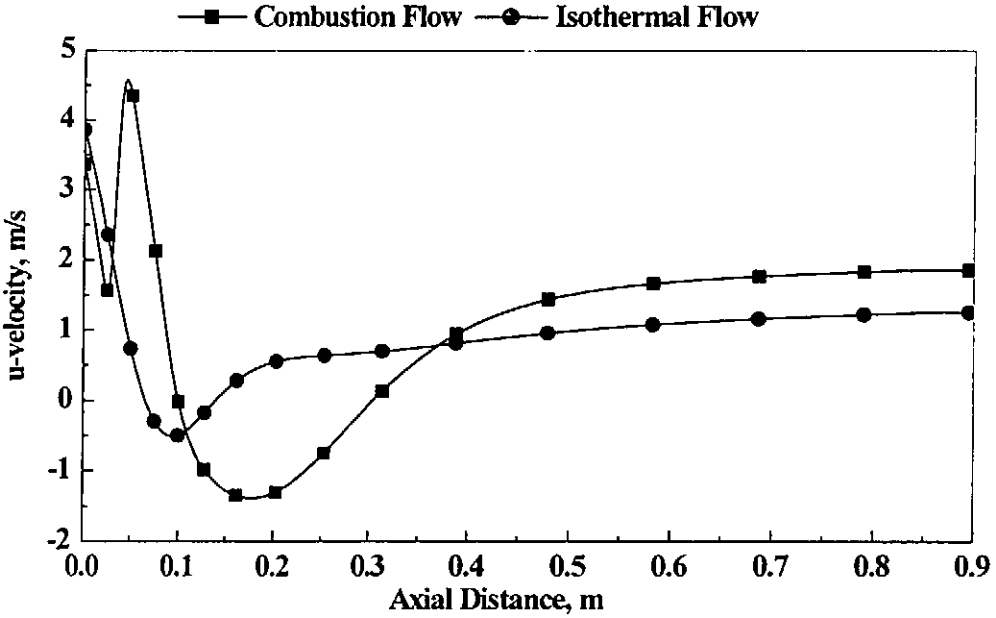

Fig. 5.2 Profiles of Axial Velocity on the Centerline

Fig. 5.2 shows the variation of axial velocity along the jet centerline. It can be seen that the axial velocity starts to decrease in the burner tube. The axial velocity at the burner exit is below 4.0 m/s. A re-circulation zone is predicted under both combustion and isothermal conditions. In non-reacting flow, the re-circulation zone locates within the testing section, with very small size and reversal velocity. When

combustion is initialized, the axial velocity tends to decrease faster at first, then followed with a sharp increase. Another outcome of combustion is that the re-circulation zone is moved downstream with increased size and velocity. It is noticed that the forward stagnation point of the re-circulation zone locates above x=0.1m, beyond the testing section in the reacting flow. This may be the reason why no re-circulation was detected in *Chan et al.*'s study [5].

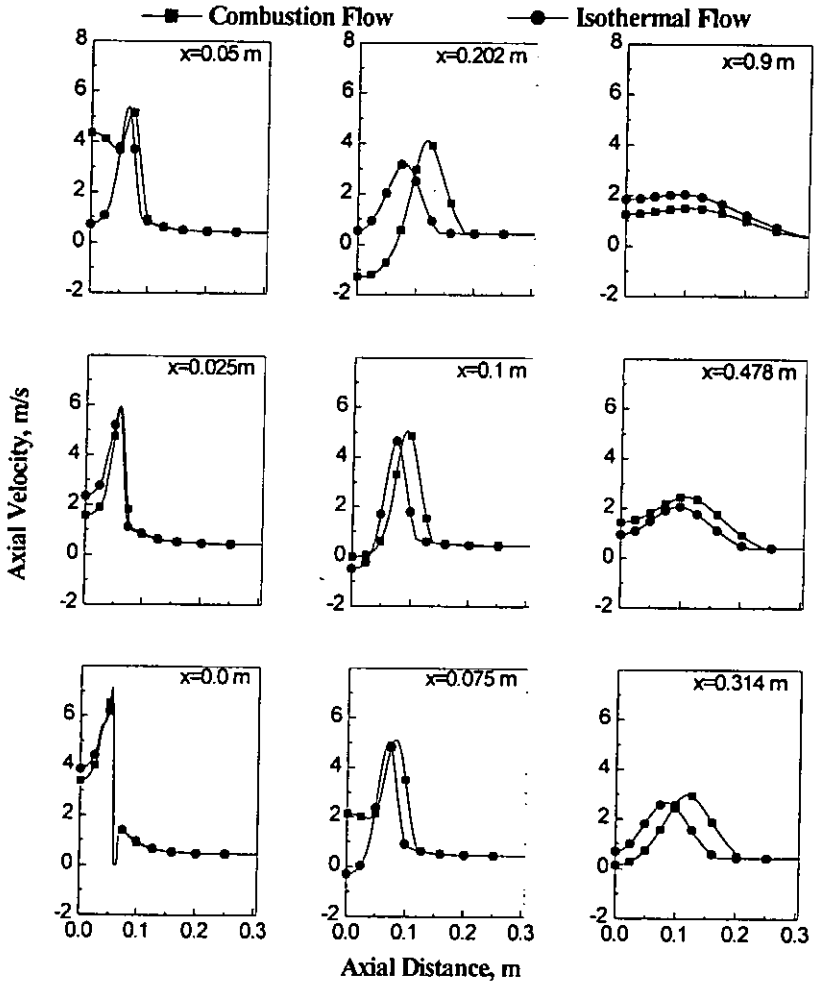

Fig. 5.3 Radial Profiles of Axial Velocity

Profiles of axial velocity at various vertical locations are shown in Fig. 5.3. On the burner exit plane, the axial velocity profile shows a sharply peaked maximum near the burner wall. This is due to the centrifugal force induced by swirl, which pushes the flow towards the wall. The axial velocity is positive at radial distance larger than 0.065m, indicating that the surrounding air is entrained into the jet through the axial entrainment boundary. Combustion occurs between x=0.025m and 0.05m. This is verified by the sharp increase in the axial velocity. The facts that higher axial velocity is located on the centerline and that the axial velocity maxima in the combustion flow change little compared with corresponding isothermal values, as are shown at x=0.05,

0.075m, indicate that major chemical reaction takes place in the core of the fuel air mixture. Upstream of the flame zone, the axial velocity is somewhat lower than that in the isothermal flow. This changing trend is also reported in other studies [18,20]. Downstream of the re-circulation zone, the centerline axial velocity recovers its positive value and higher values are predicted with combustion.

It is interesting to note that combustion moves the re-circulation zone downstream, with increased width, length and reversal velocity, as shown in Figs. 5.2 and 5.3. This phenomenon is quite different from those occurring in a confined system, where the re-circulation is suppressed by heat release under most conditions.

Several reasons for combustion to increase re-circulation are reported in the literature. These previous studies mainly attributed such phenomenon to a stronger adverse pressure gradient caused by combustion in the flame zone. For the inviscid case, the adverse pressure gradient, $\partial P/\partial x$, set up on centerline due to swirl can be determined by integrating the radial force balance $dP/dr = \rho w^2/r$ in the radial direction, then differentiating the result with respect to x to get:

$$\left.\frac{\partial P}{\partial x}\right|_{r=0} = -\frac{\partial}{\partial x}\left(\int_0^R \rho \frac{w^2}{r} dr\right) \qquad (5.4)$$

Equation (5.4) shows that as combustion causes gas density ρ to decrease in the axial direction, the adverse pressure gradient is forced to increase, which causes the flow to reverse. Physically, near the fuel exit, gas density is large so pressure on centerline will be very low; a few centimeters downstream the density is low so pressure on centerline will quickly rise to atmosphere. Thus combustion tends to increase re-circulation.

Presently, an increase in the adverse axial pressure gradient is predicted within the flame zone, as shown in Fig. 5.4. It can be seen that the adverse pressure gradient, between the burner exit (x=0.0 m) and the flame zone (x=0.025m), is larger in the reacting flow than in the isothermal flow. However, this increase is limited to a short vertical distance with moderate increment. Though this increase helps reduce the axial velocity before the flame zone (as shown in Figs. 5.2 and 5.3), it is difficult to comprehend that such an augment is the major factor for a much stronger re-circulation zone. Furthermore, the pressure gradients under combustion is much smaller than those in non-reacting flow between x=0.025m and 0.05m, as shown in Fig. 5.4.

It can be learnt that, from Figs. 5.1 to 5.3, this is a region with intense combustion.

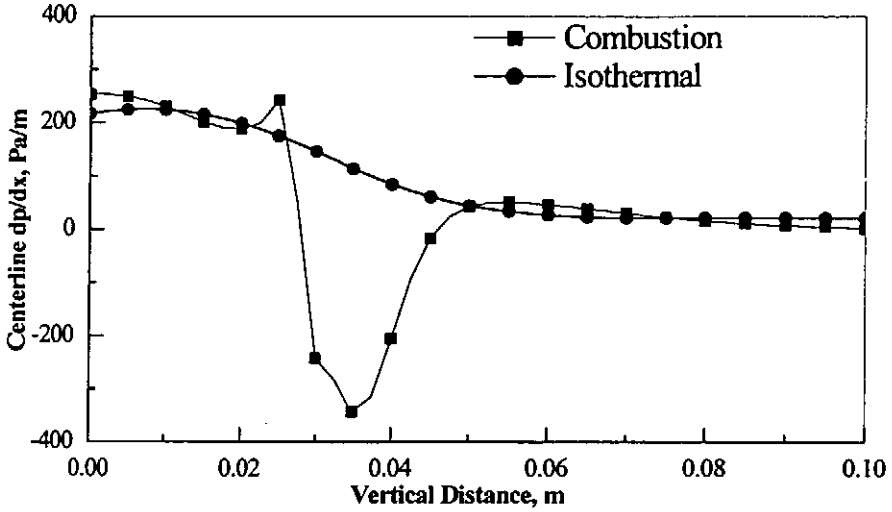

Fig. 5.4 Profile of Axial Pressure Gradient on the Centerline

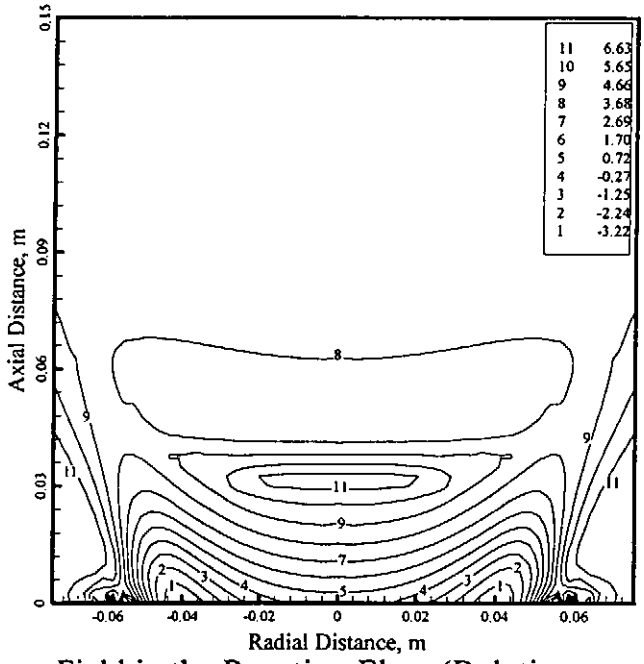

Fig. 5.5 Pressure Field in the Reacting Flow (Relative to point (0,0)), Pa

As a matter of fact, when intense combustion occurs, large amount of heat is released in a narrow space and the temperature will rise sharply. This results in a higher-pressure zone, as shown in Fig. 5.5. This figure shows that the pressure in the flame zone is higher than that in the surrounding flow. As a consequence, the fuel air mixture from upstream is difficult to penetrate this region. This implies that the flame zone acts as "blunt body" for the fuel air mixture. It is the blunt body that increases the width and length of the re-circulation zone.

In the current study, the axial flow is predominant, while turbulent diffusion is important in the radial direction. In the standard k-ε model, turbulent

viscosity, μ_t represents the ability of turbulent diffusion. Figure 5.6 shows the distribution of turbulent viscosity in the flow field. It can be seen that μ_t becomes much smaller with combustion. The smallest viscosity in the main flow field reaches a value of 1.03×10^{-3} kg/ms, located downstream of the reaction zone.

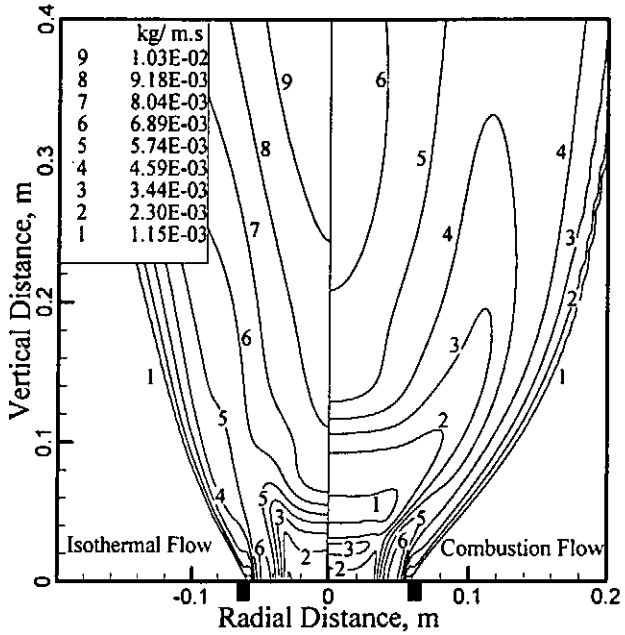

Fig. 5.6 Distribution of Turbulent Viscosity

The decrease of μ_t results in a decay of turbulent diffusion of mass and momentum, from the shear layer of the swirl jet towards the centerline. On the other hand, combustion tends to spread the flow wider in the open system. Thus, the re-circulation zone becomes wider and longer with increased reversal velocity under combustion.

5.1.2 Radial Velocity

Figure 5.7 shows the profiles for the radial velocity. Positive values of the radial velocity from r=0 to 0.057m at the burner exit plane indicate that, swirl flow is thrown outward in the radial direction. The existence of sharp peaks in the radial velocity profiles shows that strong flow divergence exists in the combustion space. This is quite different to the free jet. At radial locations larger than 0.3m, radial velocities become negative, indicating that surrounding air is entrained into the swirling jet.

As the vertical distance is lesser than 0.128m, radial velocities under combustion are higher within main flow region. At x=0.025m, the increase in radial velocity results from the decrease of axial velocity. When combustion

takes place, the adverse vertical pressure gradient increases before the reaction zone, as shown in Fig. 5.4. This leads to a decrease in axial velocity. Correspondingly, the radial velocity increases to satisfy mass conservation.

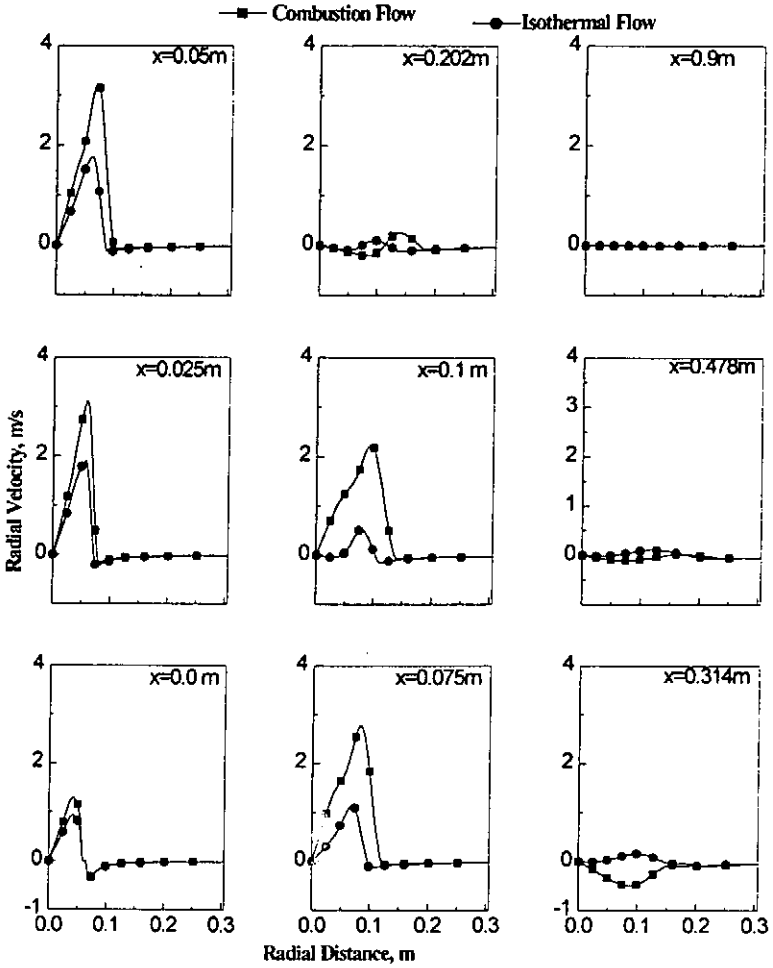

Fig. 5.7 Profiles of Radial Velocity

Heat release causes flow expansion in the combustion zone. This results in a sharp increase in radial velocity, as shown at x=0.05m. Near the forward stagnation point region of the re-circulation zone, strong impingement between swirling jet and reverse flow occurs under combustion. This can be verified by the higher values of radial velocity at x=0.075 and 0.1m. In the rear part of the re-circulation zone, the presence of negative radial velocity shows that flow is entrained into the re-circulation zone, as shown at x=0.202 and 0.314m.

5.1.3 Tangential Velocity

The profiles of tangential velocity are shown in Fig. 5.8. Similar to the axial and radial velocities, the tangential velocity has a sharp peak near the wall at x=0.0m. Values of tangential velocity at small radial distance are negligible, indicating that swirl hasn't spread into the inner fuel/air mixture at the burner

exit. Compared with axial and radial velocities, tangential velocity decreases rapidly and the maximal tangential velocities under combustion are lower than their corresponding isothermal values. This is not surprising since the angular momentum behaves as a conserved scalar. In the current open system, swirl induces strong flow divergence, as shown in Fig. 5.7. Combustion drives the flow to spread even wider. Thus, tangential velocity tends to drop rapidly.

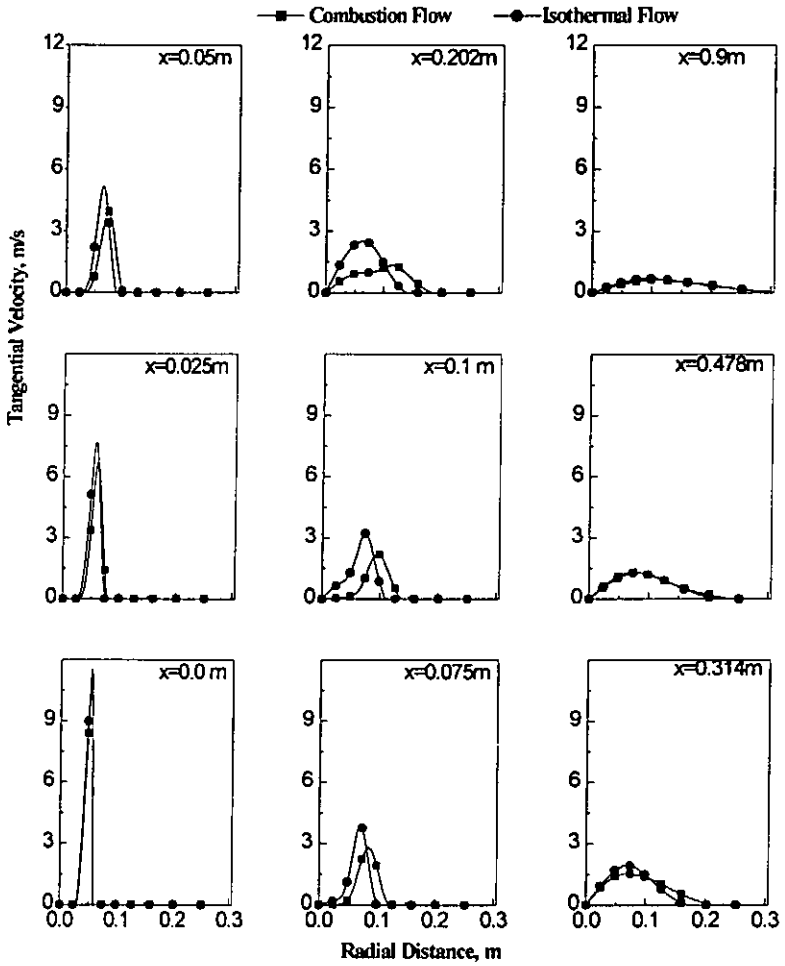

Fig. 5.8 Profiles of Tangential Velocity

At x=0.025, 0.05, 0.075m, swirling motion is only significant outside the 0.025m radius fuel/air core. The tangential velocity remains negligible at the radial distance smaller than 0.025m. This indicates that the flame zone is in fact free of swirl though the flame is stabilized by swirl. Such prediction is verified by measurements in *SWF4* [5]. Fig. 5.8 shows that there is little swirl within most of the re-circulation zone (at x=0.202m), as had been noted by *Syred* and *Beer* [61]. Further downstream of the re-circulation zone, the tangential velocity is seen to evolve into a distribution of conventional *Rankine*-type.

5.1.4 Turbulent Kinetic Energy and its Dissipation Rate

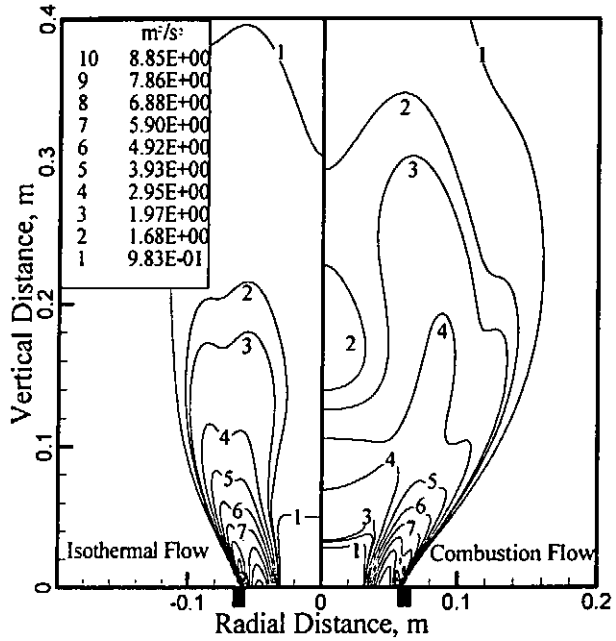

Fig. 5.9 Distribution of Turbulent Kinetic Energy

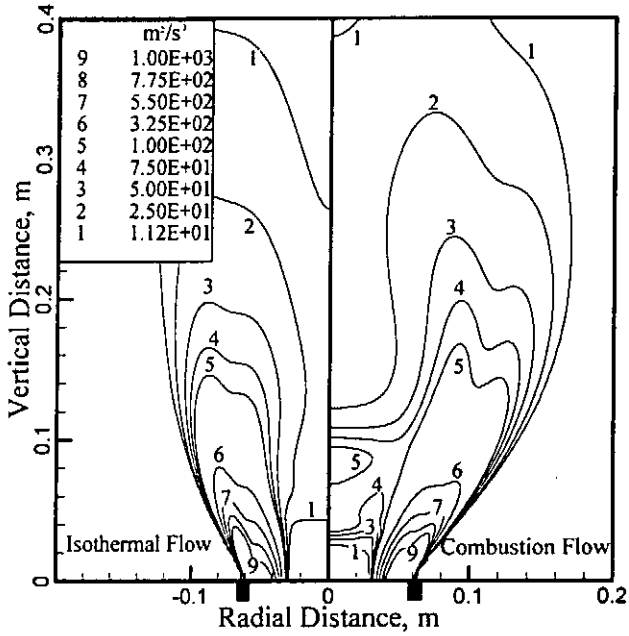

Fig. 5.10 Distribution of Turbulent Dissipation Rate

Figs. 5.9 and 5.10 show the distribution of turbulent kinetic energy and its dissipation rate, respectively. It is seen that the turbulence is most intense about the burner exit lip. There is significantly more turbulence in the flame than in the isothermal flow. Turbulent kinetic energy is generated where the velocity gradient is sharp. As a consequence, the production of turbulent kinetic energy is intense near the flame where large velocity gradient occurs. The turbulent kinetic energy is smaller along the centerline of the burner than at the shear layer due to smaller production of the turbulence along the centerline. The

steep velocity gradients near the forward stagnation point of the re-circulation zone produce again some turbulent kinetic energy.

The turbulent kinetic dissipation rate is a very complicated function. However, it can be considered to be large where turbulent kinetic energy is large. Similar to the turbulent kinetic energy, the dissipation rate reaches its highest level at the exit lip, too. Both distributions of turbulent kinetic energy and its dissipation rate show a wider spread of flow with combustion.

5.2 Flame Properties

The aerodynamic characteristics of the open swirl stabilized turbulent premixed flame are discussed in previous sections. The following sections will provide some information about the flame properties, including the distribution of temperature, species mass fraction, turbulent flame speed, fuel burning rate, reactedness, and so on. The mechanism of the formation of planar flame is also discussed in the follow sections.

5.2.1 Temperature and Fuel burning Rate

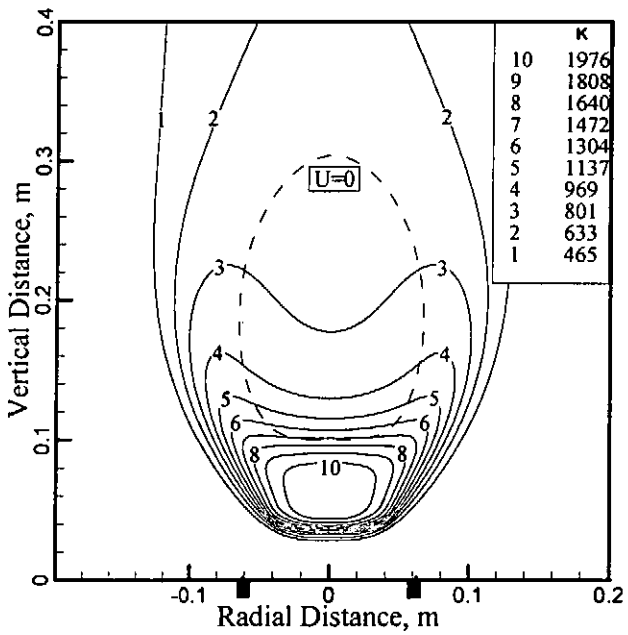

Fig. 5.11 Temperature Field

Mean temperature field is shown in Fig. 5.11. It can be seen that the largest temperature gradient (i.e., closely spaced isotherms) is the axial gradient occurring between x=0.025 and 0.05m. This indicates that chemical reaction takes place in a region locally normal to the centerline. This can also be seen clearly from Fig. 5.12, in which the distribution of fuel burning rate is shown.

Fig. 5.12 shows that the reaction zone is localized between x=0.025 and 0.05m, and that intense combustion begins at 0.030m from the burner exit. The zone of maximum burning rate is very close to a one-dimensional plane normal to the centerline. Such intense reaction leads to a sharp increase in temperature. Fig. 5.11 shows that mean temperature is only 373 K at x=0.0275 m on the centerline, while it is as high as 2009 K at x=0.045 m. The averaged heating rate of the gas is about 9.46×10^4 K/m, based on the vertical distance. It can be learnt from Fig. 4.1 that the averaged axial velocity is about 3.0 m/s within the same vertical distance. Thus, the time averaged heating rate reaches a value of 2.84×10^5 K/s. This indicates that temperature rises very quickly in the flame zone.

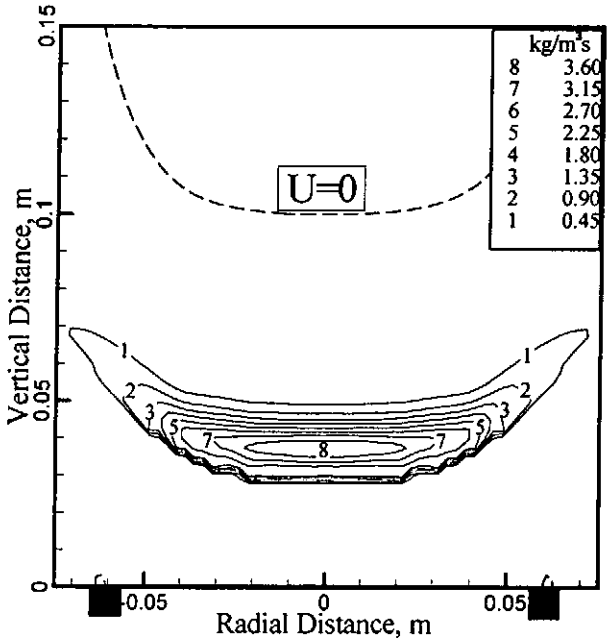

Fig. 5.12 Distribution of Fuel Burning Rate

During combustion, the flame expands radially outwards and spreads to an area equal to that of the burner exit. It is also found that there is no reaction at the edge of the re-circulation zone, or within the impingement region of opposed jets at the forward stagnation point, as shown in Fig. 5.12.

The stoichiometric adiabatic flame temperature for methane/air mixture is 2210 K [19]. In our study, the predicted maximum temperature is 2115 K, about 100 K lower than the corresponding adiabatic flame temperature. This difference indicates that the central fuel/air mixture isn't burnt under adiabatic conditions and that the co-flow air enters the core mixture earlier than expected.

The distribution of methane to air equivalence ratio in the isothermal flow is shown in Fig. 5.13. It can be seen that the equivalence ratio is smaller than 0.985 at the burner exit on the centerline, though the ratio is 1.0 at the burner

inlet. This means that some co-flow air has penetrated to the core mixture in the burner tube. When the fuel/air mixture reaches the flame front (at x=0.0275m), the equivalence ratio is reduced to as low as 0.977. In Chapter 6, we will explore how to maintain the fuel to air equivalence ratio before combustion is initiated.

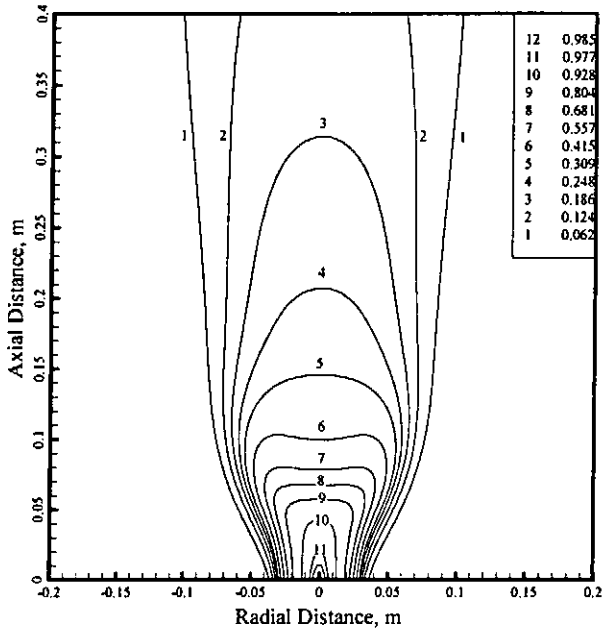

Fig. 5.13 Distribution of fuel to air equivalence ratio in the isothermal flow

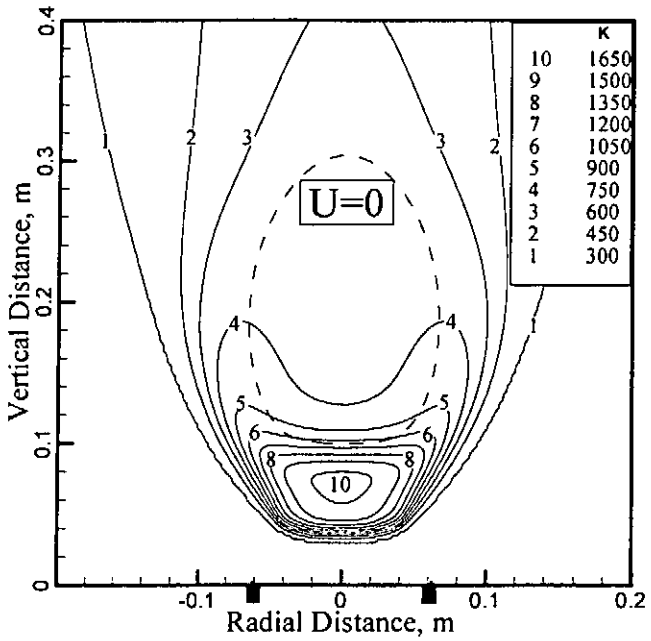

Fig. 5.14 Fresh Mixture Temperature

Fig. 5.14 shows the temperature distribution of fresh mixture. It can be seen that the temperature of fresh mixture increases abruptly as it passes through the flame. The fresh mixture temperature is almost proportional to the

mean gas temperature, as can be ascertained from Figure 5.14. In *Lagrangian* sense, the net temperature change of the fresh mixture is due to radiative heating and heat conduction from other fresh mixture packets. Note that conduction from the burned gas may be neglected because the interface between the fresh mixture and product or the flame film moves fast with respect to the fresh mixture. In other words, the temperature gradients in the fresh mixture near the flame may be neglected, and the fresh mixture is assumed to be heated only by radiation and mixing of the fresh mixture.

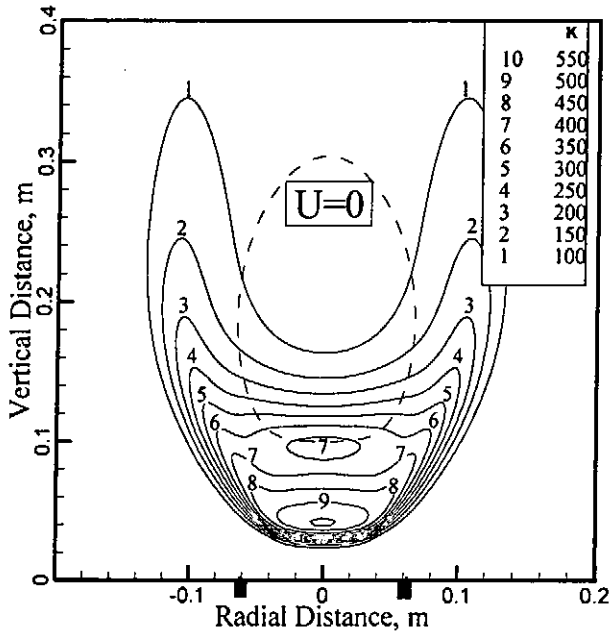

Fig. 5.15 Temperature Fluctuation, $\sqrt{\overline{T'^2}}$

Distribution of temperature fluctuation, $\sqrt{\overline{T'^2}}$, is shown in Fig. 5.15. The temperature fluctuation is greatest near the flame. It reaches a maximal value of 583 K, located at x=0.0375 m on the centerline. It can be learnt that, from Figs. 5.12 and 5.15, the maximal temperature fluctuation is located at about the same position as that of the maximal fuel-burning rate. This coincidence is reasonable. Owing to the intense reaction, the turbulent flame zone is alternatively occupied by the cold fresh mixture and by the products. This leads to the large temperature fluctuation in the flame zone. The steep temperature gradients near the forward stagnation point of the re-circulation zone produce again some large temperature fluctuation, but decays rapidly. Further downstream, temperature fluctuation is smaller along the centerline of the burner than at the shear layer, due to the mixing of hot products and surrounding cold flow at the shear layer.

5.2.2 Species Concentrations

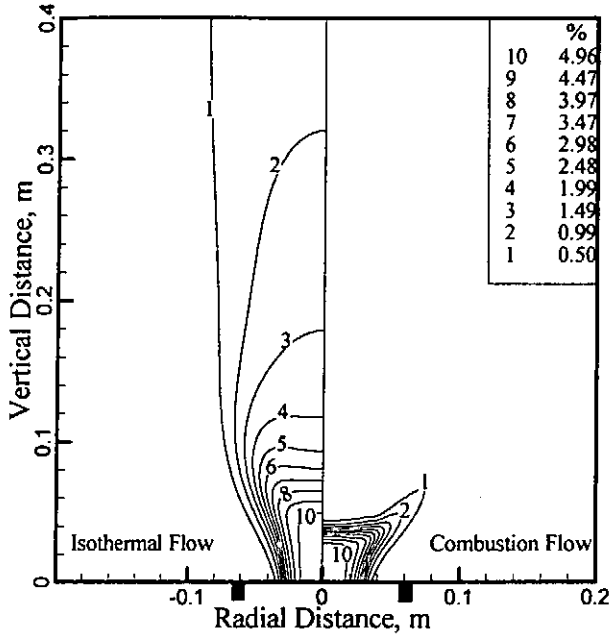

Fig. 5.16 Mass Fraction Distribution of CH_4

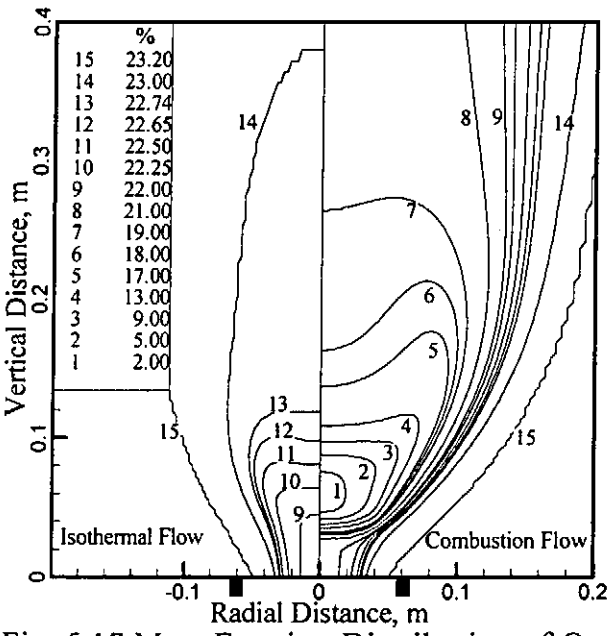

Fig. 5.17 Mass Fraction Distribution of O_2

Figs. 5.16 to 5.18 show the mass fraction distributions of methane (CH_4), oxygen (O_2) and carbon dioxide (CO_2) in the flow field. The mass fraction distribution of another product, water vapor (H_2O), is similar to that of carbon dioxide, and is not shown. The flame structure can also be determined from these figures. Figs. 5.16 to 5.18 show that steep vertical gradients for every mass fraction are formed between x=0.025 and 0.05m, indicating that this is a region with intense combustion. It can be seen from Fig. 5.16 that the mass fraction of methane is very small when the vertical height is greater than 0.05m in the combustion flow, whilst the fuel concentration remains very high in the

isothermal flow. This shows that most fuel has been consumed in the flame zone.

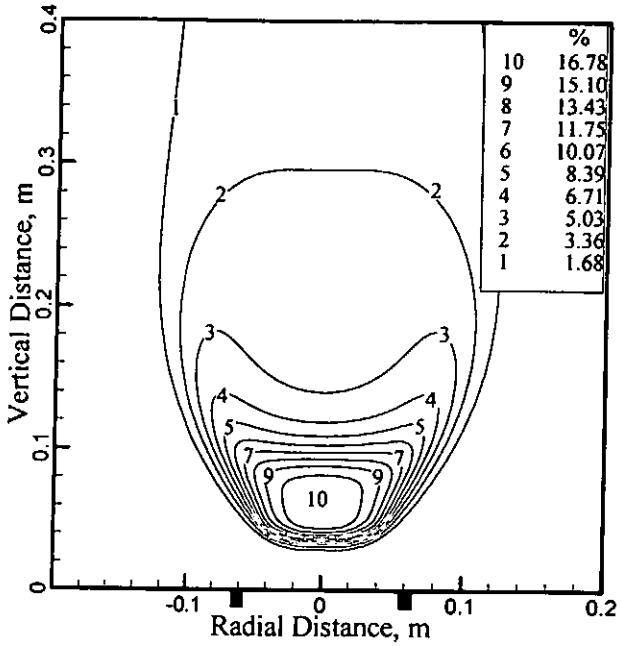

Fig. 5.18 Mass Fraction Distribution of CO_2

Fig. 5.17 shows that combustion consumes most oxygen from the inner fuel/air mixture. The coflow air enters the hot flow gradually. The minimal mass fraction of oxygen in the flame zone is 1.6%, indicating that coflow air has diffused into the core before the flame zone. Both Figs. 5.16 and 5.17 show a wider spread of the flow in combustion than in isothermal conditions. It can be seen from Figs. 5.18 and 5.11, that fraction contours of carbon dioxide are similar to those of the mean temperature. This is an inevitable outcome of *SCRS* (Simply Chemical Reacting System).

5.2.3 Reactedness

In the current study, the reactedness parameter is used to describe the combustion progress. The reactedness is defined as [53]

$$c = \frac{M_{fu} - M_{fu,u}}{M_{fu,b} - M_{fu,u}} \tag{5.5}$$

Where, c is the reactedness, $M_{fu,u}$ is the fuel mass fraction in the fully unburned conditions. For a confined premixed flame, $M_{fu,u}$ is identical to that at the inlet boundary. Presently, $M_{fu,u}$ can be obtained by solving the transport equation similar to that of M_{fu}, but with zero source term, i.e.,

$$\frac{\partial}{\partial x}(\rho u M_{fu,u})+\frac{\partial}{r\partial r}(r\rho v M_{fu,u})=\frac{\partial}{\partial x}\left(\frac{\mu_T}{\sigma_Y}\frac{\partial M_{fu,u}}{\partial x}\right)+\frac{\partial}{r\partial r}\left(r\frac{\mu_T}{\sigma_Y}\frac{\partial M_{fu,u}}{\partial r}\right) \qquad (5.6)$$

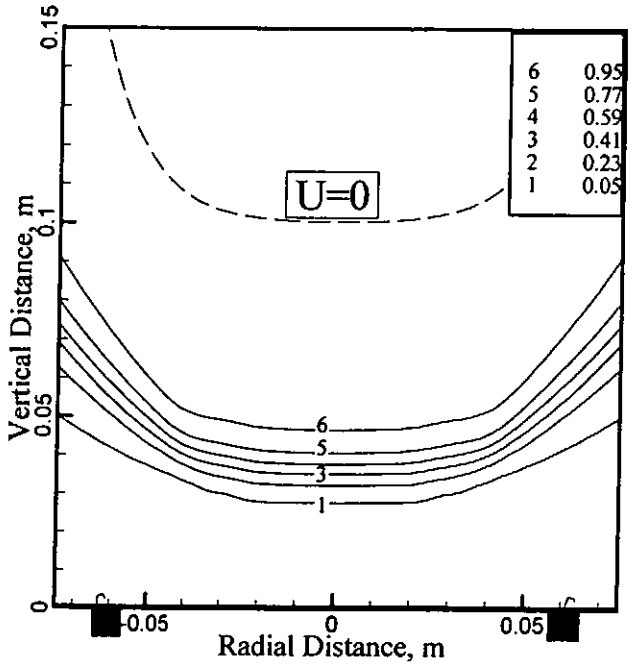

Fig. 5.19 Reactedness within Flame

Equation (5.5) shows that, that c equals to 0 denotes that there is no combustion in the flow, while that c equals to 1 means that combustion has finished.

Fig. 5.19 provides the reactedness in the reacting flow. It shows that reactedness arrives to a value of 0.05 at x=0.03m, indicating that combustion begins at this position. At x=0.0425m on the centerline, the reactedness rises to a value of 0.95, implying that combustion is almost complete. Though the reactedness is lower in the outer region of the flame (r>0.07m), the mass fraction of fuel is negligibly small in the same region. Fig. 5.19 shows that combustion has already completed before arriving to the forward stagnation point of the re-circulation zone.

From above results, it can be learnt that the flame brush is locally normal to the centerline. Consequently, the axial velocity at the reactant boundary provides a convenient means to estimate the turbulent flame speed, as in the stagnation flow stabilized flames. In the current study, the flame front is defined as c=0.05 contour. As is shown in Fig. 5.19, this contour intersects the jet centerline at x=0.03 m. The axial velocity at this point is 1.617 m/s, as shown in Fig. 5.1. Therefore, the corresponding turbulent flame speed is 1.617 m/s.

5.3 Effects of Re-circulation on Combustion

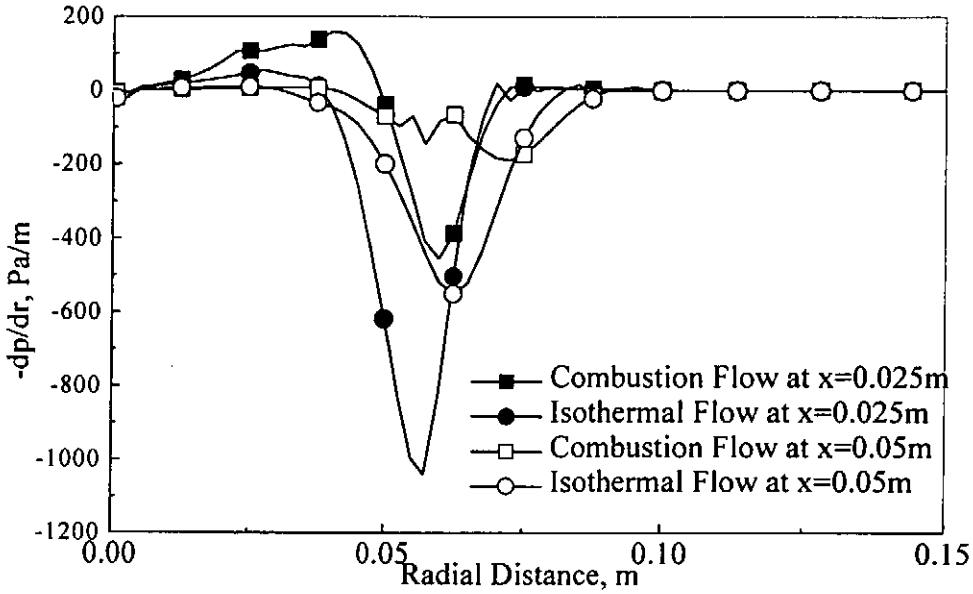

Fig. 5.20 Radial Pressure Gradients at x=0.025m and 0.05m

The above results clearly show that flow divergence is the key flame stabilization mechanism. When swirl flow enters an open space, the sudden expansion of flow will intensify on the centerline an imposed adverse pressure gradient. This tends to decrease the axial velocity rapidly. Swirl also induces radial mean pressure gradients, as shown in Fig. 5.20. All these factors increase the radial velocity and cause flow divergence in the open system.

When combustion is initialized by some means, the adverse vertical pressure gradient in the reaction zone increases, as shown in Fig. 5.4. This forces the flame to advance to the fresh mixture and further decreases the axial velocity before the reaction zone. Meanwhile, the radial pressure gradients are increased with combustion. Fig. 5.20 shows that there is significant increase in the radial pressure gradient before the reaction zone (i.e., at x=0.025m). This increases the radial velocity before the flame and results in a decrease in the axial velocity, as verified by Figs. 5.3 and 5.6. These help build a region where the turbulent flame speed matches that of the local flow. Consequently, the flame is stabilized in such region.

In the current study, a re-circulation zone is predicted in both isothermal and combustion flows. However, there is no reaction at the edge of the re-circulation zone, or within the impingement region, as reported in previous sections. Actually, combustion has already completed before impingement occurs. Figs. 5.21 and 5.22 show that there is a peak of the axial velocity between flame and the re-circulation zone. All these facts show that flame is

not stabilized by the re-circulation zone. Actually, the reverse flow acts as opposed jet.

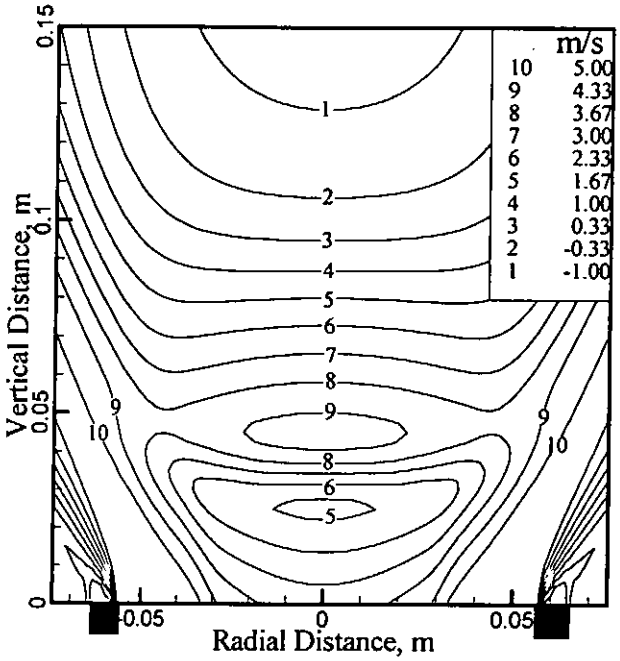

Fig. 5.21 Contours of Axial Velocity under Combustion

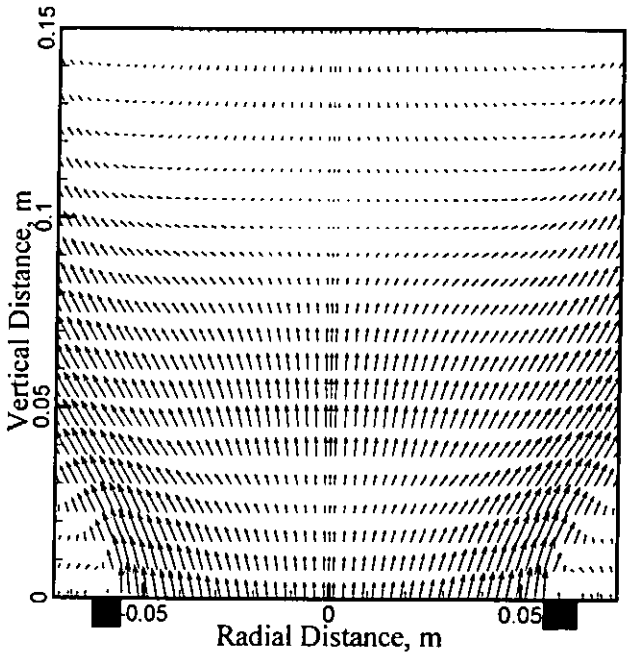

Fig. 5.22 Velocity Vectors under Combustion

It can be seen from Fig. 5.20 that strong impingement occurs between hot products and re-circulated flow. It is this impingement that makes the flame approximates to the one-dimensional planar flame. As shown in Fig. 5.21, the contours for axial velocity within flame zone are nearly parallel to the radial coordinate, indicating that axial velocities are uniform along the radial direction within the flame zone. Similarly, the axial velocities between the maximal

temperature zone and re-circulation zone are uniform along the radial direction, as the radius is less than 0.04m. Compared with our study, *Chigier* and *Cherivinsky* [9] reported a weak swirl-stabilized premixed flame in the shape of an annular ring. This is because that no re-circulation zone was formed in their study.

5.4 Comparison with other Combustion Models

As reported in Chapter 2, the combustion model used in our current study is a modified version of *Spalding*'s Stretch-Cut-Slide Model (*SCS* model). In this section, numerical results from the original *SCS* model are presented. In addition, the results from Eddy-Break-Up (*EBU*) model are also compared with those from the *SCS* model. In *EBU* model, the mixing controlled fuel-burning rate per unit volume is written as [31]:

$$S_{fu,EBU} = -A\rho \min\left[M_{fu}, \frac{M_{ox}}{s}, \frac{M_{pr}}{B(1+s)}\right]\frac{\varepsilon}{k} \tag{5.7}$$

Where,

A, B: Empirical constants, A=4.0, B=0.5

M_{pr}: Mass fraction of combustion products, including CO_2 and H_2O

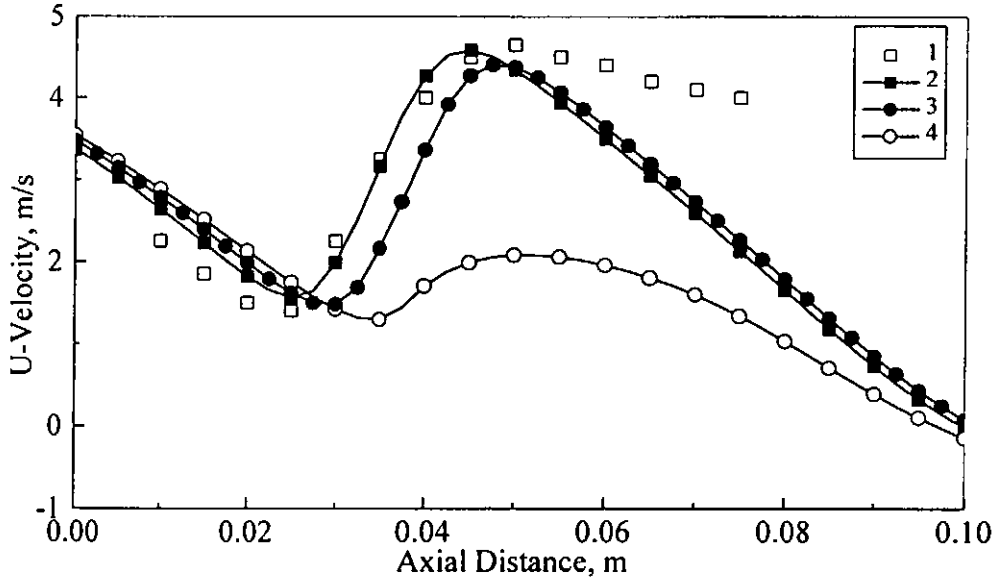

Fig. 5.23 Predicted vs. Measured Axial Velocities on the Centerline

1. Experiment; 2. Modified *SCS* Model; 3. *SCS* Model; 4. *EBU* model

Fig. 5.23 shows the profiles of axial velocity on the centerline with combustion. It can be seen that *EBU* model gives very poor prediction of the

axial velocity. The results from *SCS* models match the experiment very well, and the modified *SCS* model gives the best prediction in the flame zone.

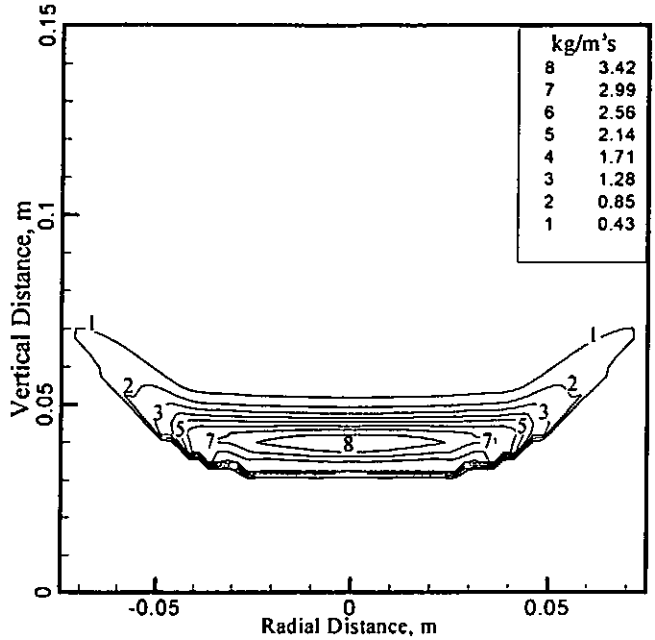

Fig. 5.24 Fuel Burning Rate Based on *SCS* Model

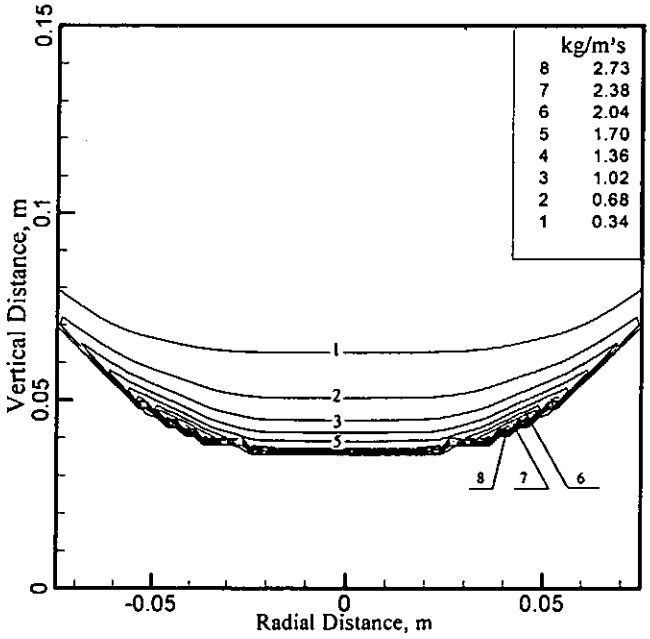

Fig. 5.25 Fuel Burning Rate Based on *EBU* Model

Figs. 5.24 and 5.25 give the distribution of fuel burning rate per unit volume in the combustion space. It can be seen that *SCS* model also predicts a planar flame, similar to that of the modified *SCS* model, as shown in Fig. 5.11. *EBU* model gives a different flame structure. The burning rate is much smaller than that of *SCS* model, and the maximal burning rate is located at the periphery of the flame, not on the centerline. This is not strange, since *EBU* model is valid where *Reynolds* number is high and there exists strong shear flow. Figs. 5.9 and 5.10 show that turbulence is very high at the shear layer. Experimental

study shows that current flame approximates to the one-dimensional planar flame. Thus, *EBU* model is unfit for our current study.

Figs. 5.11, 5.23 and 5.24 show that there is little difference between the modified *SCS* model and the original *SCS* model. In fact, the quantity, $l_1|\partial u/\partial y + \partial v/\partial x|/S_L$, is very small in the major reaction zone. Fig. 5.26 shows the distribution of this quantity in the flame.

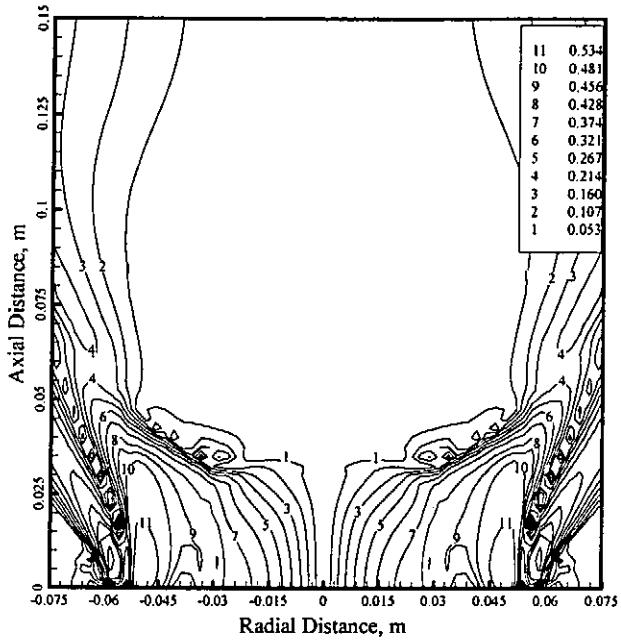

Fig. 5.26 Distribution of $l_1|\partial u/\partial y + \partial v/\partial x|/S_L$ in th Flame

It can be seen that $l_1|\partial u/\partial y + \partial v/\partial x|/S_L$ is smaller than 0.5 in the major reaction zone. In most part of the flame, this quantity is smaller than 0.35. This introduces very small error in simplifying the original *SCS* model. Though $l_1|\partial u/\partial y + \partial v/\partial x|/S_L$ is large in the shear layer, the temperature is low in this region. It is expected that chemical kinetics dominate in this region.

6. Effects of Aerodynamics and Burner Configuration

It is well known that burner configurations and operating aerodynamic parameters affect the burner performance. Thus, they are very important in view of energy efficiency, optimum design and operation of the burner. Among those parameters affecting the burner performance, the following ones are considered to be of greatest interest: swirl number and fuel to air equivalence ratio. Presently, parametric calculations are carried out to determine the effects of these parameters. A typical burner is considered as the reference case, and one of these parameters is varied at a time from the base case for each simulation. The reference condition is the one described in Chapter 5. Variation of more than one parameter at a time is avoided, because this makes it difficult to interpret the individual effects.

6.1 Influence of Swirl Intensity

Swirl affects the overall performance of the premixed flames. In order to assess how swirl affects the flame, it is decided to keep the inlet flow rate and burner configuration constant. Swirl intensity is changed via varying the tangential mass flow rate. In the current study, calculations are carried out for three geometric swirl numbers: S_1=0.05, 0.07 and 0.09. Figs. 6.1~6.7 provide the changing trend of flame properties under above three swirl intensity.

6.1.1 Influence of Swirl on Centerline Velocity

Fig. 6.1 shows the vertical velocity profile on the centerline. Under non-reacting conditions, the decaying rate of the vertical velocity with stream wise distance, seen in Fig. 6.1, increases as swirl number increases. No re-circulation zone is predicted for S_1=0.05. There exists a re-circulation zone for both S_1=0.07 and 0.09. The length of the re-circulation zone for S_1=0.09 is longer than that for S_1=0.07. That is to say, an increase in swirl number of the isothermal flow causes an increase in the mass of gas re-circulated, and this in turn causes an increase in the re-circulation zone length.

Chemical reaction alters the flow field drastically. Heat release causes flow gas expansion, which results in a sharp increase in the vertical velocity within the flame zone. Such increase is characteristics of turbulent premixed flames under similar flow and mixture conditions. Beyond the flame zone, the vertical velocity resumes its decrease. It is interesting to note that, from Fig. 6.1, for swirl number of 0.05, the isothermal flow doesn't have re-circulation. However, the re-circulation zone appears in the corresponding combustion flow.

The flames of S_l=0.07 and 0.09 have much larger re-circulation zones than their corresponding isothermal flows. Thus, it is concluded that chemical reaction helps to drive the re-circulation. Compared with the non-reacting flows, there is no significant change in the length of re-circulation zone as swirl number increases. This indicates that heat release has stronger effect on the re-circulation zone length than swirl intensity in our current study.

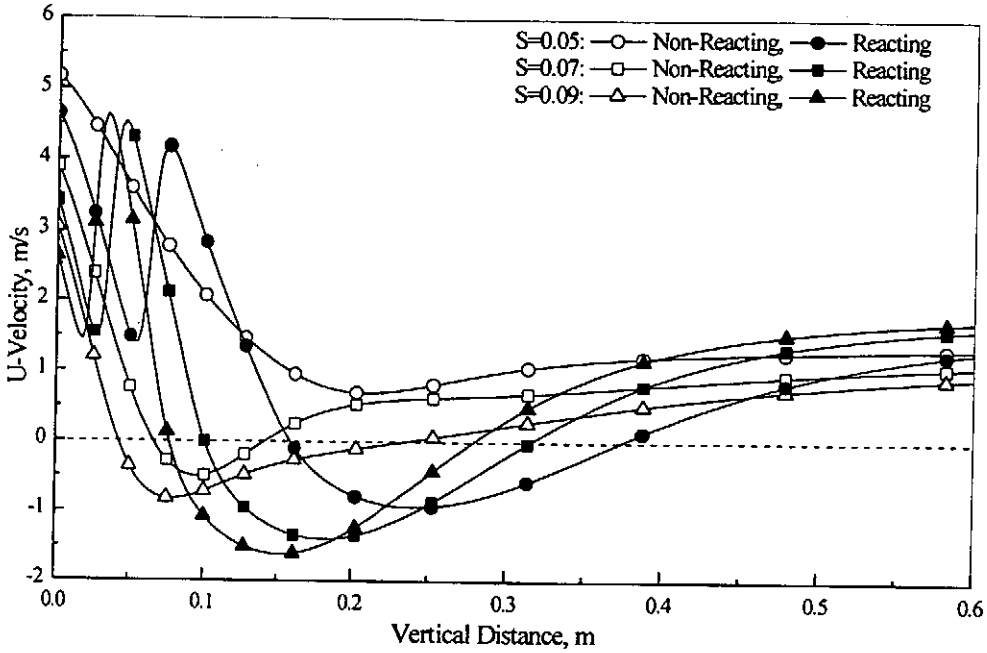

Fig. 6.1 Variation of Axial-Velocity with Swirl along the Centerline

Fig. 6.1 also shows that varying swirl changes the position of the flame brush. Weaker swirl pushes the flame downstream, while stronger swirl pulls the flame closer to the burner exit, as reported in the experimental study [5].

6.1.2 Influence of Swirl on Turbulent Kinetic Energy, k

Fig. 6.2 shows the profile of turbulent kinetic energy on the centerline. It can be seen that k increases drastically with increasing swirl at the burner exit. For the isothermal swirl jets, the development of k with stream wise distance is strongly influenced by swirl number. For S_l=0.05, k begins to increase near the burner exit and rise monotonically to an asymptotic value on the order of 0.3 m^2/s^2. For S_l=0.09, k increases even more sharply near the burner exit. It reaches a peak of approximately 2.2 m^2/s^2 at x=0.05m, and then decays gradually.

There is significantly more turbulence in the flames than in the isothermal flows. As shown in Fig. 6.2, there is sharp increase in turbulent kinetic energy within the flame zone. This is because that there exist large velocity gradients in the combustion space. There are two peaks in the turbulent kinetic energy

profile for S_1=0.07 and 0.09, respectively. The forward peak locates within the reaction zone, while the rear peak are formed due to the sharp decrease in the axial velocity, as a result of impinging between the flame and the reverse flow.

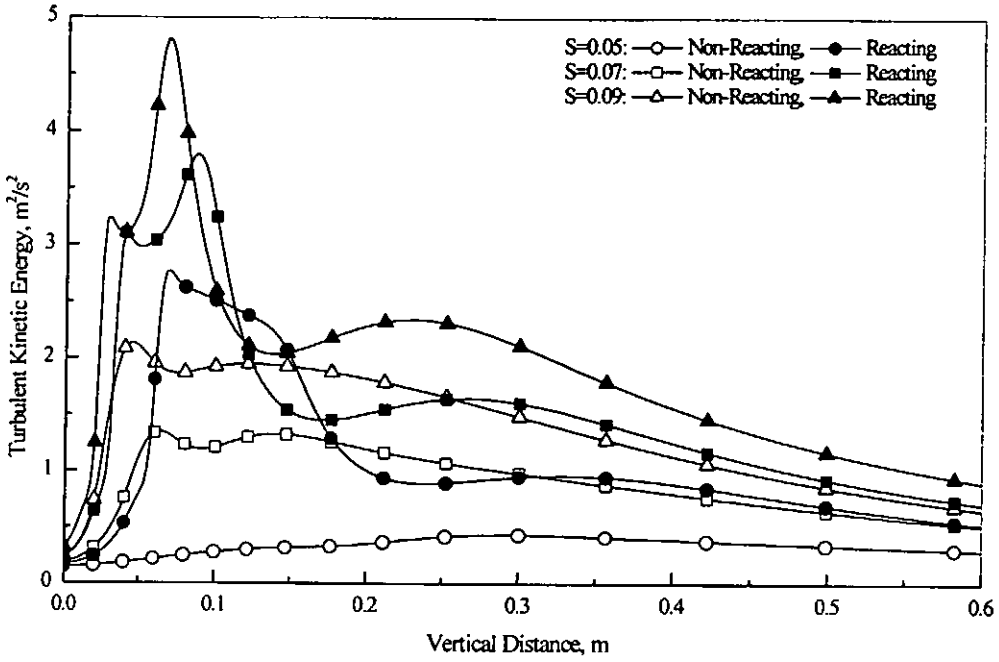

Fig. 6.2 Variation of Turbulent Kinetic Energy with Swirl on the Centerline

6.1.3 Influence of Swirl on Flame Temperatures

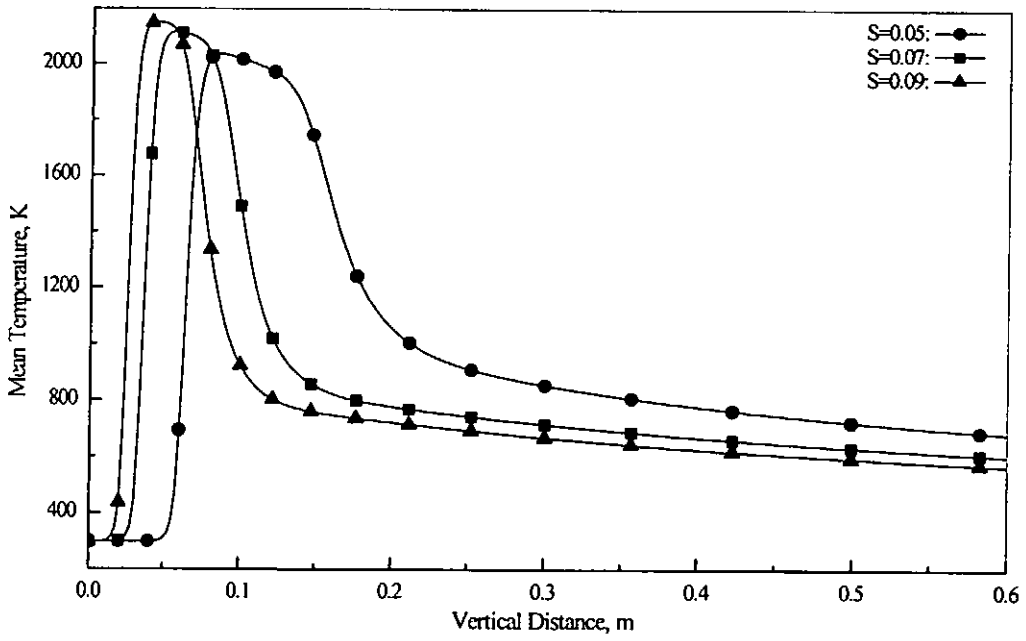

Fig. 6.3 Variation of Mean Temperature with Swirl on the Centerline

It can be seen from Fig. 6.3 that, the maximal flame temperature increases as swirl number increases. This is not surprising, because the length of stronger swirl flame is shorter than that of weaker swirl flame. This can be verified from

Fig. 6.4, in which variations of fuel-burning rate with swirl are presented. Fig. 6.4 shows that, as swirl number becomes larger, fuel-burning rate becomes faster and that chemical reaction occurs in a narrower space. This means that combustion heat is released in a reduced volume as swirl increases. This leads to an increase in flame temperature. Fig. 6.3 shows that maximal temperatures for S_l=0.05, 0.07, and 0.09 are 2036 K, 2115 K and 2151 K, respectively.

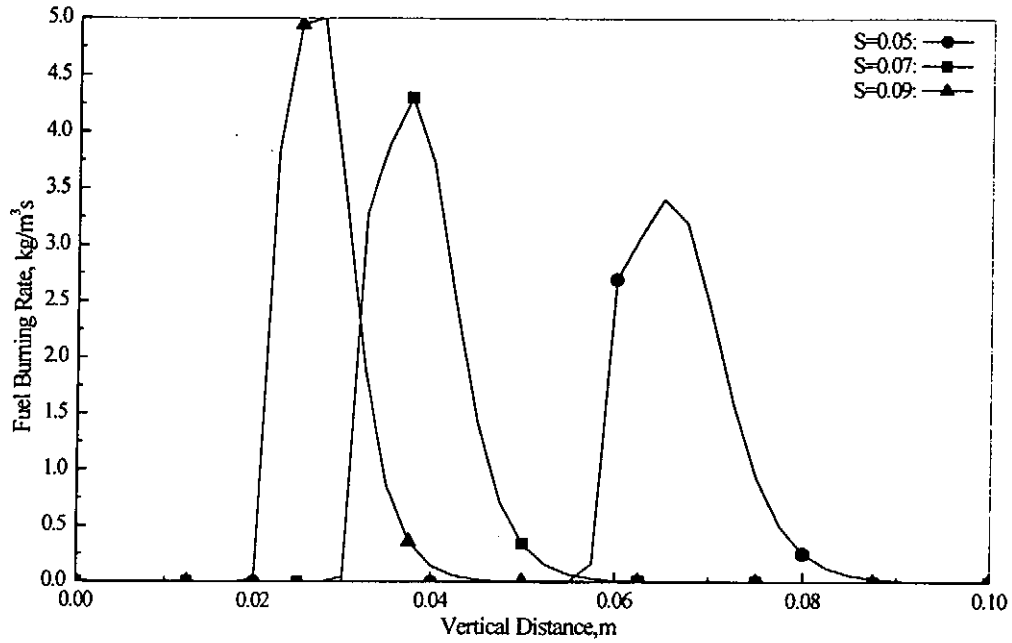

Fig. 6.4 Variation of Fuel Burning Rate with Swirl

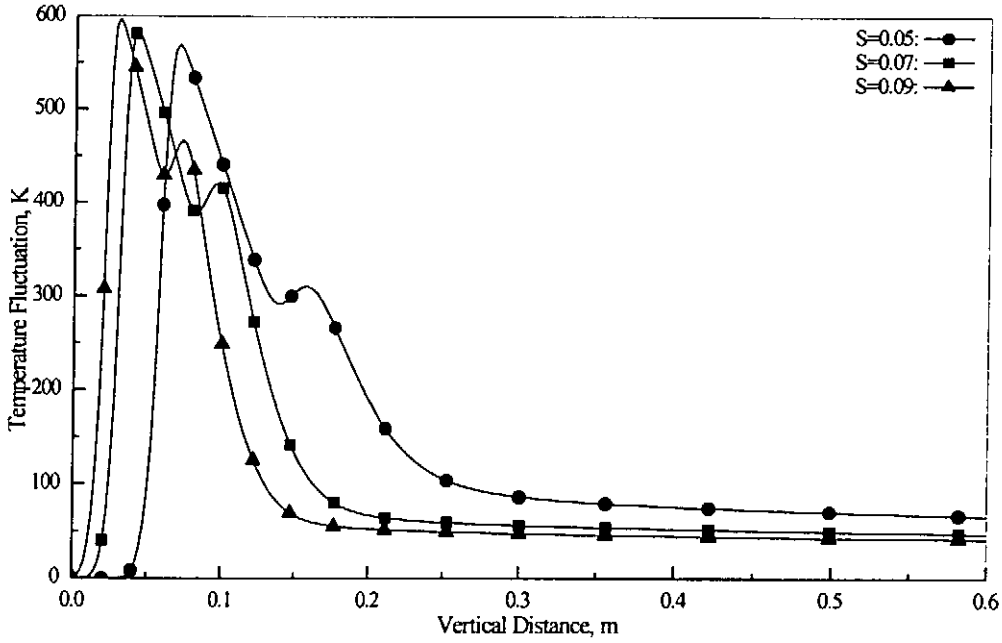

Fig. 6.5 Variation of Temperature Fluctuation with Swirl

Variation of temperature fluctuation with swirl is shown in Fig. 6.5. It can be seen that temperature fluctuation also increases with swirl within the flame. As reported in Section 5.2, there are two peaks in the vertical profile of

temperature fluctuation. One is located at about the same position as that of the maximal fuel-burning rate, the other is located within the impingement region between the flame and re-circulation zone. The predicted maxima of temperature fluctuation for S_1=0.05, 0.07 and 0.09 are 569 K, 583 K and 597 K, respectively.

6.1.4 Influence of Swirl on Species Mass fraction

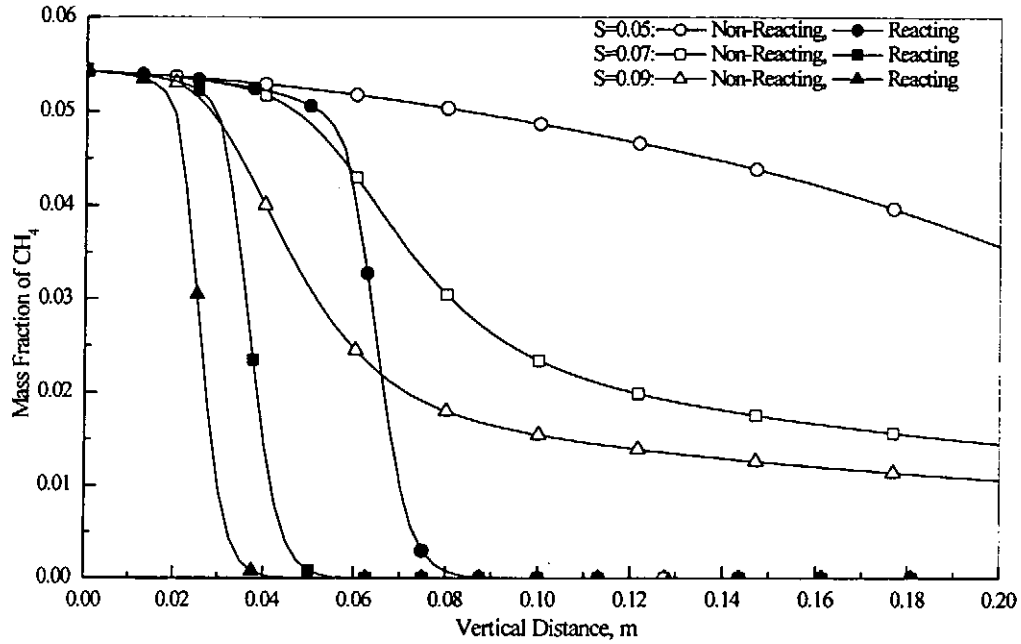

Fig. 6.6 Variation of CH_4 Mass Fraction with Swirl

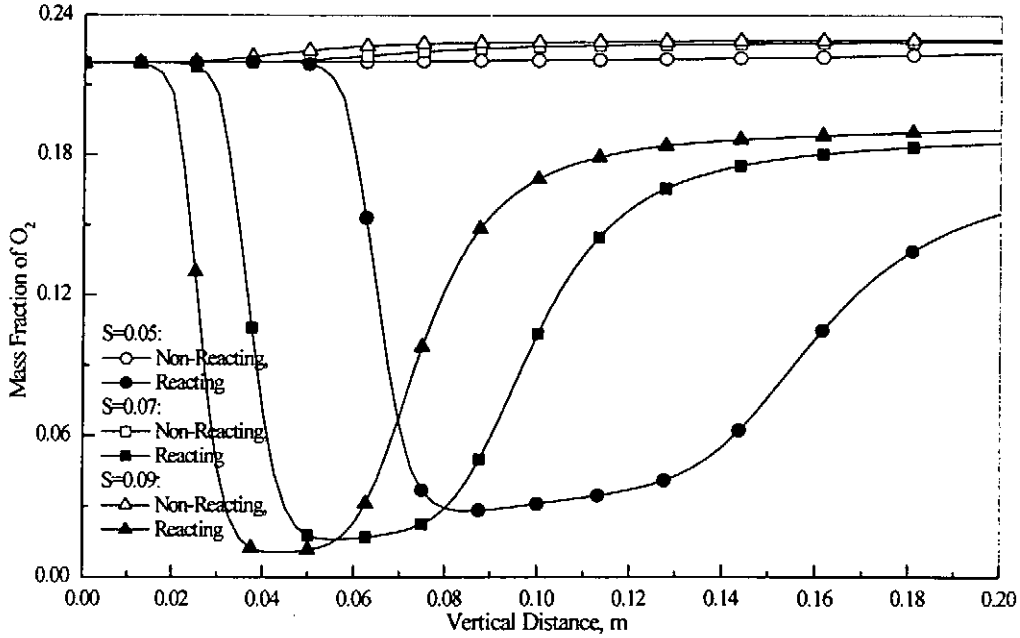

Fig. 6.7 Variation of O_2 Concentration with Swirl

Figs. 6.6 and 6.7 show the variation of concentration of methane and oxygen on the centerline, respectively. For the cold swirl jets, the concentration

of CH_4 along the flow axis decreases significantly as swirl number increases. This shows that as swirl number increases, the diffusion of CH_4 to the surrounding coflow air is strengthened. In addition, when a re-circulation zone is formed downstream of the burner exit, as for S_1=0.07 and 0.09, the intense mixing between the core mixture and the reverse flow also contribute to the sharp decrease in concentration of methane gas. This is because that concentration of CH_4 is very low in the re-circulation zone. Correspondingly, concentration of oxygen increases as swirl number increases for the cold flow. Both Fig. 6.6 and 6.7 show that there exists sharp decrease of concentration of combustion gases within the flame zone, indicating that intense combustion occurs. It can also be seen that the position of the flames moves closer to the burner exit as swirl number increase. The reason that the flame moves upstream is that an increase in swirl increases the adverse pressure gradient, $\partial p/\partial x$, which contribute a force acting in the negative axial direction.

6.2 Influence of Methane to Air Equivalence Ratio

In turbulent premixed flames, the fuel to air equivalence ratio, Φ, has an important influence on flame stability, combustion process and temperature field in the reacting flow. Presently, a lean premixed flame where Φ=0.8, a stoichiometric flame and a rich flame where Φ=1.2 are studied systematically.

6.2.1 Influence of Equivalence Ratio on Axial Velocity

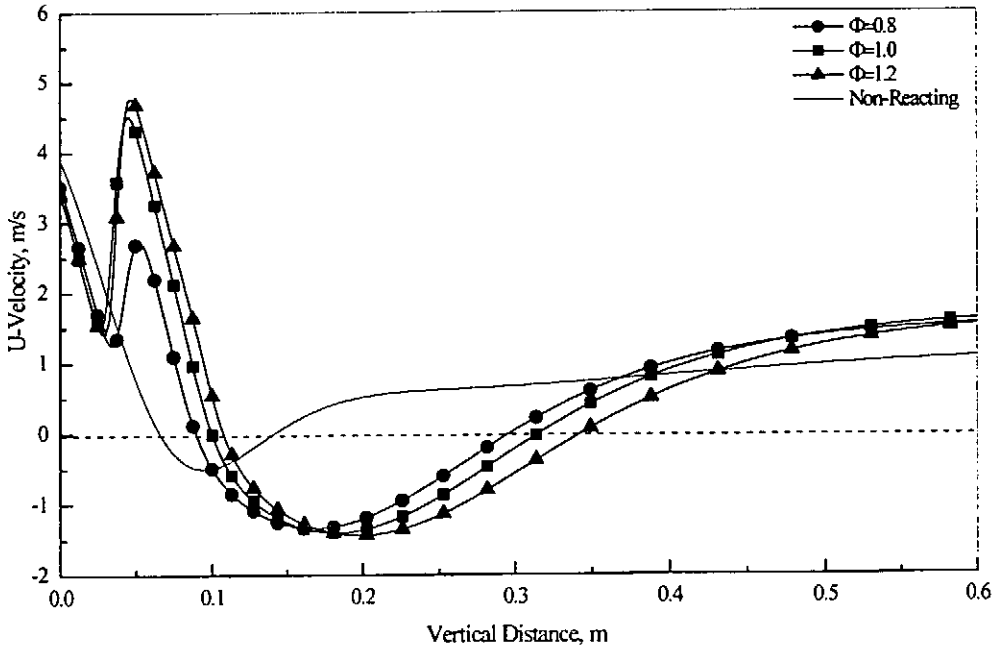

Fig. 6.8 Variation of Axial Velocity with Equivalence Ratio

Fig. 6.8 depicts the variation of centerline axial velocity in the stream wise direction for Φ=0.8, 1.0, and 1.2, respectively. As is shown in this figure, there is significant difference in the increment of axial velocity between lean and the other two flames within the flame zone. This indicates that the amount of heat released within the reaction zone drastically changes the flow field.

For lean flame, the overall amount of heat that can be released is small. This only leads to a moderate increment of vertical velocity associated with combustion-induced acceleration. For rich premixed flame, chemical reaction depends on the availability of oxygen. There is not enough oxygen in the core mixture to burn all methane for Φ=1.2. Additional oxygen must be supplied from coflow air. However, the surrounding air diffuses into the flame gradually. This restricts the heat release rate. That is why there is little difference in the profiles of vertical velocity for Φ=1.0 and 1.2 within the flame zone, as shown in Fig. 6.8.

It is interesting to note again that the axial length of re-circulation zone under combustion does not vary much with equivalence ratio. In section 5.1.1, it has been discussed that swirl number has little effect on the axial length of re-circulation zone under combustion. These facts indicate that chemical reaction itself has stronger effect on the re-circulation zone length than swirl intensity or equivalence ratio. This isn't a unique phenomenon of our current study. *Tangirala* and *Chen* [63] measured the same trends of re-circulation zone length in their diffuse flame in an open swirl flow.

6.2.2 Influence of Equivalence Ratio on Turbulent Kinetic Energy, k

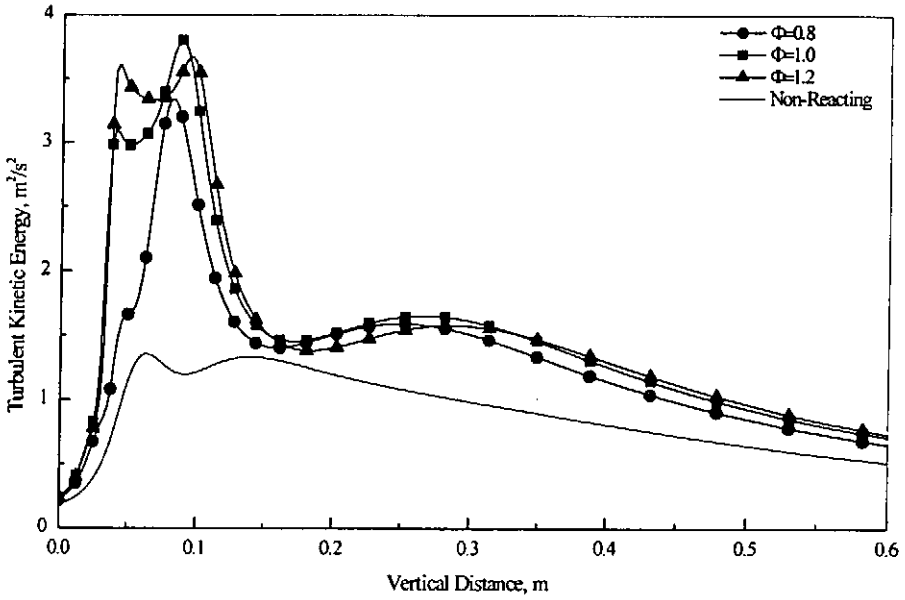

Fig. 6.9 Variation of Turbulent Kinetic Energy with Equivalence Ratio

Fig. 6.9 shows the variation of turbulent kinetic energy with Φ. This figure also shows that there is significant more turbulence in flames than in the non-reacting flow. Variations of turbulent kinetic energy along the axis are different with Φ. In downstream region of the combustion space (above x=0.35 m), turbulent kinetic energy increases with Φ.

For lean flame of Φ=0.8, there exists only one maximum of turbulence kinetic energy in the axial direction, while there are two maxima of turbulence kinetic energy for Φ=1.0 and 1.2 respectively. This is affected by the variation of velocity in the flow field. For lean flame, the chemical heat release is finite. Thus, there is no sharp increase or decrease in velocity, as shown in Fig. 6.8. This isn't the case for Φ=1.0 or 1.2. As shown in Fig. 6.8, there is much steeper increase or decrease in velocity for Φ=1.0 and 1.2, respectively. In addition, the maximum reversal velocity of Φ=1.0 or 1.2 is faster than that of Φ=0.8. As a result, stronger impingement occurs between flame and reverse flow for Φ=1.0 or 1.2. Consequently, two maxima of turbulence kinetic energy are formed for Φ=1.0 or 1.2.

6.2.3 Influence of Equivalence Ratio on Flame Temperature

Fig. 6.10 shows the variation of mean temperature with Φ. It can be seen that mean temperature increases with Φ. For the flame of Φ=1.2, the maximum temperature reaches a value of 2203K. For Φ=1.0, the maximum temperature arrives to a value of 2115K, while the lean flame has a maximum temperature of 1786K only. Furthermore, as equivalence ratio increases, the region that identifies a certain level of temperature increases in axial length.

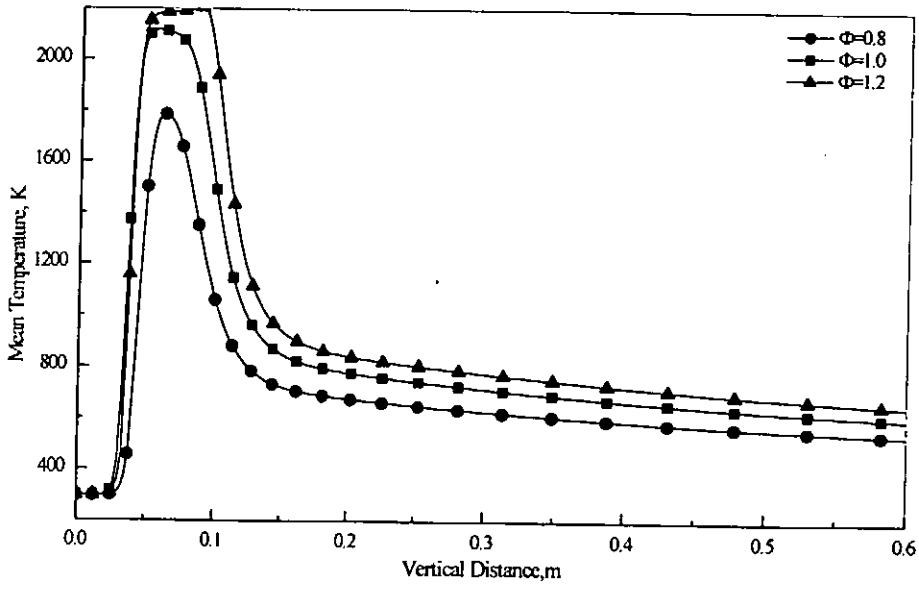

Fig. 6.10 Variation of Mean Temperature with Equivalence Ratio

It can be seen from Fig. 6.10 that, there exists a plateau of temperature for the rich flame. That is to say, the mean temperature remains about 2190K for about 0.05m in the vertical direction. While for the other two flames, the mean temperature drops rapidly after reaching its maximum value. This indicates that intense mixing between flame and reverse flow has different influence on flame.

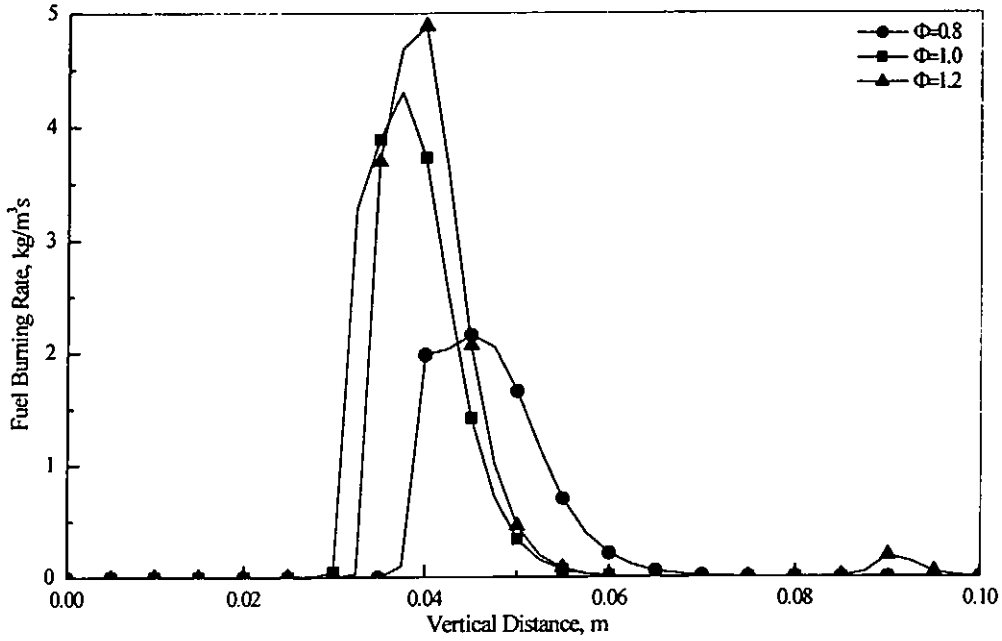

Fig. 6.11 Variation of Fuel Burning Rate with Equivalence Ratio

For lean or stoichiometric flame, fuel is completely burned after passing through the reaction zone. There is no chemical reaction or heat release in the impingement region. This results in the sharp decrease in the mean temperature, since the temperature in the reverse flow is relatively low. On the other hand, the reverse flow brings oxygen to the impingement region. For rich flame, the core mixture doesn't have enough oxygen for combustion. Excessive fuel passes through the flame zone and is burned completely in the impingement region. Consequently, heat released in the impingement region helps maintain a zone with relatively high temperature. Fig. 6.11 depicts the variation of fuel burning rate with Φ. This figure shows that intense combustion occurs in a narrow space for all these flames. However, apparent combustion also occurs in the impingement region for the rich flame.

6.2.4 Influence of Equivalence Ratio on Species Mass Fraction

Variation of CH_4 mass fraction with equivalence ratio is shown in Fig. 6.12. It can be seen that CH_4 mass fraction decreases in a similar trend for the cold swirl flows. For lean and stoichiometric flames, methane gas is consumed completely within the reaction zone, as indicated by the sharp decrease in methane

concentration and negligibly low value of CH_4 mass fraction in the downstream region of the flame. It can be seen from Fig. 6.12 that, the curves representing combustion depart from their corresponding non-reacting curves at about the same vertical position. This indicates that flame is stabilized at about the same position with fixed swirl number, irrespective of equivalence ratio.

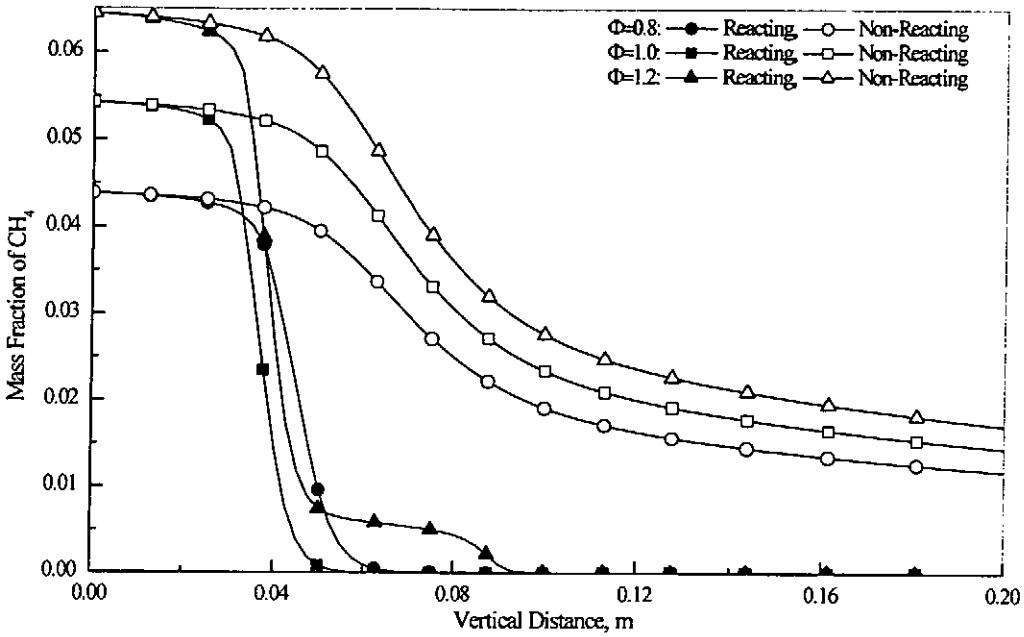

Fig. 6.12 Variation of CH_4 Concentration with Equivalence Ratio

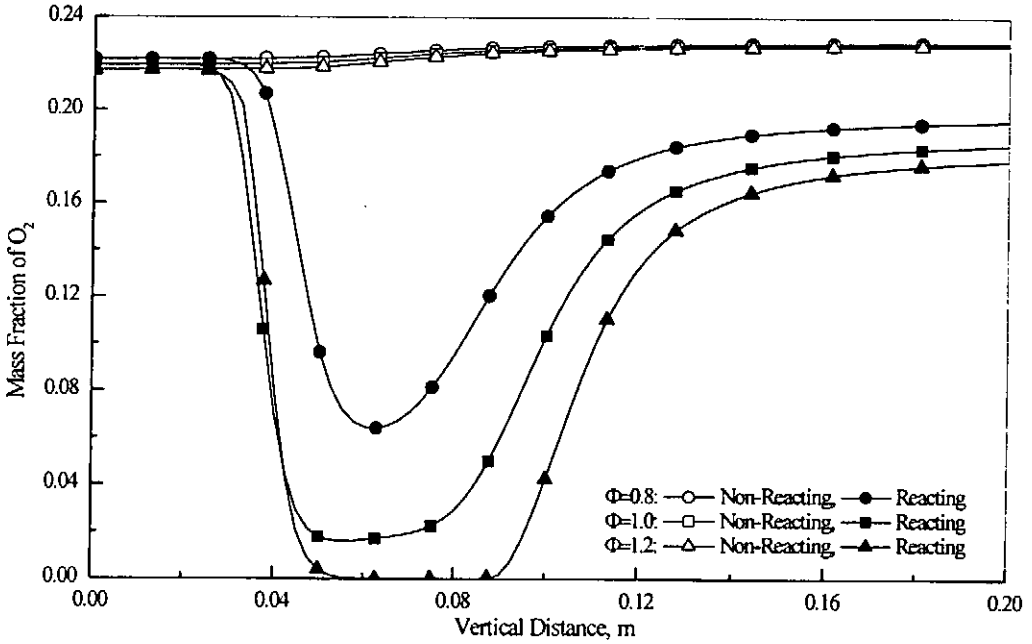

Fig. 6.13 Variation of O_2 Concentration with Equivalence Ratio

For rich flame, methane mass fraction also drops significantly within the main reaction zone. During this process, oxygen is depleted for rich flame, as shown in Fig. 6.13. Owing to the shielding effect of combustion products, little surrounding oxygen diffuses to the post-flame zone to complete combustion.

As a result, flame is smothered. That is why methane concentration decays very slowly between x=0.05m and x=0.08m.

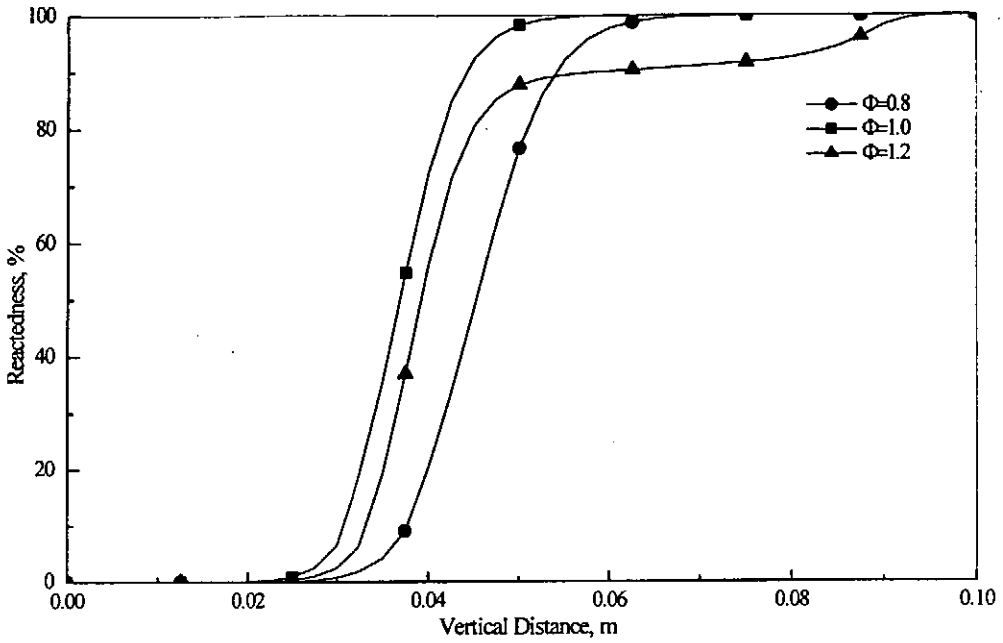

Fig. 6.14 Variation of Reactedness with Equivalence Ratio

Fig. 6.14 shows the profiles of reactedness for these three flames. It can be seen that the lean and stoichiometric flames finished their combustion within very short vertical distance, while the rich flame is elongated to the impingement region. As shown in Fig. 6.14, there is little combustion between x=0.05 m and x=0.08 m for rich flame. The reverse flow transports enough oxygen to the impingement region. Then, excessive hot fuel is burned out and the combustion is eventually finished.

6.3 Influence of Burner Configuration

In *Chan et al*'s experiment [5], there was no wall boundary between the fuel/air mixture and co-flow air inside the burner tube. The co-flow will prevent surrounding air from entering the fuel/air mixture. It is expected that there is little mass exchange between the core mixture and co-flow inside the tube, when the velocity of co-flow matches that of the mixture. Thus, the equivalence ratio of the mixture could remain constant before reaching the flame brush. This is true when there is no swirl in the flow.

When swirl is introduced inside the burner tube, the flow structure may be altered significantly by swirl. If swirl is weak, the pressure gradient induced by centrifugal force is insufficient for a reverse flow to form in the near wall region. It results only in decreased axial velocity. In our current study, the tangential velocity is very high in the near wall region and a re-circulation zone

is predicted, as shown in Fig. 6.15. The reverse flow impinges with inlet co-flow and forms a centripetal flow. This brings more co-flow air into the fuel/air mixture and decreases the overall equivalence ratio of the mixture. In order to prevent co-flow air from entering the core mixture earlier than expected, some methods should be taken to maintain the equivalence ratio of the mixture. A commonly used method is to set up a membrane between the core mixture and co-flow to the burner exit, as shown in Fig. 6.16.

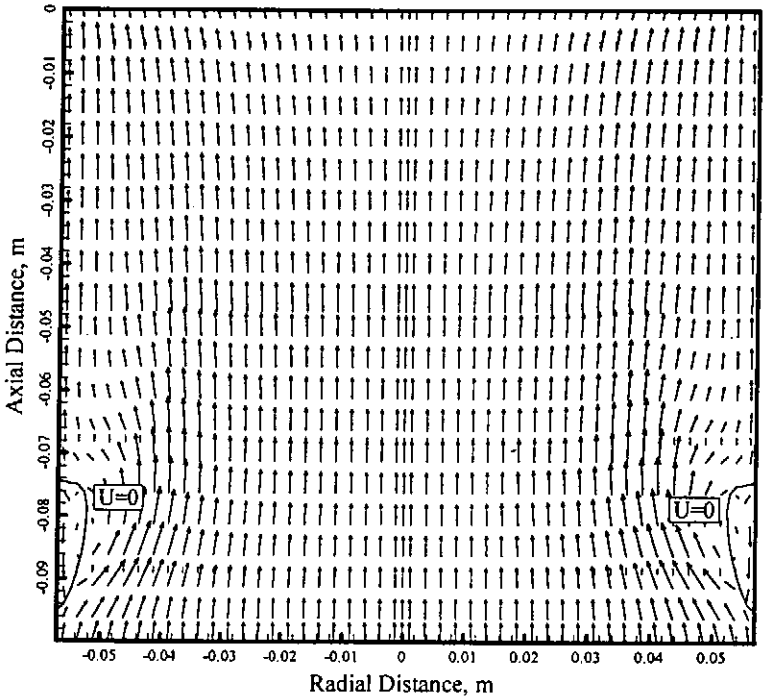

Fig. 6.15 Velocity Field inside the Burner without Wall

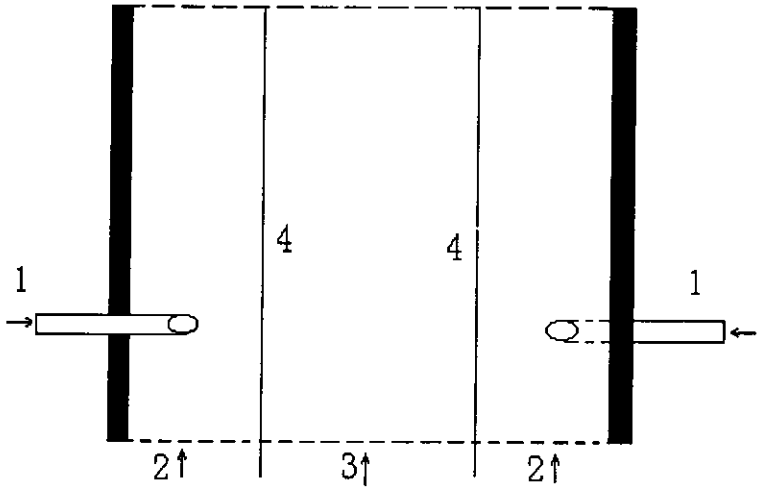

Fig. 6.16 Modified Burner Configuration

1. Tangential Air, 2. Coflow Air, 3. Fuel-Air Mixture, 4. membrane

Presently, calculations are carried out for the premixed flame using the burner configuration of Fig. 6.16. The wall boundary inside the tube is assumed to be infinitely thin. The radial velocity on it is zero and there is no diffusive

flux through this membrane. In addition, the near wall effect is not taken account of in the current study. All the operating parameters are same as those of the reference case.

6.3.1 Influence of Burner Configuration on Axial Velocity

Fig. 6.17 depicts the variation of centerline axial velocity with burner configuration. When there exists wall inside the burner tube, swirl has little effect on fuel-air mixture inside the tube. The centerline axial velocity decreases very slowly till the burner exit. The velocity is still as high as 4.78 m/s at the exit. After ejecting to the stagnant air, the axial velocity decreases sharply under the influence of swirl, and a re-circulation zone is formed between x=0.086m and x=0.2m for the cold swirl flow.

The flame zone is marked by the increase in centerline axial velocity. Fig. 6.17 shows that chemical reaction occurs further downstream of the swirl flow, when there exists wall boundary inside the burner tube. It can also be seen that, the current flame has a longer re-circulation zone than the flame without wall boundary inside the tube. Our predictions show that the current re-circulation zone is also wider than the flame without wall boundary inside the tube.

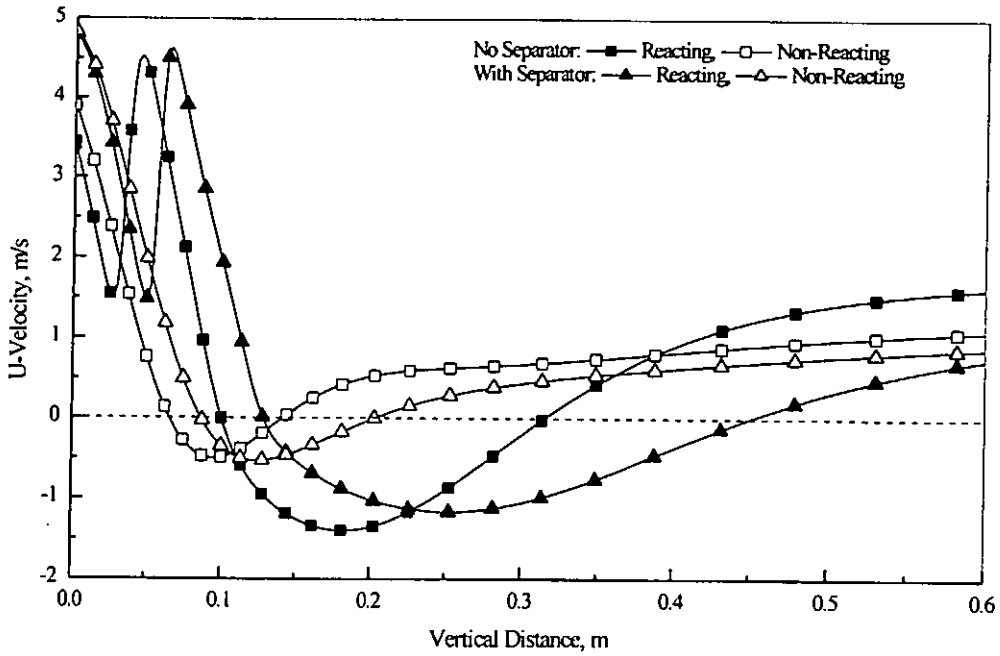

Fig. 6.17 Variation of Axial Velocity with Burner Configuration

Fig. 6.18 shows the distribution of relative pressure field under combustion. The point locating on the centerline at the burner exit is taken as reference point for both burner configurations. It can be seen from this figure, that the pressure increases along the flow axis and high-pressure zones are formed in the

combustion space for both burner configurations. The maximal pressure is 12.9 Pa in the current flame, while corresponding value is 6.9 Pa for the flame without wall boundary inside the tube. It has been discussed in Chapter 5 that, the high-pressure zone acts as blunt body for upstream fuel-air flow. The pressure is higher in the current flame. Consequently, a longer and wider re-circulation zone is formed in the flow.

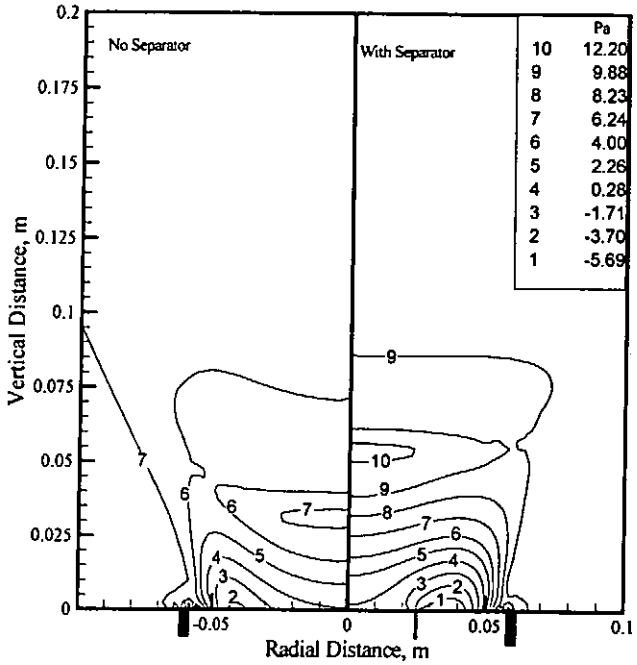

Fig. 6.18 Relative Pressure Field under Combustion

6.3.2 Influence of Burner Configuration on Flame Properties

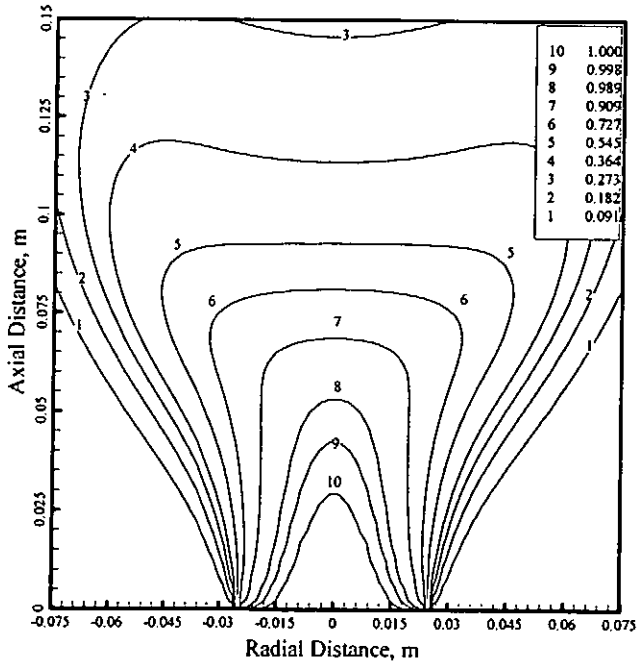

Fig. 6.19 Distribution of Φ for Isothermal Flow (Wall inside)

As stated previously, the purpose of adding a wall between core mixture and coflow air is to maintain the equivalence ratio constant before the flame. Distribution of fuel to air equivalence ratio is shown in Fig. 6.19 for the non-reacting flow under the modified burner configuration. This figure shows that

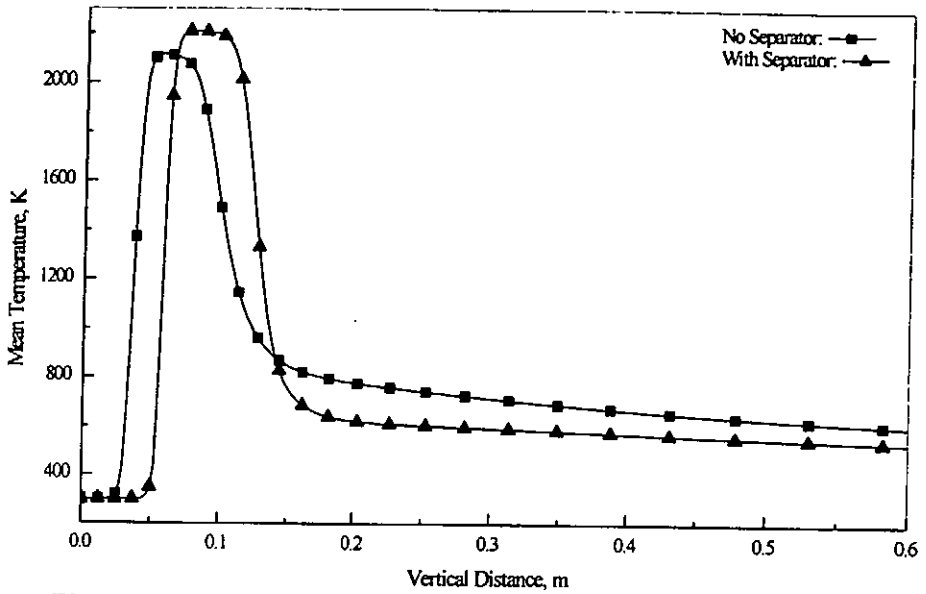

Fig. 6.20 Variation of Temperature with Burner Configuration

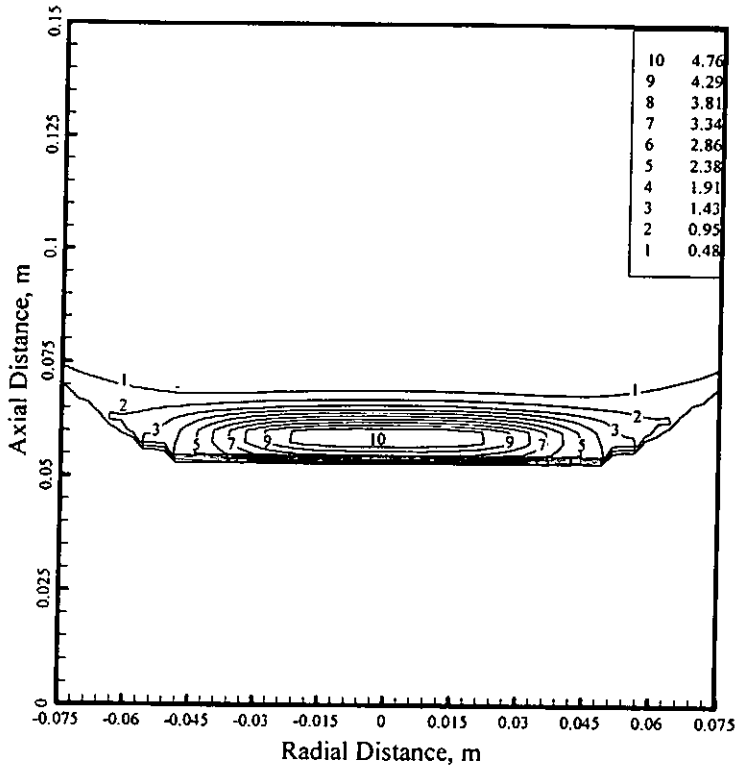

Fig. 6.21 Fuel Burning Rate for Flame with Wall inside Burner Tube

fuel to air equivalence ratio remains unchanged (i.e., Φ=1.0) within an axial distance of 0.03 m above the burner exit. The equivalence ratio is still as high as 0.99 at x=0.05 m on the centerline. Fig. 6.18 indicates that chemical reaction

is initialized at x=0.05 m. This means that the equivalence ratio before flame front is almost the same as that at the inlet boundary. Under such circumstance, the maximal flame temperature should be very close to corresponding adiabatic flame temperature of the same equivalence ratio. Fig. 6.20 depicts the variation of centerline mean temperature along the axial direction. It can be seen that, when there exists a wall inside burner tube, mean temperature maintains very high level within the flame zone. The maximal temperature is 2208 K in the current flame, while corresponding adiabatic flame temperature is 2210 K.

The distribution of fuel burning rate for the current flame is shown in Fig. 6.21. It can be seen that intense combustion occurs almost within two parallel planes normal to the centerline. In other words, chemical reaction takes place between x=0.055m and x=0.065m. Compared with Fig. 5.11, cross-sectional area of the current flame is larger than that of the flame without wall inside burner tube, and the current flame zone is thinner in the axial direction. It is expected that current flame behaviors in a more planar manner and is more suitable for investigating fundamental properties of turbulent premixed flames.

7. Conclusions

Flame stabilization by swirl is a common feature of many turbines and combustors. However, most swirl burners are enclosed, there have been relatively few studies of unconfined swirl stabilized flames. An open swirl stabilized turbulent premixed flame is studied numerically. Flow field, combustion process and heat transfer are simulated in a larger open space. The primary aim has been to improve understanding of the fundamental physics and to examine the effect of many burner parameters on flame properties. Based on the results obtained, the following conclusions can be drawn.

1. *Spalding*'s Stretch-Cut and Slide model (*SCS*) is modified and extended to fit our current study. In the modified *SCS* model (*MSCS*), fuel-burning rate per unit volume is simply defined as the sum of turbulent mixing controlled and chemical kinetically determined fuel-burning rate. Thus, effect of turbulence and chemical kinetics on combustion can be clearly seen from *MSCS* model. Numerical results show that *MSCS* model gives better prediction of flame properties than *SCS* and *EBU* models.

2. Predictions reveal that a re-circulation zone is located far downstream of the flame zone, though previous experimental study [5] detected no reversal flow. It is found that combustion helps to drive re-circulation zone. The re-circulation zone becomes wider and longer under combustion than in isothermal flow. The maximum reversal velocity also increases with combustion. These phenomena are quite different from those occur in a confined reacting flow.

3. Intense combustion occurs in a narrow space. A stationary planar flame is maintained above the burner exit, where the turbulent flame speed is equal to local flow velocity. Although flame is stabilized by swirl, the flame zone is in fact free of swirl. Thus, it is very convenient to measure the turbulent flame speed based on the flow field. Predictions reveal that flame stabilization does not rely on re-circulation zone, but on flow divergence.

4. Distribution of reaction rate, temperature and species concentration indicate that the current flame features that of a one-dimensional turbulent planar flame. It is shown that strong impingement occurs between flame zone and re-circulation zone. It is this impingement that makes the flame approximate to the one-dimensional planar flame.

5. Chemical reaction itself has stronger influence on re-circulation zone length than swirl intensity and fuel to air equivalence ratio. It is found that the length of re-circulation zone changes little with swirl number or equivalence ratio in the reacting flow.

6. A more planar one-dimensional flame can be obtained via modifying the burner configuration. At the same time, the fuel to air equivalence ratio is well maintained before the flame front when operating on the modified swirl burner.

These conclusions are drawn based on our numerical simulations. However, there can be artifacts generated due to the inadequacies of the mathematical models in any numerical study (i.e. assuming constant values for the empirical parameters throughout the computational domain despite significant variation in viscosity and density). In our study, apparent discrepancy between predictions and measurements exists for both isothermal flow and reacting flow. This indicates that more work is needed on this kind of swirl flame, both experimentally and theoretically. Due to the unique application of this swirl burner in studying turbulent premixed flame, it is recommended that future work on this kind of swirl flame is done in the following areas:

1. Numerical simulation of this swirl flame under three-dimensional cylindrical coordinates.
2. A more comprehensive validation of the empirical constants employed in the turbulence and combustion models.
3. Consideration of the flame with advanced combustion models, taking into account of chemical kinetics.
4. Measurements of the swirl flame in a larger open space, so as to provide new opportunities for investigating flame propagation phenomenon and for comparison between experimental and theoretical work.

References:

1. Bach, T.V. and Gouldin, F.C., "Flow Measurements in a Model Swirl Combustor", *AIAA Journal*, Vol. 20, No. 5, pp.642-651 (1982)
2. Bedat, B. and Cheng, R.K., "Experimental Study of Premixed Flames in Intense Isotropic Turbulence", *Combustion and Flame*, Vol. 100, pp. 485-494 (1995)
3. Beer, J.M., and Chigier, N.A., *Combustion Aerodynamics*, Applied Science Publishers, London (1972)
4. Bray, K.N.C., "Turbulent Flows with Premixed Reactants", in Libby, P.A. et al., ed., *Turbulent Reacting Flows*, Springer-Verlag Press, pp. 115-183 (1980)
5. Chan, C.K., Lau, K.S., Chin, W.K., Cheng, R.K., "Freely Propagating Open Premixed Turbulent Flames Stabilized by Swirl", *Twenty-Fourth Symposium (International) on Combustion*, The Combustion Institute, pp. 511-518 (1992)
6. Chen, R.H. and Driscoll, J.F., "The Role of the Recirculation Vortex in Improving Fuel-Air Mixing within Swirling Flames", *Twenty-Second Symposium (International) on Combustion*, The Combustion Institute, pp. 531-540 (1988)
7. Cheng, R.K., Yegian, D.T., Miyasato, M.M., Samuelsen, G. S., "Scaling and Development of Low Swirl Burners for Low-Emission Furnaces and Boilers", *Twenty-eighth Symposium (International) on Combustion*, The Combustion Institute, to be published (2000)
8. Chigier, N.A., and Chervinsky, A., *Transactions of ASME, Journal of Applied Mechanics*, Vol. 34, pp. 443-451 (1967)
9. Chigier, N.A., Chervinsky, A., "Aerodynamic Study of Turbulent Burning Free Jets with Swirl", *Eleventh Symposium (International) on Combustion*, The Combustion institute, pp.489-499 (1967)
10. Chou, P.Y., "On Velocity Correlations and Solution of the Equations of Turbulent Fluctuation", *Quarter Journal of Applied Mathematics*, Vol. 3, pp. 38-54 (1945)
11. Chuang, S., Yang, C. and Wu, N., "Prediction of Swirling Flow in Sudden-Expansion Dump Combustor with Flame holder Side-inlet Using Two-step Combustion Model", *International Journal of Numerical Methods for Heat & Fluid Flow*, Vol. 9, No. 7, pp.764-787 (1999)
12. Claypole, T.C. and Syred, N., "Effect of Swirl Burner Aerodynamics on NO_x Formation", *Eighteenth Symposium (International) on Combustion*, The Combustion Institute, pp. 81-92 (1981)
13. Dugger, G.L., Heimel, S. and Weast, C., *Industrial and Engineering Chemistry*, Vol.47, pp.114-125 (1955)

14. Edelman, R.B. and Harsha, P.T., "Laminar and Turbulent Gas-Dynamics in Combustors-Current Status", *Progress in Energy and Combustion Sciences*, Vol. 4, No. 1 (1978)

15. Edwards, C.F. and Rudoff, R.C., *Twenty-third Symposium (International) on Combustion*, The Combustion Institute, pp. 1353-1360 (1991)

16. Fan, W.C., *Computer Modeling of Combustion Processes*, International Academic Publishers (1991)

17. Feikema, D., Chen, R.H. and Driscoll, J.F., "Enhancement of Flame Blow out Limits by the Use of Swirl", *Combustion and Flame*, Vol. 80, pp. 183-193 (1990)

18. Fujii, S. Eguchi, K. and Gomi, M., "Swirling Jets with and without Combustion", *AIAA Journal*, Vol. 19, No. 11, pp. 1438-1442 (1981)

19. Glassman, I., *Combustion*, 3rd Edition, Academic Press (1996)

20. Gouldin, F.C., Depsky, J.S., and Lee, S.L., "Velocity Field Characteristic of a Swirling Flow Combustor", *AIAA Journal*, Vol. 23, No. 1, pp. 95-102 (1985)

21. Gupta, A.K., Lilley, D.G., and Syred, N., *Swirl Flows*, Abacus Press (1984)

22. Halthore, R.N. and Gouldin, F.C., "Laser Scattering Measurements for Gas Densities in a Swirling Flow Combustor", *AIAA Journal*, Vol. 24, No.7, pp. 1129-1136 (1986)

23. Harlow, F.H. and Welch, J.E., "Numerical Calculation of Time-dependent Viscous Incompressible Flow of Fluid with Free Surface", *Physics of Fluids*, Vol. 8, No. 12, pp. 2182-2189 (1965)

24. Hinze, J.O., *Turbulence*, 2nd Edition, McGraw-Hill, New York (1975)

25. Khalil, E.E., *Modeling of Furnaces and Combustors*, Abacus Press (1982)

26. Kuo, K.K., *Principles of Combustion*, A Wiley-Interscience Publication, New York (1986)

27. Launder, B.E. and Spalding, D.B., *Lectures in Mathematical Models of Turbulence*, Academic Press, London (1972)

28. Launder, B.E. and Spalding, D.B., "The Numerical Computation of Turbulent Flows", *Computer Methods in Applied Mechanics and Engineering*, Vol. 3, pp. 269-289 (1974)

29. Libby, P.A., "Theory of Normal Premixed Turbulent Flames Revisited", *Progress in Energy and Combustion Science*, Vol. 11, pp. 83-96 (1985)

30. Lilley, D.G., "Swirl Flows in Combustion: A Review", *AIAA Journal*, Vol.15, No.8, pp. 1063-1078 (1977)

31. Magnussen, B.F. and Hjertager, B.H., "On Mathematical Models of Turbulent Combustion with Special Emphasis on Soot Formation and Combustion", *Sixteenth Symposium (International) on Combustion*, The Combustion Institute, pp. 719-728 (1976)

32. Milosavljevic, V.D., Taylor, A.M.K.P. and Whitelaw, J.H., "The Influence of Burner geometry and Flow Rates on the Stability and Symmetry of Swirl-Stabilized Non-premixed Flames", *Combustion and Flame*, Vol. 80, pp.196-208 (1990)

33. Mitchell, R.E. Sarofim, A.F. and Clomburg, L.A., "Experimental and Numerical Investigation of Confined Laminar diffusion Flames", *Combustion and Flames*, Vol. 37, pp. 227244 (1980)

34. Morse, A.P., *Axisymmetric Free Shear Flows with and without Swirl*, Ph.D. Thesis, Department of Mechanical Engineering, Imperial College of Science and Technology, London (1980)

35. Pan, W.Q., *Engineering Fluid Mechanics* (in Chinese), Publishers of Tsinghua University (1987)

36. Patankar, S.V. and Spalding, D.B., "A Calculation Procedure for Heat, Mass and Momentum Transfer in Three-dimensional Parabolic Flow", *International Journal of Heat and Mass Transfer*, Vol. 15, pp. 1787-1805 (1972)

37. Patankar, S.V., Ramadhyani, S. and Sparrow, E.M., "Effects of Circumferentially Non-uniform Heating in Laminar Combined Convection in a Horizontal Tube", *Journal of Heat Transfer*, Vol. 100, pp.63-70 (1978)

38. Patankar, S.V., *Numerical Heat Transfer and Fluid Flow*, Hemisphere, Washington D.C. (1980)

39. Patankar, S.V., "A Calculation Procedure for Two-Dimensional Elliptic Situations", *Numerical Heat Transfer*, Vol. 4, pp. 405-425 (1981)

40. Peters, N., *Fifteen Lectures on Laminar and Turbulent Combustion at ERCOFTAC Summer School*, Aachen, Germany (1992)

41. Peters, N., *Four Lectures on Turbulent Combustion at ERCOFTAC Summer School*, Aachen, Germany (1997)

42. Plessing, T., Kortschchik, C., Mansour, M.S., Peters, N. and Cheng, R.K., "Measurements of the Turbulent Burning Velocity and the Structure of Premixed Flames on a Low Swirl Burner", *Twenty-eighth Symposium (International) on Combustion*, The Combustion Institute, to be published (2000)

43. Pope, S.B., "A Monte Carlo Method for the P.D.F. Equations of Turbulent Reactive Flow", *Combustion Science and Technology*, Vol. 25, pp. 159-174 (1981)

44. Pope, S.B., "Methods for Turbulent Reactive Flows", *Progress in Energy and Combustion Science*, Vol. 11, pp. 119-192 (1985)

45. Pope, S.B., "Monte Carlo Calculations of Premixed Turbulent Flames", *Eighteenth Symposium (International) on Combustion*, The Combustion Institute, pp. 1001-1010 (1980)

46. Ramos, J.I. and Somer, H.T., "Swirling Flow in a research Combustor", *AIAA Journal*, Vol. 23, No. 2, pp. 241-248 (1985)

47. Ribeiro, M.M. and Whitelaw, J.H., "Coaxial Jets with and without Swirl", *Journal of Fluid Mechanics*, Vol. 96, pp. 769-795 (1980)

48. Rodi, W. and Spalding, D.B., "A Two-Parameter Model of Turbulence, and its Application to Free Jets", *Warme-Stoffubertrag*, Vol. 3, pp. 85-95 (1970)

49. Rose, W.G., "A Swirling Round Turbulent Jet, 1-Mean-Flow Measurements", *Transaction of ASME, Journal of Applied Mechanics*, Vol. 29, pp. 615-625 (1962)

50. Siegel, R. and Howell, J.R., *Thermal Radiation Heat Transfer*, McGraw-Hill, New York (1981)

51. Smooke, M.D., "Numerical Modeling of Two-dimensional Axisymmetric Laminar Diffusion Flames", in Hussaini, M.Y. et al., ed., *Major Research Topics in Combustion*, Sprnger-Verlag Press, pp.23-44 (1992)

52. Song, T.H., *Simulation of Flow, Combustion and Heat-Transfer in a Two-dimensional Natural Gas-fired Industrial Furnace*, Ph. D. Thesis, Purdue University (1986)

53. Spalding, D.B., "Mixing and Chemical Reaction in Steady Confined Turbulent Flames", *Thirteenth Symposium (International) on Combustion*, The Combustion Institute, pp. 649-657 (1971)

54. Spalding, D.B., "A Two-Equation Model of Turbulence", *VDI-Forschungsheft*, pp. 5-16 (1972)

55. Spalding, D.B., "Mathematical Models of Turbulent Flames: A Review", *Combustion Science and Technology, Special Issue on Turbulence Reactive Flows*, Vol. 13, pp. 1-25 (1976)

56. Spalding, D.B., *Combustion Theory Applied to Engineering*, HTS-1 (1977)

57. Spalding, D.B., *GENMIX: A General Computer Program for Two-Dimensional Parabolic phenomena*, Pergamon Press, Oxyford (1978)

58. Spalding, D.B., "Development of the Eddy-Break-Up model of Turbulent Combustion", *Sixteenth Symposium (International) on Combustion*, The Combustion Institute, pp.1657-1663 (1978)

59. Spalding, D.B., *Combustion and Mass Transfer*, Pergamon Press, London, (1979)

60. Starner, S.H. and Bilger, R.W., "Joint Measurements of Velocity and Scalars in a Turbulent Diffusion Flame with Moderate Swirl", *Twenty-First Symposium (International) on Combustion*, The Combustion Institute, pp. 1569-1576 (1988)

61. Syred, N. and Beer, J., "Combustion in Swirling Flows: A Review", *Combustion and Flame*, Vol. 23, pp. 143-201 (1974)

62. Takeno, T., Nishioka, M. et al., "Effects of Local Flow Field on Chemical Reactions in Thin Reaction Zone of Premixed Flames", in: *Modeling in Combustion Science*, Springer Press, pp. 36-43 (1994)

63. Tangirala, V., Chen, R.H. and Driscoll, J.F., "Effect of Heat Release and Swirl on the Recirculation within Swirl-Stabilized Flames", *Combustion Science and Technology*, Vol. 51, pp. 75-95 (1987)

64. Williams, F.A., "Turbulent Reacting Flows", in: ***Combustion Fundamentals***, EXXON Research and Engineering Co., Florhem Park, NJ (1983)

65. Williams, F.A., *Combustion Theory*, 2nd Edition, Benjamin-CUmmings, Menlo Park, CA (1985)

66. Zhou, L.X., *Theory and Numerical Modeling of Turbulent Gas-Particle Flows and Combustion*, Science Press and CRC Press Inc. (1993)

67. Zhou, L.X., *Numerical Simulation of Turbulent Two Phase Flow and Combustion* (in Chinese), Publisher of Tsinghua University (1991)